APPLYING ADAPTIVE PROGNOSTICS TO ROLLING ELEMENT BEARINGS

A Thesis
Presented to
The Academic Faculty

by

Tara Reeves Lindsay

In Partial Fulfillment
of the Requirements for the Degree
Masters of Science in the
School of Mechanical Engineering

Georgia Institute of Technology
December 2005

APPLYING ADAPTIVE PROGNOSTICS TO ROLLING ELEMENT BEARINGS

Approved by:

Dr. Steven Liang, Co-Advisor
School of Mechanical Engineering
Georgia Institute of Technology

Dr. Richard Cowan, Co-Advisor
School of Mechanical Engineering
Georgia Institute of Technology

Dr. Shreyes Melkote
School of Mechanical Engineering
Georgia Institute of Technology

Date Approved: November 28, 2005

To Michael Karl Maelzer, for his continuous portrayal of humility, compassion and fervent quest for knowledge.

ACKNOWLEDGEMENTS

I wish to thank my father for teaching me the importance of both humor and humility and my mother for instilling in me a strong sense of persistence and pride in my work. I also would like to thank all of my close friends who have aided me in several aspects of academics, research, and life in general.

I would like to sincerely thank my thesis committee members, Dr. Rick Cowan, Dr. Shreyes Melkote, and especially Dr. Steven Liang, for their time, guidance, and insight during the research process. Whenever I had questions, these gentlemen always met me with a smile and knowledge that helped me with not only my research, but also in time management, career searching, and broader thinking.

I would like to give special recognition to Spaceworks, Inc. Without the company's support, my research and continued education would not have been possible. This company gave me the opportunity to achieve one of the most important milestones in my life. For this gift, I am eternally grateful.

TABLE OF CONTENTS

ACKNOWLEDGEMENTS IV

LIST OF TABLES VIII

LIST OF FIGURES IX

LIST OF SYMBOLS XII

LIST OF ABBREVIATIONS XIV

SUMMARY XV

CHAPTER 1: INTRODUCTION 1

Importance of Prognostics 1

Cost Association and Savings 1

Proposed Research's Contribution to Maintenance and Reliability Field 3

CHAPTER 2: BACKGROUND INFORMATION 4

The Presented Research's Relatedness and Importance 4

Previous Work at Other Institutions 5

Georgia Tech's Contributions 6

Digital Signal Processing 7

Rolling Element Bearings 8
Rolling Element Bearing Components 8
Lifetime of Rolling Element Bearings 11

CHAPTER 3: MATHEMATICS AND ENGINEERING THEORY 13

Manipulation of Paris Equation 14
Paris's Law 14

Paris-Erdogan Equation 15
Proposed Alteration to Paris Equation 16

Digital Signal Processing 18
Fast Fourier Transform 18
Power Spectrum 19
High Frequency Resonance Technique 21
Adaptive Line Enhancer 23

Frequencies of Failures 25

Least Squares Algorithm 26
Linear Least Squares Algorithm 27
Weighted Linear Least Squares Algorithm 27
Weighting Data Points Chronologically 28

CHAPTER 4: EXPERIMENTAL PROCEDURE 30

Equipment 31
Bearing Test Stand 31
Timken Bearing Description 32

Accelerometer 34
Acoustic Emissions Sensor 37
EDM Groove Initialization 38
Profilometer 40

Experiment Component Descriptions 41
Resonant Frequency 41
Determining System Constants 41
Experimental Design and Data Collection 45

CHAPTER 5: WORK DONE TO PREVIOUSLY ACQUIRED DATA 47

Paris Equation Constants 47

Filtering FFT and PSV description 48

Envelope Spectrum Analysis 50

Frequency Spectrum Analysis 51

Calculation of the Critical PSV 60

Other Signal Characteristics Analyzed 63

CHAPTER 6: SIMULATED DATA POINTS 65

Development of Simulated Data 65

Least Squares Algorithm 69

Validity of the Paris Equation with Respect to the Simulated Data 73

CHAPTER 7: EXPERIMENTALLY EXTRACTED DATA 76

Filling Out the Voids in Acquired Data 76

Applying a Least Squares Algorithm to Increasing Amount of Data 80

Closeness to Actual Failure Point 84

CHAPTER 8: CONCLUSION 91

Simplicity of the Presented Research 91

Drawbacks of Presented Research 92

Proposed Future Work 93

Contributions 93

APPENDIX A 95

Chronologically Weighted Least Squares Matlab Code 95

APPENDIX B 96

FFT and HFRT Code 96

APPENDIX C 98

Power Spectrum Value Extraction Code 98

APPENDIX D 99

Simulated Data Points Plots 99

APPENDIX E **102**

Naturally Propagating Figures **102**

APPENDIX F **106**

Naturally Propagating Data ΔC and ΔPSV **106**

REFERENCES **109**

LIST OF TABLES

Title **Page**

Table 1: Frequencies for Experiment Analyzed in this Thesis **33**

Table 2: Naturally Propagating Defect Pertinent Information **60**

Table 3: Difference Between Paris Estimation and Actual Cycles Remaining Using Weighted Least Squares Approximation with c=4 **85**

Table 4: Difference Between Paris Estimation and Actual Cycles Remaining Using Weighted Least Squares Approximation with c=8 **86**

Table 5: Difference Between Paris Estimation and Actual Cycles Remaining Using Standard Least Squares Approximation **86**

Table 6: Comparison of Differences between Actual and Estimated Remaining Cycles for Three Least Squares Algorithms **87**

LIST OF FIGURES

Title **Page**

Figure 1: Component Parts of (a) deep-groove ball bearing (b) ball thrust bearing (c) angular contact ball bearing (d) tapered roller bearing (Williams, 2000) **10**

Figure 2: Illustration of Paris Equation (Key to Metals Task Force, 2005) **15**

Figure 3: Illustration of Modified Paris Equation **17**

Figure 4: Raw Data **20**

Figure 5: Fast Fourier Transform of Same Raw Data Set **20**

Figure 6: Envelope Spectrum of Same Data Set **22**

Figure 7: Envelope Spectrum using ALE for Same Data Set **23**

Figure 8: Block Diagram of ALE (Li, 1999) **24**

Figure 9: Tapered Roller Bearing (Li, 1999) **26**

Figure 10: Bearing Test Housing **31**

Figure 11: Photograph of Timken tapered roller bearing (Billington) **33**

Figure 12: Basic Piezoelectric Accelerometer Design (sensorland, 2005) **34**

Figure 13: Kistler 8792A50 Tri-axial K-Shear Accelerometer [Billington, 1997] **36**

Figure 14: Wilcoxand 736T High Frequency Accelerometer [Billington, 1997] **36**

Figure 15: Sensitivity of Acoustic Emission Sensor with Respect to Frequency [Billington, 1997] **38**

Figure 16: Electrical Discharge Machine [Billington, 1997] **39**

Figure 17: Hommelwerke Profilometer [Billington, 1997] **40**

Figure 18: Stochastic Crack Growth Propagation **42**

Figure 19: Comparison of Material Constant P_o to defect propagation **44**

Figure 20: Comparison of Material Constant m to defect propagation **45**

Figure 21: Schematic of Data Acquisition from Propagating Defect **46**

Figure 22: Raw Data **49**

Figure 23: Respective Power Spectrum **49**

Figure 24: Envelope of Data Indicating Failure is Located Around 220 Hz **50**

Figure 25: September 24 Frequency Spectrum **52**

Figure 26: October 21 Frequency Spectrum **53**

Figure 27: November 14 Frequency Spectrum **54**

Figure 28: November 16 Frequency Spectrum **55**

Figure 29: November 20 Frequency Spectrum **56**

Figure 30: November 22 Frequency Spectrum **57**

Figure 31: November 25 Frequency Spectrum **58**

Figure 32: December 17 Frequency Spectrum **59**

Figure 33: Defect PSV versus Area **61**

Figure 34: Power Spectrum Value as a Function of Cycles **62**

Figure 35: Comparison of Signal Characteristics **63**

Figure 36: Simulated Data—Linear Equidistant Points **66**

Figure 37: Simulated Data—Gaussian White Noise Applied **67**

Figure 38: Simulated Data—Random Points Selected from Previous Plot **68**

Figure 39: Simulated Data Set 1—Weighted Least Squares Algorithm **69**

Figure 40: Simulated Data Set 2—Weighted Least Squares Algorithm **70**

Figure 41: Simulated Data Set 3—Weighted Least Squares Algorithm **71**

Figure 42: Simulated Data Set 4—Weighted Least Squares Algorithm **72**

Figure 43: Plot of Simulated Data as Compared to Modified Paris Equation **73**

Figure 44: Percent Difference between Estimated Cycles of Simulated and Theoretical Data **74**

Figure 45: Cycle Difference between Theoretical and Simulated Points **75**

Figure 46: Plot of PSV as a Function of Cycles **77**

Figure 47: Equidistant Points Filling Out Experimental Data **78**

Figure 48: Application of Gaussian White Noise to Equidistant Points **79**

Figure 49: Random Selection of Equidistant PSV Points Obtained from Naturally Propagating Defect **80**

Figure 50: Propagating Experimental Data up to 8.1 Million Cycles and its Respective LS Fit **81**

Figure 51: Propagating Experimental Data up to12.8 Million Cycles and its Respective LS Fit **82**

Figure 52: Propagating Experimental Data up to 18 Million Cycles and its Respective LS Fit **83**

Figure 53: Propagating Experimental Data up to 20.7 Million Cycles and its Respective LS Fit 84

Figure 54: Estimation of Cycles to Failure for Modified Paris Equation 88

Figure 55: Percent Difference between Estimated Cycles of Experimental and Theoretical Data 89

Figure 56: Cycle Difference between Theoretical and Experimentally Extracted Points 90

LIST OF SYMBOLS

α	contact angle
ΔK	stress intensity factor
ΔT	cycles
ω	weight
ξ	colorness parameter
a	defect width
c	weighting constant
C_o	material constant for original Paris Equation
D	average roller diameter
D	defect area
d_m	pitch diameter
E	energy or power spectrum value
f_{cage}	frequency of cage
f_{bpir}	frequency of ball pass inner race
f_{bpor}	frequency of ball pass outer race
f_r	frequency of rolling elements
m	data point of interest
m	material constant for modified Paris Equations
N	number of cycles
N_i	frequency
n	number of data points collected
n	material constant for original Paris Equation
P_o	material constant for modified Paris Equations

Z	number of rolling elements
$Z(t)$	stochastic variable

LIST OF ABBREVIATIONS

ASTM	American Society for Testing and Materials
DSP	Digital Signal Processing
DFT	Discrete Fourier Transform
EI	Energy Index
FFT	Fast Fourier Transform
HFRT	High Frequency Resonance Technique
LSA	Least Squares Algorithm
PS	Power Spectrum
PSV	Power Spectrum Value

SUMMARY

Rolling element bearing failure can cause problems for industries ranging from mild inconveniences such as simple replacement to catastrophic damage such as large production-line equipment failure. Rolling element bearing failure has plagued industries for many years. Bearings are currently monitored to determine whether or not there is a defect in the bearing, but the remaining lifetime of the bearing remains unknown. This research estimates the bearing's remaining lifetime through digital signal processing in conjunction with a modified version of Paris's equation—a fatigue-failure equation well known in rotating machinery prognostics.

An energy quantity, coined the Power Spectrum Value (PSV), is the maximum amplitude of the frequencies within a relatively small band around the resonant frequency of the system. The current PSV is estimated and updated using a chronologically weighted least squares algorithm. It is this PSV which is implemented in the modified Paris equation to determine the remaining lifetime of the bearing. This research presents a non-intrusive method of determining the lifetime of the bearing so that the bearing's utility is maximized and reactive maintenance procedures are minimized.

CHAPTER 1

INTRODUCTION

Importance of Prognostics

Understanding how equipment works and determining how it will fail prove to be important concepts in industry. Knowing when equipment approaches the failure point is another important aspect of maintaining equipment. Methods such as vibration monitoring indicate the stage of defects in components, and enable workers to change them as needed. The concept of fixing or replacing equipment just prior to it reaching failure is known as condition-based maintenance.

Condition-based monitoring utilizes technology to determine the condition of machinery. Thermography, acoustic monitoring, tribological testing, and digital signal processing are methods used to monitor problems in a system. Once these methods indicate a possible threat, replacement or adjusting of the machinery is scheduled for the near-future. Conditon-based monitoring is much different from time-based maintenance in that the useful life of the component is maximized; the part is only removed when it is near failure. The fault should be detected early enough so that replacement procedures can take place before the component fails and at a time that is convenient for the production lines.

Cost Association and Savings

Manufacturing plants heavily consist of rotating machinery such as gearboxes, bearings, motors and fans. Common problems associated with these components are cyclic fatigue, improper lubrication, and dirt and debris damage. Sometimes the failure of these components is relatively harmless. Those failure types could cause production

downtimes and also result in other machinery failing. There is a cost associated with the machinery replacement and the cost of products not being manufactured.

There is a large cost savings associated with maintenance and reliability. As far as general maintenance and reliability is concerned, money is saved through a reduction of replacement part purchases, possible air leaks resulting in a pressure loss, equipment loss due to excessive heat and temperature problems. There are some costs incurred from the lack of a good maintenance and reliability program which cannot be measured monetarily. If employees are continuously reactive to the environment in which they work, it lowers morale to be fixing the same machine or system. This, in turn, lowers productivity.

As far as bearings are concerned, there are four primary cost concerns: the bearings themselves, other connected machinery, labor costs, and downtime of the system. Bearings are not considered expensive components when compared to the entire system which the bearing supports. Therefore, it is important to recognize both the cost of the bearing as well as all components it affects. If a bearing does reach the failure point while it is in the system, the vibration related to the bearing can cause failure to other, more costly components such as motors, shafts, pumps, etc. If these parts break down, then it takes time to replace the broken components. This also requires paying more for labor. If the worker had just monitored the bearing, the only time associated with the system would be the bearing replacement. If the bearing does affect larger, more complicated parts, they must be either fixed or replaced. One of the more expensive costs incurred by the failure of a bearing is the production downtime. While the system is down, nothing is being manufactured or produced. If nothing is being produced, the company cannot make money.

It is possible that the complete product can be deemed useless if it is not monitored correctly. This is the case with satellites whose bearings no longer are effective or have destroyed other components.

There are also some instances where prognostics could save lives. Thermography can detect the amount of heat being generated by an electrical box. If an ill-connected wire were to catch fire, it could be catastrophic and fatal. If gearboxes or bearings fail in a helicopter or another transport vehicle, lives are directly endangered.

Proposed Research's Contribution to Maintenance and Reliability Field

The work presented in this thesis involves the condition-based monitoring technique of digital signal processing. Rotating machinery has a distinct time signature due to its rotating speed, size, and type found when an accelerometer is connected to the system. The vibration signature is a strong indicator of wear and fatigue [Cembel, 1995]. If a flaw begins to emerge, the Power Spectrum Value (PSV) gathered from the accelerometer data increases. This thesis describes the relationship between this PSV and the time remaining until the rotating piece of machinery is considered to have failed through manipulation of the Paris Equation.

CHAPTER 2

BACKGROUND INFORMATION

In order to determine whether or not research is a new concept, useful in industry, or can relate to other work, a background search must be completed. Much research has been focused on rotating equipment for dozens of years. Some research focuses on loading and manufacturing concerns, others look into tolerances and precision, and still more delve into preservation of the quality of the rotating equipment. It takes all three of these concepts, as well as several other, smaller factors, to meet the demands of today's manufacturing environment.

The Presented Research's Relatedness and Importance

Work developed in this thesis builds on knowledge acquired previously from engineers at Georgia Institute of Technology and from universities across the world. Some of the most notable work describes the manipulation of the Paris Equation, the monitoring of a signal's energy, and the correlation of the peak amplitude to the defect width. Combining this background information results in a simple, but effective, means of predicting a bearing's remaining life.

Much of the previous research performed on rotating machinery involves defects which have been artificially inscribed that are then analyzed. Defects described in this thesis were initiated by an EDM machine, and then the spall propagation was monitored. The information gathered as the defect propagates requires the system to be shut down in order for the bearing condition to be analyzed. A method needs to be developed to

accurately monitor a naturally propagating defect without losing the valuable time and money due to a work-stoppage; this is one of the purposes of this research.

The work presented in this thesis describes a method in which one can estimate the remaining cycle time of a bearing with a defect through digital signal processing and manipulation of the Paris-Erdogan equation. It builds upon and combines prior research and requires little *a priori* information of the system. All of the data analyzed in this thesis comes from the information gathered from naturally propagating defects.

Previous Work at Other Institutions

Modeling the crack propagation time proves to be an ongoing quest in bearing prognostics. Lin and Yang [1983] sought to develop closed form solutions for the statistical moments of the time it takes a crack to propagate to any specified width for rotating machinery. The research began by looking at the Paris Equation which has been used extensively in rotating machinery prognostics. A Markov random process was applied to the Paris equation in order to approximate the crack sizes. A more thorough description of Markov processes can be found in the Davis text [1993]. Once the crack size is treated as a diffusive Markov process, the energy can be replaced by a constant mean plus a Gaussian white noise. This information is useful in that it shows that a recursive relationship can be developed given certain system characteristics when a power law governs the crack propagation rate.

Al-Balushi and Samanta [2002] have also previously monitored and diagnosed machine conditions through monitoring the signal energy. Their analysis was based on a relative energy value coined to be the energy index, EI. The EI was used for acoustic emission signals gathered from gearbox failure. The extensive work completed by Al-

Balushi and Samanta show that the energy can indicate a rotating component's failure. This is useful information for the proposed research, because it involves monitoring of the signal's energy and compares it to the defect size. One notable difference between Al-Balushi and Samanta and the research presented in this thesis is that they utilized acoustic emission sensors instead of accelerometers.

An advantage of acoustic emission sensors is that they are more sensitive to higher frequencies associated with friction, wear, and impacts for gearboxes. One notable disadvantage of acoustic emission sensors as opposed to accelerometers is that the acoustic emission sensors require a high sampling rate due to the high frequency rate of the sensor itself [Al-Balushi, and Samanta, 2002].

Georgia Tech's Contributions

For almost a decade now, researchers at Georgia Institute of Technology have been interested in monitoring bearing conditions, failure modes, and prognostics. There has been focus on system features such as RMS, kurtosis, peak amplitude, and crest factor determined through accelerometer and acoustic emission data digital signal processing.

Shiroishi et al. [1997] first concentrated on determining the quantitative level of bearing defects with a strong focus on signal to noise ratio. It was determined that the peak amplitude value increases with increasing crack width on both the cone and the cup components of a rolling element bearing. His research also indicates that from the characteristics determined from digital signal processing, the peak ratio is the most

correlated characteristic to the defect size. Once the peak ratio indicates a failure is present in a bearing, the peak value can give a direct indication of the defect width.

A bearing's lifetime can also be predicted through monitoring the changes in the dynamic stiffness of the system through vibration analysis and digital signal processing. Furthermore, other methods of determining the lifetime of a bearing are the damage curve approach and the double linear damage approach. It was also confirmed that the crack propagation and spalling of a bearing is short compared to the crack initiation phase [Qiu et al., 2002].

A visiting scholar working at the Georgia Institute of Technology, Cheng Zhang [Zhang et al., 2000], showed there is a connection between the energy of a bearing and the defect size when a roller strikes a defect on a bearing's outer race. He developed a rigid body impact dynamic model in order to determine the defect severity under different system conditions. In addition to these contributions, he also shows that an accelerated life test model closely estimates the life expectancy of a bearing in corrosive environments.

Digital Signal Processing

Digital Signal Processing (DSP) pertains to analysis and processing of data that is acquired in the digital form. This field of study came into existence as far back as the seventeenth century from Sir Isaac Newton's work; over the last 60 years, it has been prevailing as a useful means of manipulating information due to the increased processor speeds and data storage capabilities.

A time signal is a sequence of real numbers that are sampled in uniform increments of time. The discrete-time system transforms input signals from machinery into digital output signals. The digital output signals are a combination of signals emitted by each component of the rotating apparatus. The measured signal can be decomposed into the component functions which can then be analyzed individually by using Fourier Transforms [Roberts and Mullis, 1987].

The mathematics, theory, and application of digital signal processing in this research will be further explained in Chapters 3 and 5.

Rolling Element Bearings

The purpose of a rolling element bearing is to allow radial motion between two loaded components while maintaining a small distance between them. Rolling element bearings can hold radial loads, thrust loads, or a combination of both. The most frequently used rolling element bearing is a deep groove ball bearing. This type of bearing is designed to carry a radial load, but it can also withstand a heavy thrust load if applied. The bearings whose energy is monitored in this thesis are tapered roller element bearings.

Rolling Element Bearing Components

The rolling element bearing consists of four components: the inner race, outer race, cage, and rolling elements. Figure 1 indicates the different parts of a rolling element bearing as well as the different types of rolling element bearings.

The outer race of the bearing is the ring which is the furthest from the center of the bearing. It is usually the stationary race which is mounted to the machine casing or bearing pedestal. The inner race, which is concentric with the outer race, is the inner-most ring of the bearing. The inner race rotates along with the center shaft and shares the same center as the outer race. The cage is the component that maintains the distance between the rolling elements, and the rolling elements are the balls, cylinders, or spheres.

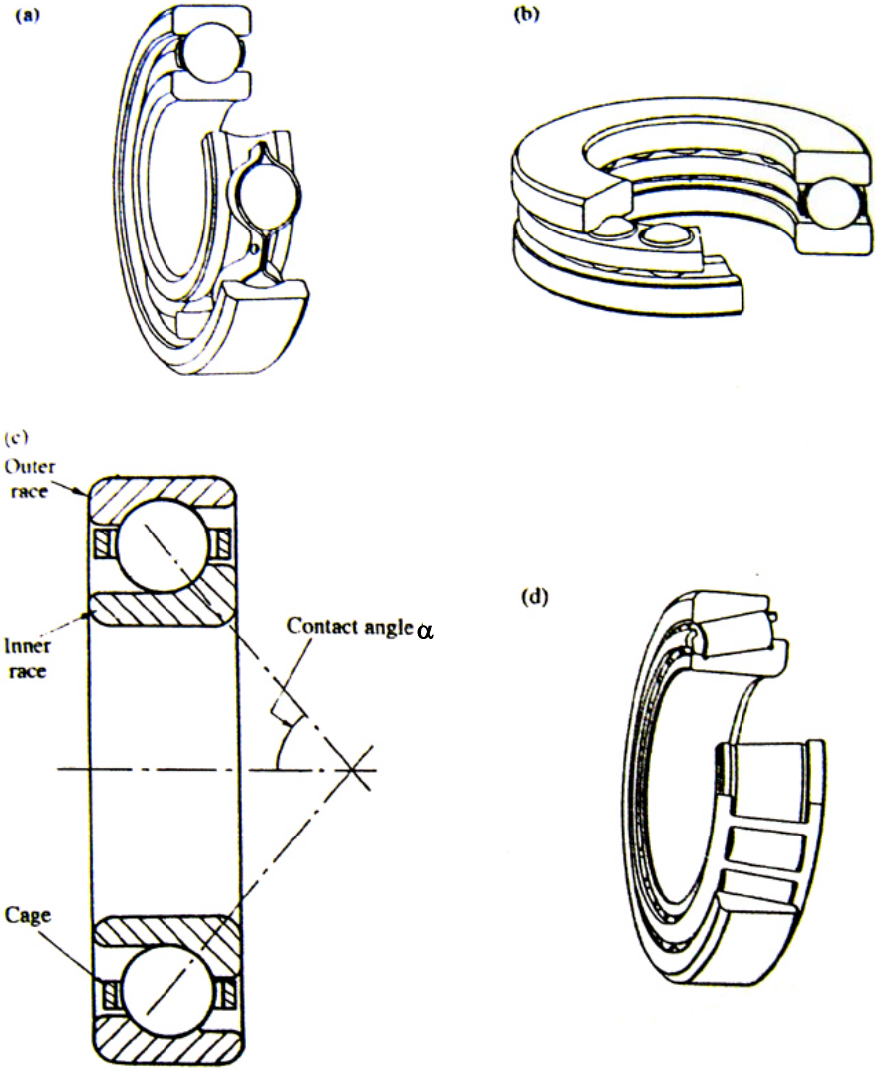

Figure 1: Component Parts of (a) deep-groove ball bearing (b) ball thrust bearing (c) angular contact ball bearing (d) tapered roller bearing (Williams, 2000)

The thrust bearing shown in Figure 1 (b) is unable to carry any sort of radial load. Since inertia effects from the rotating inner race results in a radial load component, they are usually paired with radial bearings. The angular contact bearing which is shown in Figure 1 (c) is designed to withstand both radial and thrust loads. The amount of the

sustainable thrust load is dependent on the contact angle, α. As the angle increases, the bearing tends to act more as a thrust bearing.

The tapered rolling element bearings shown in Figure 1 (d) are used when the load-carrying capacity is greater than that which a spherical element is able to carry (Figure 1 (a)). The cylindrical bearings cost more than the spheres, but they have a greater fatigue life, and they are stiffer than the spherical elements. The cylindrical bearings are often tapered in order to increase the bearing's ability to withstand both radial and thrust loads at high rotating speeds. The qualities of the tapered rolling element bearing result in utilization of them in important applications such as automobile wheels and transmissions [Williams, 2000]. Due to the benefits of the tapered rolling element bearing and the important applications, this type of bearing is used in all experiments on the bearing test stand at Georgia Tech.

Lifetime of Rolling Element Bearings

Lubrication is essential to the performance and lifetime of a rolling element bearing. However, even with proper lubrication, bearings will eventually fail. Failure can be caused by cyclic fatigue resulting in spalls which usually appear on the bearing's races. A spall is simply a crack in a bearing which is caused by cyclic fatigue and crack propagation due to inclusions within the metal. Debris can also find its way into the bearing; this results in pits on the rolling elements.

If the bearing fails due to cyclic fatigue, it is caused by an inclusion or a defect in the material which propagates to the surface after the rolling elements pass over the defect with every turn of the shaft. This spall is the criterion determining the

instantaneous quality of the bearing. Since the locations and sizes of the inclusions or defects in materials as well as the metal's resistance to fatigue propagation, the time it takes for a bearing to fail varies tremendously. For this reason, when specifying a bearing for a particular application, the lifetime of the bearing must be treated statistically. This is also why it is especially difficult to determine the remaining lifetime of any given rolling element bearing [Williams, 2000].

CHAPTER 3
MATHEMATICS AND ENGINEERING THEORY

As common with engineering research, most of the work presented in this thesis is based off the combination of mathematics and engineering theory. The remaining portion of the research comes from practical knowledge, bearing guidelines, and industrial standards.

In regards to mathematics, the most important equation considered for implementation in the research is the Paris Equation. The Paris Equation is the primary focus of this research, and the manipulation of this equation that aids in the estimation of the remaining lifetime of a bearing.

Another useful mathematical concept pertaining to the data collected is the Fast Fourier Transform. Without the digital signal processing equations and theory, it would be impossible to decompose the signals generated by a rotating piece of machinery.

A third contributing factor, a chronologically weighted least squares algorithm, comes from both mathematics and standard engineering methods in numerical methods. Calculating the approximate value of the instantaneous energy can be done in several ways. The method used in this research is a modification of the weighted linear least squares algorithm in which greater weights are applied to the most recently collected data points. The amount of weight placed on the points is dependent on the person implementing the code.

Manipulation of Paris Equation

The work presented in this thesis is a continuation and an adaptation of the work previously completed by Georgia Tech researchers. The concept began after reviewing Yawei Li's research involving the Paris-Erdogan Equation.

Paris's Law

The aircraft industry was the first to really push for a means of predicting fatigue crack propagation. P.C. Paris then began researching crack propagation, and derived and equation known today as the Paris Equation. The Paris Equation is a correlation of system constants (C_o and n), defect width (a), and change in stress intensity (ΔK) with the number of remaining cycles of a piece of rotating machinery. The Paris Equation is defined in Equation (1).

$$\frac{da}{dN} = C_o(\Delta K)^n \tag{1}$$

Figure 2 illustrates the monitoring of the fatigue-crack length as a function of number of cycles as done in the Paris Equation. It is important to note the relatively long time it takes for the crack to start propagating and then the rapid propagation after more cycles have passed.

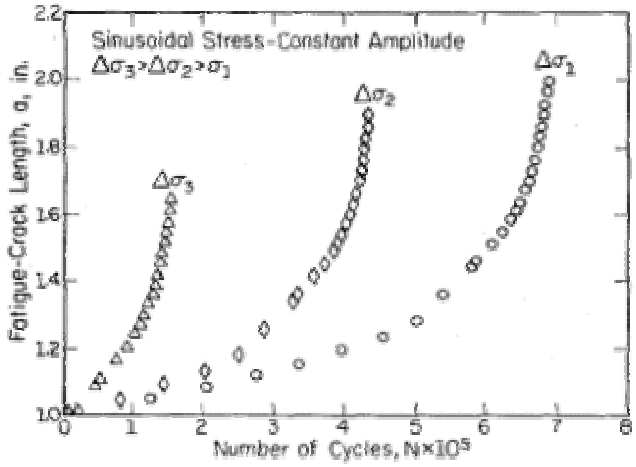

Figure 2: Illustration of Paris Equation (Key to Metals Task Force, 2005)

Paris-Erdogan Equation

After many years of implementing the original Paris Equation, Paris began working with Erdogan to modify the first equation in order to relate the defect area with the number of remaining cycles; this equation is known as the Paris-Erdogan Equation and is given as Equation (2). In the Paris-Erdogan Equation, D represents the defect area. P_o and m are characteristics defined by the system and can be determined by tests previously designed and developed by the American Standard for Testing and Materials (ASTM) "Standard Test Method for Measurement of Fatigue Crack Growth Rates". The full description of the loading tests for the Georgia Tech System is described in Chapter 4.

$$\frac{dD}{dt} = P_o D^m \tag{2}$$

Proposed Alteration to Paris Equation

The use of the Paris-Erdogan equation in Li's work shows that the bearing defect area is a direct indication of time to failure. The drawback to this research is that the system would have to be shut down and the defect measured by a profilometer every time the updated time to failure is desired. The primary proposal of this thesis is to convert the Paris-Erdogan equation from a function that requires stopping the system into a form that can estimate the time to failure without interrupting the process flow. The conversion of the Paris-Erdogan equation from monitoring defect area to defect energy is possible due to the correlation shown by Zhang et al. [2000]. Equation (3) proposes this modified version of the Paris Equation; the presented research focuses on proving the relevancy of this modification.

$$\frac{d(PSV)}{dt} = P_0(PSV)^m \tag{3}$$

The constants used for Equation (2) are the same values found in Equation (3). This is true due to the combination of two factors: Zhang previously showed that the defect size is directly correlated to the energy of a bearing, and the variables on the left-hand side of the equation are a function of the same variable on the right-hand side for both equations. Since there are no unit conversions needed when switching between the two equations, the values for P_o and m remain the same.

The graphical counterpart for Equation (3) is shown in Figure 3. From Figure 3, one can see the rapid decrease in the remaining number of cycles as the power spectrum value approaches the critical power spectrum value for the P_o and m which define the bearing test stand at Georgia Tech.

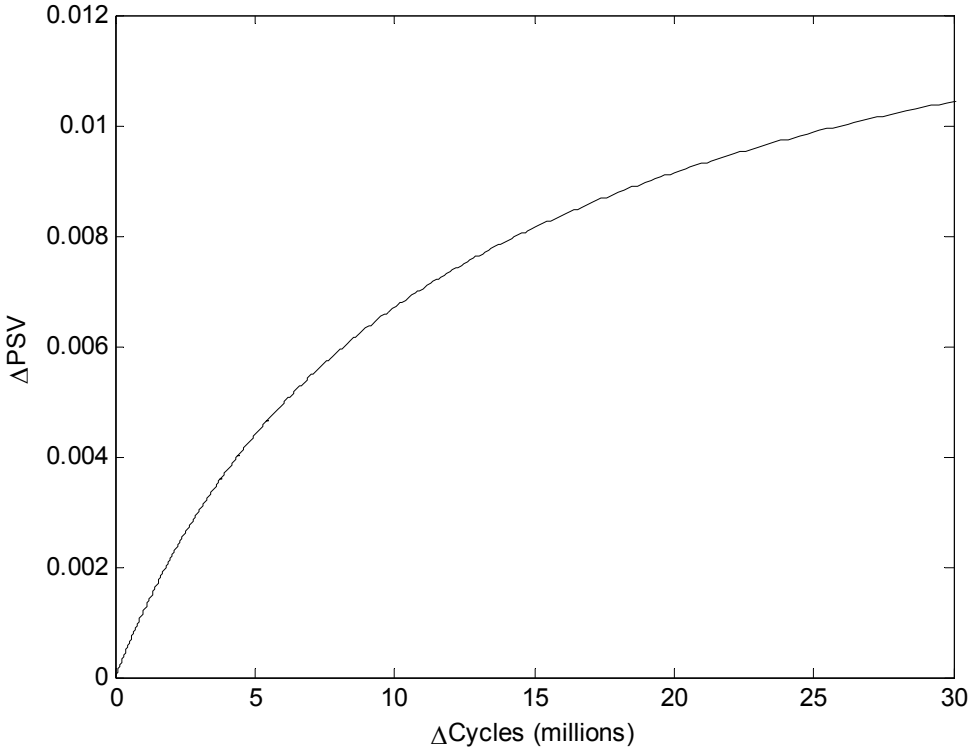

Figure 3: Illustration of Modified Paris Equation

This figure also implies that once a defect is initially detected, there is a relatively long time for it to begin propagation. This concurs with the information Qiu et al. presented [2002]. In proceeding chapters there are comparisons between this theoretical Modified Paris Equation plot to simulated data as well as experimental data. These comparisons identify the theoretical and actual relationships as well as the validity of the proposed research.

Digital Signal Processing

Fast Fourier Transform

The Fast Fourier Transform, FFT, has been in existence since the early nineteenth century, but it was not widely accepted until approximately 40 years ago. Gauss is credited as being the first mathematician to discover the transform, and several mathematicians have since then built upon his initial work. Since the calculations of the discrete transform consumed much time when done by hand, it was not until the 1960's when J. W. Cooley and J.W. Tukey outlined an algorithm that calculated the FFT quickly via computer.

The theory behind the FFT is that it decomposes a Discrete Fourier Transform, DFT, into successively smaller DFT's which are simpler to analyze [Chapra and Canale, 1998].

A signal that is discrete in frequency and discrete in time can be analyzed using the Discrete Fourier Transform (DFT). If the collected signal, $f(k)$, has a finite signal energy, then it is defined as Equation (4). If equation (4) is calculatable, then the Fast Fourier Transform (FFT) can be applied to the data. The FFT is an algorithm devised to analyze a signal needed to undergo a DFT in few computations. A standard DFT analysis requires N^2 applications, and the FFT Equation (5) is completed in $Nlog_2N$ operations.

$$Energy = \sum_{k=0}^{N-1} \left| f(k) \right|^2 \tag{4}$$

$$F(n) = \sum_{k=0}^{N-1} f(k) e^{(j2\pi/N)-kn} \tag{5}$$

Since each calculation takes time and memory, it is desirable to use algorithms that minimize the "cost" associated with the Discrete Fourier Transform [Chapra and Canale, 1998].

In addition to the faster computation time linked with the FFT, it can be applicable to approximating other transforms, fast convolution, and filter design. It is also the only Fourier transform that is capable of being parameterized [Roberts and Mullis, 1987].

Power Spectrum

In general, the Power Spectrum (PS) is developed from the power output of electrical systems. The power spectrum is the square of the absolute value of the components of the Fast Fourier Transform as shown in Equation (5) [Goldman, 1999].

$$Power(n) = \left|F(n)\right|^2 \tag{6}$$

According to Parseval's energy theorem, the energy of the time domain signal is equal to the energy in the frequency domain. Therefore, all of the energy shown in the time domain is also in the frequency domain, but it is in a more usable form [Kay and Marple, 1981]. The power spectrum is simply a measure of how much power or energy a signal has at a particular frequency [Simmons, 1996]. As a side note, the values along the y-axis will be referred to as the power spectrum values.

Figure 4 shows a sample of raw data, and Figure 5 illustrates the result after the data are converted to the power spectrum.

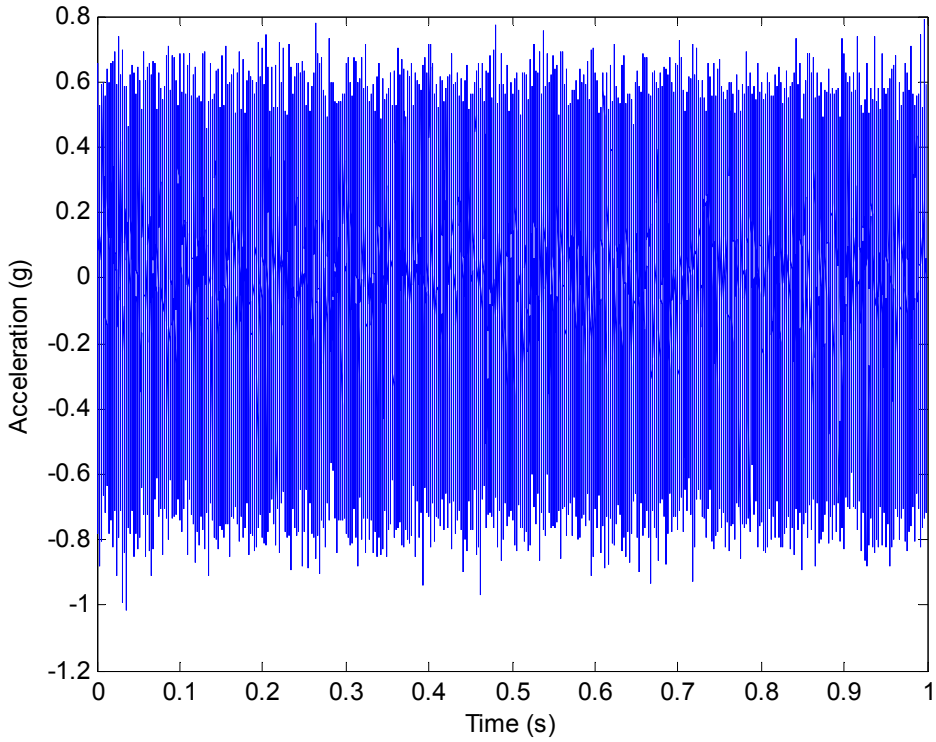

Figure 4: Raw Data

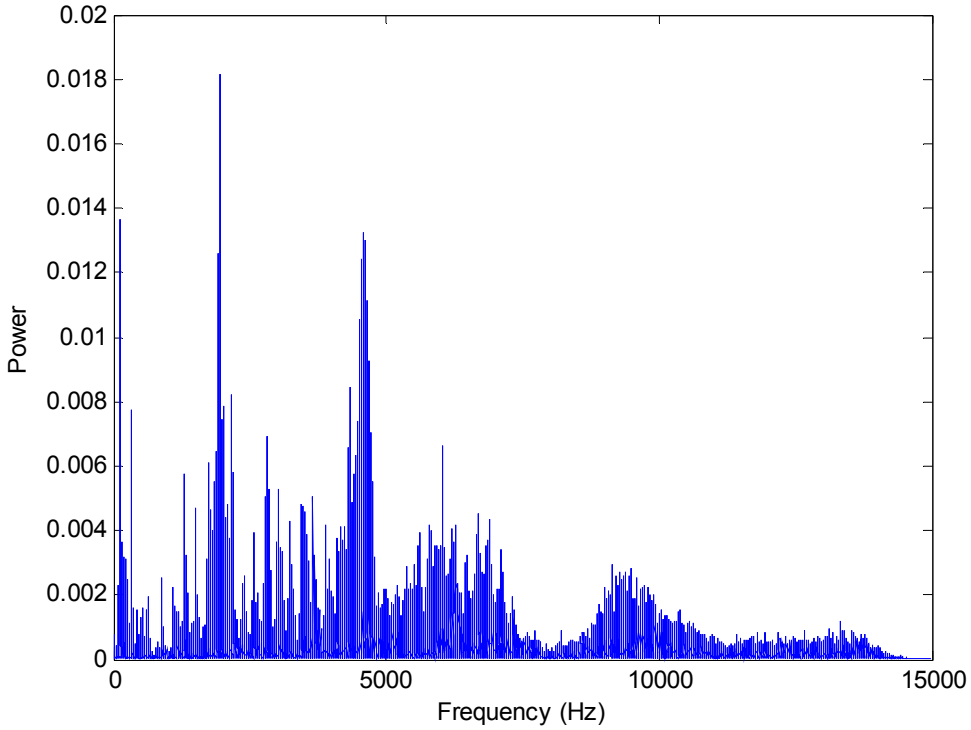

Figure 5: Fast Fourier Transform of Same Raw Data Set

High Frequency Resonance Technique

When analyzing a bearing's condition, it is not only important to understand how damaged the bearing is, but also where the damage has taken place. As mentioned in Chapter 2, for rolling element bearings, there are four main components which can become damaged: outer race, inner race, rolling elements, and cage. These components each have their own distinct frequency shown in Chapter 4.

The method of enveloping effectively eliminates the high frequency components of the signal gathered by the accelerometer and creates a dominant peak where the highest impact repetition frequency lies in the frequency spectrum. A signal is first obtained from the rotating machinery. The next three steps of signal processing follow the HFRT method. A band pass filter is placed on the signal at a high frequency band so as to remove the frequencies around a chosen high resonant frequency of a system. The bandpassed signal is then demodulated by a non-linear rectifier. Since bearing defects are usually associated with low frequency signals, a low pass filter is placed on the demodulated signal. At this point, the signal is resampled at a low rate. The frequency spectrum is then analyzed for indication of bearing failure.

Equation (7) defines the Enveloping method, and Figure 6 illustrates this concept.

$$Env(x_i) = \frac{1}{N} = \sqrt{\sum_{j=(i-N)}^{i} x_j^2} \tag{7}$$

In Equation (7), N is the number of points, and x is the value of the signal.

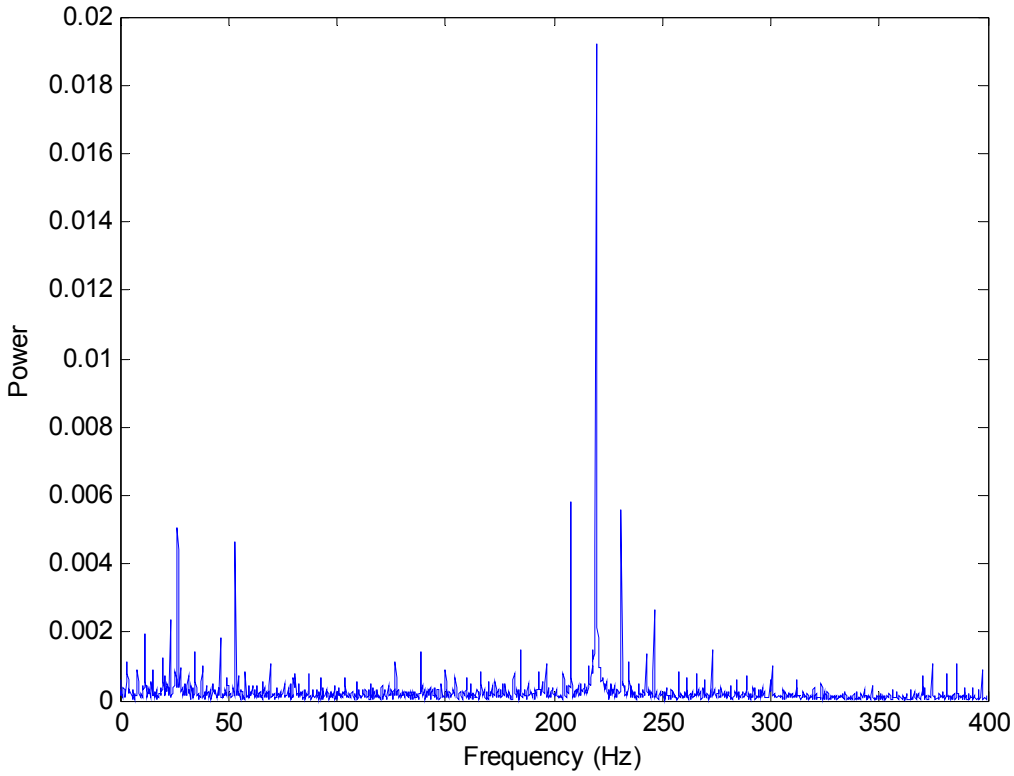

Figure 6: Envelope Spectrum of Same Data Set

There is another method of filtering the data to find the highest impact frequency, and it is called the Envelope Method. The Enveloping Method is typically used in the frequency domain, but it can be useful in the time domain as well. The primary difference between the two is that the envelope spectrum takes a moving average of within the time domain. The two methods have virtually the same results and are conceptually the same, so the High Frequency Resonant Technique is the one used for the purpose of this research [Shiroishi, 1996]. The next step in DSP is utilizing an adaptive line enhancer which allows the narrow band signals to be separated from the broadband noise. These signals can then be analyzed to determine the level of bearing crack propagation.

Adaptive Line Enhancer

The envelope signal is basically a combination of all the narrow band signals which are spaced with the harmonics of the defect frequencies as well as some broad-band noise. Looking at Figure 6, the information appears somewhat noisy, but the most important peak is still intelligible. With a few simple steps, known as the Adaptive Line Enhancer (ALE) algorithm, the envelope spectrum plot can be "cleaned" up.

ALE reduces the noise components in the signals by separating narrow band signals from the broad band noise. If Figure 7 is compared with Figure 6, then the noise reduction due to the ALE is obvious. It is important to note that the largest peak still falls at the same frequency as before ALE was applied.

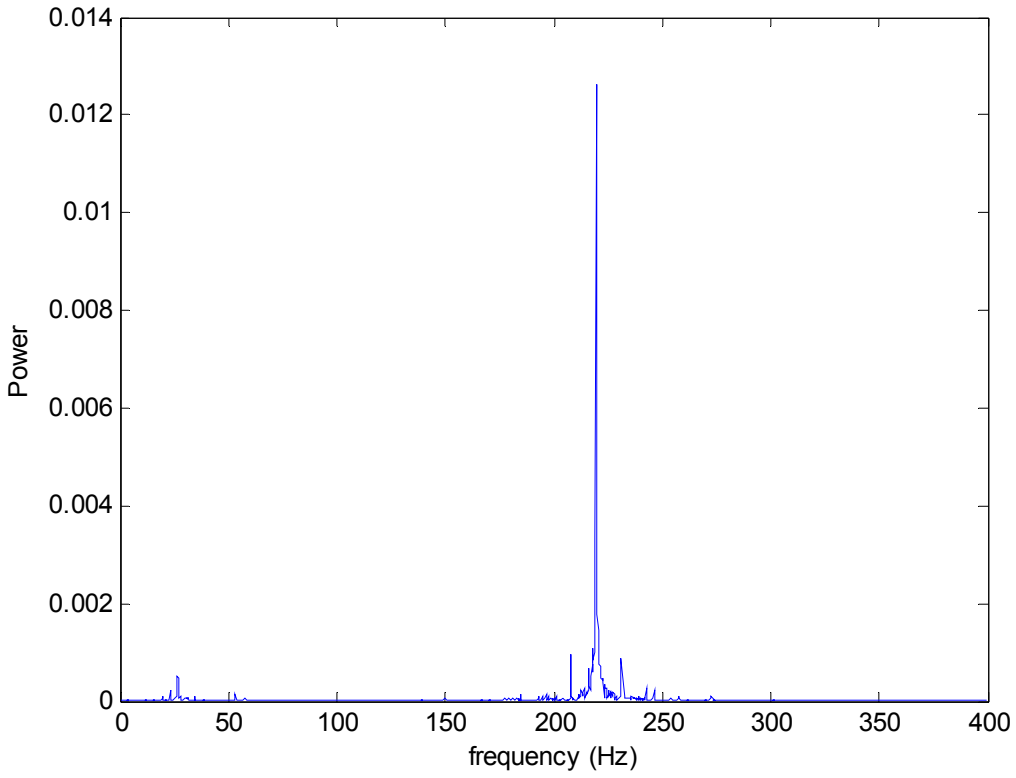

Figure 7: Envelope Spectrum using ALE for Same Data Set

The next step is to describe how the narrow band signal is separated from the noise. Figure 8 illustrates the controls used to manipulate the signal from the envelope signal.

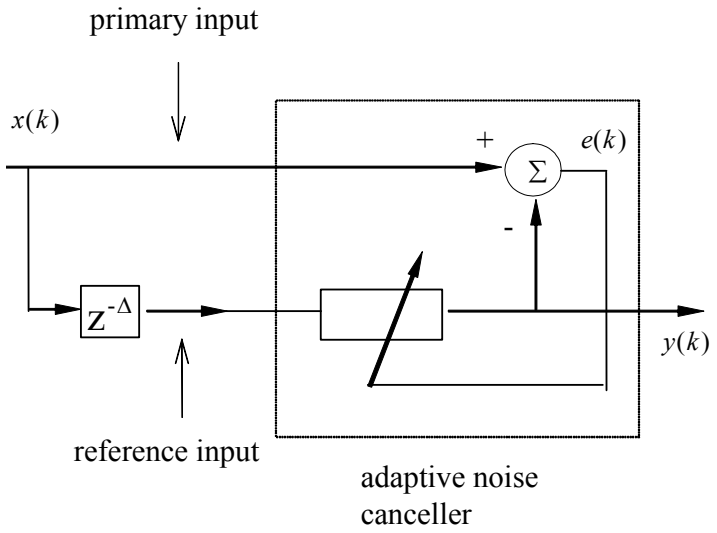

Figure 8: Block Diagram of ALE (Li, 1999)

The signal is input twice, and the delay is monitored. If the signal paths are well correlated, then it is a narrow band signal. If the signal paths do not follow a trend, then they can be considered white noise. The adaptive noise canceller is a filter which is able to compensate for the offset and correlated narrow-band signals. Since the broad-band signals cannot be compensated, they are dismissed. Only the narrow-band signals are able to be output from the system. This output is what was shown in Figure 7.

Frequencies of Failures

Since the primary purpose of taking the envelope spectrum and applying the adaptive line enhancer on a set of data are to determine the location of a failure, it is important to know the frequencies of the components which could fail.

Each rolling element bearing is comprised of four components: outer race, inner race, the rolling elements and the cage. Each part emits a signal at its unique frequency which contributes to the final signal acquired by the accelerometer. These frequencies are listed in Equations (8)-(11) [Harris 1991].

$$f_{bpor} = Z\frac{N_i}{2}\left(1-\frac{D}{d_m}\cos\alpha\right) \tag{8}$$

$$f_{bpir} = Z\frac{N_i}{2}\left(1+\frac{D}{d_m}\cos\alpha\right) \tag{9}$$

$$f_r = \frac{N_i d_m}{2D}\left[1-\left(\frac{D}{d_m}\cos\alpha\right)^2\right] \tag{10}$$

$$f_{cage} = \frac{N_i}{2}\left(1-\frac{D}{d_m}\cos\alpha\right) \tag{11}$$

Figure 9 indicates the dimensions needed to analyze Equations (8)-(11) on the Timken bearings analyzed in this research.

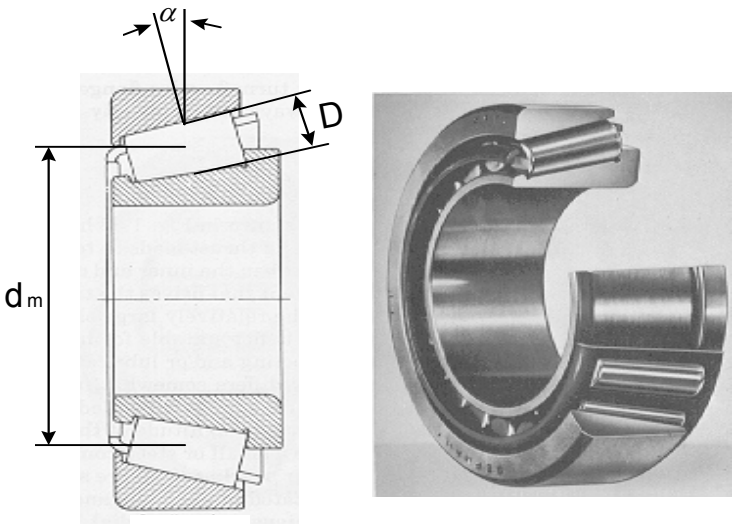

Figure 9: Tapered Roller Bearing (Li, 1999)

In this figure, α is the taper angle, D represents the average roller diameter, and d_m is the pitch diameter [Li, 1999].

Least Squares Algorithm

It is understood and proven that crack propagation is linear with respect to time. Sometimes, however, the collected data deviates from the trend line. When acquiring accelerometer data from a rotating piece of machinery, there is some variance due to the stochastic nature of the system, environmental conditions, and inconsistent placement. In order to get a better estimate of the most probable power spectrum value, a least squares algorithm is applied to the data. Since the most important bearing information is that which is most recent, a weighting system is applied to the data points. The earliest points carry the least amount of weight, and the latter points carry the most.

Linear Least Squares Algorithm

The least squares algorithm (LSA) was introduced by Gauss and Legendre in the late 1700's to early 1800's. There are several advantages of linear least squares such as it uses data efficiently. The LSA also models many science and engineering processes well. Once a LSA is applied to data, it is easily interpreted and results in clear answers. The downside to the LSA is that extrapolation of the data can be poor, and it has a strong sensitivity to outlying data points. The sensitivity to the outlying points can also result in skewed results. Equation (12) shows the basic linear least squares algorithm.

$$f\left(\vec{x};\vec{\beta}\right)=\beta_0+\beta_1 x_1+\beta_2 x_2+\ldots \tag{12}$$

Weighted Linear Least Squares Algorithm

The basic linear least squares algorithm places an equal emphasis on all points no matter the importance to the experiment. Since this is not always the optimal method of fitting a linear trend to the data, there is a method which weights the points depending upon the standard deviation of the point to the other data points. This method is optimal if there are few points, and some of those points hold greater importance than others. Equation (13) represents the weighted least squares algorithm, and Equation (14) defines the weights implemented in Equation(13) .

$$Q=\sum_{i=1}^{n}\omega_i\left[y_i-f\left(\vec{x}_i;\hat{\vec{\beta}}\right)\right]^2 \tag{13}$$

$$\omega_{ij} = \frac{1}{\left[\frac{\sum_{j=1}^{n}\left(y_{ij} - \bar{y}_i\right)^2}{n_i - 1}\right]} \tag{14}$$

The weighted linear least squares algorithm does have some disadvantages, however. This algorithm assumes the weights of the points are explicitly known. One noticeable disadvantage comes from weighting primarily from the point's standard deviation. Data points oftentimes need to have greater emphasis placed on them for reasons other than standard deviation values. Similar to the basic linear least squares algorithm, outliers have a strong pull on the data trend due to the large error margins [NIST, 2005 and Hoffman, 2001].

Weighting Data Points Chronologically

Since the data in this research holds stronger value to the most recently gathered points and is not reliant upon the standard deviation of the data, the standard definitions of weights in the weighted linear least squares algorithm do not apply. Since this method of weighting the points is completely arbitrary depending on how much more weight needs to be placed on the most recent point. Instead of having the weight inversely proportional to the standard deviation, it is inversely proportional to the placeholder which the point is in the sequence of data points.

Equation (15) shows the correlation between the weight and the point's location in the collected set. In this equation, ω represents the weight, *n* represents the total

number of data points collected, m is the number of the data point of interest, and c is an arbitrary constant determined by the person utilizing the equation.

$$\omega = \frac{1}{n - m + c} \tag{15}$$

The weight defined in Equation (15) is now implemented in Equation **Error! Reference source not found.** to develop an algorithm that is weighted based on chronological order instead of standard deviation. One note of interest is the value chosen for c. As $c \to \infty$, then the most recent points become less and less important due to the comparatively like denominators being used. Likewise, as $c \to 0$, the most recent points have increasingly greater pull toward them. For the purpose of the presented research, a value of $c = 4$ is selected. This results in a strong pull from only the first 6 points. The Matlab code written for the chronologically weighted least squares algorithm can be found in Appendix A.

CHAPTER 4

EXPERIMENTAL PROCEDURE

As previously stated, the experimental work for the research presented in this thesis was completed by Yawei Li. For Li to begin his research, he utilized the bearing test stand, Hommelwerke profilometer, and the same Timken bearings from previous experiments initiated at Georgia Institute of Technology. Since Li's work is a continuation of prior work, he was able to utilize important information such as resonant frequency and previously developed experimental procedures.

As previously stated, all work from Georgia Tech utilizes the same bearing test stand which is able to withstand several different types of loads of varying amounts. Most research was based on the same type of Timken bearings.

Both accelerometers and acoustic emission sensors were placed on the housing holding the Timken bearings with defects inscribed by an electric discharge machine. The defect sizes were measured by a profilometer at different stages of the bearing's defect propagation. This chapter defines and describes each of these instruments as well as explaining their contributions to the experiments performed by Li.

In addition to the equipment information, collection of pertinent system information such as resonant frequency and system constants are fully explained.

Equipment

The three most important pieces of equipment for the described research are the bearing test stand, accelerometers, and the rolling element bearings. Other equipment is used to further analyze information from these three, but without a thorough understanding of them, it would be impossible to complete the work described in this thesis.

Bearing Test Stand

Most bearing research done at Georgia Tech has been executed on a bearing test stand illustrated in Figure 10.

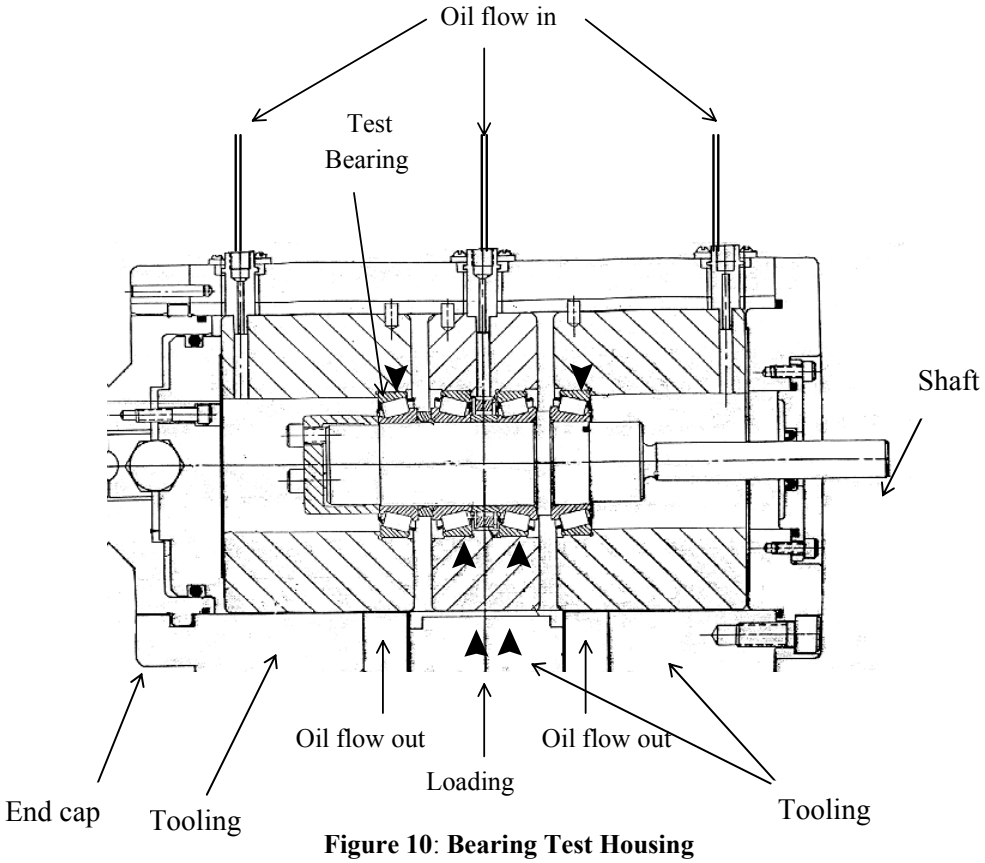

Figure 10: **Bearing Test Housing**

The housing of this test stand is made of cast iron with a 12.7 cm (5") bore with a 2.54 cm (1") wall thickness. The housing contains three pieces of steel tooling which hold two bearings in place. The hydraulic cylinder piston used to apply a radial load to the tooling has a 9.53 cm (3.75") diameter [Billington, 1997]. There is also a lubrication flow and handling system which can be closely monitored for debris and temperature if need be. The lubrication fluid used in this setup relative to this research had a viscosity of 57 SSU [Li, 1999].

Timken Bearing Description

The bearings used for most research on the specified bearing test stand are Timken bearings. The Timken LM50130 cup and the Timken LM501349 cone comprise the outer and inner races, respectively. Nineteen tapered rolling elements with a taper angle 13.13° are in the bearing cage. The bore diameter is 41.275 mm (1.625"), and the outside diameter is 73.431 mm (2.891").

For calculating the frequencies of each bearing component, the pitch diameter and the average diameter of the rollers need to be known. For these particular Timken bearings, the average roller diameter and pitch diameter are 7.84 mm (0.31") and 57.15 mm (2.25"), respectively (Li, 1999).

Research utilized Timken bearings with the identification numbers LM50130 cup (outer race) and LM 501349 cone (inner race) shown in Figure 11. If an accelerometer was placed on the Timken bearing shown, and the signal was decomposed using the fast Fourier transform, the frequency values associated with the components would match

those listed in Table 1; these values are calculated from Equations

Error! Reference source not found. - Error! Reference source not found..

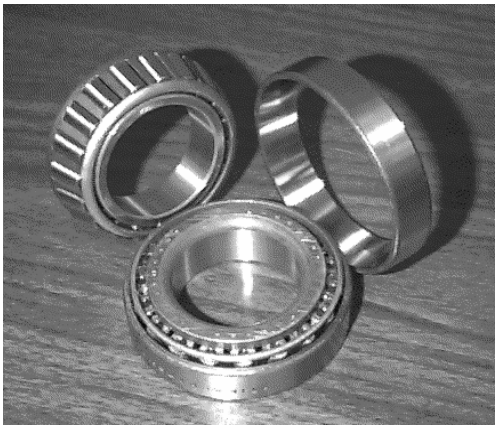

Figure 11: Photograph of Timken tapered roller bearing (Billington)

Table 1: Frequencies for Experiment Analyzed in this Thesis

Component	Frequency (Hz)
Inner Race	283.21
Outer Race	219.45
Rolling Element	559.8
Cage	11.55

The inner race and outer race are the bearing components most likely to have defect crack propagation due to cyclic fatigue. In the experiment conducted by Li, the defect was placed on the outer race, so there should be a significant peak around 220 Hz after the data is filtered.

Accelerometer

Accelerometers are seismic instruments which typically are comprised of a small mass mounted on a piezoelectric crystal which acts as a stiff spring whose change in height is measured as an electric charge. Simply put, an accelerometer is an electromechanical device that determines acceleration through measuring its own motion. The acceleration monitored can be either static (gravity) or dynamic (vibration). The accelerometer can be either digital or analog. There are dozens of different types of accelerometers, so research needs to be done to determine which accelerometer is right for the given situation.

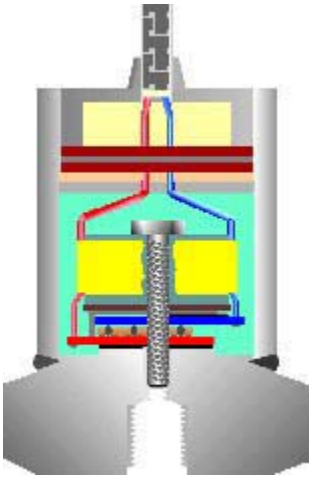

Figure 12: Basic Piezoelectric Accelerometer Design (sensorland, 2005)

There are several different types of accelerometers. As previously mentioned, some use piezoelectric crystals which are microscopic crystals that produce a voltage when stressed by acceleration. Another type of accelerometer measures changes in capacitance between two microstructures. When the two microstructures are next to each other, a certain capacitance can be measured. Once an acceleration force is applied to the microstructures the distance between them changes. The change in distance results in a

change in capacitance. This capacitance change is converted to a voltage change, and from there, the acceleration can be measured [Goldman, 1999].

Accelerometers have a few characteristics which need to be considered when purchasing—such as the sensitivity of the accelerometer. If an accelerometer has a greater sensitivity, it will emit a greater change in the generated signal.

The number of reading samples per second is a term coined "bandwidth." A large bandwidth is desirable for quick acceleration changes such as vibration monitoring and fast moving machines.

An accelerometer can also have two or three axes which it measures the acceleration. If a three-axis accelerometer is needed and none is available, two two-axis accelerometers can be used ninety degrees offset to create the same effect (Wikipedia, 2005).

For the purpose of Li's experiment, a Kistler 8792A50 tri-axial K-Shear accelerometer and a Wilcoxan 736T high frequency single-axis accelerometer were used to acquire data. These voltage-mode accelerometers have built-in microprocessors that are able to convert changes in charge to voltage. The benefit of this type of accelerometer to the experiment is that they are not very sensitive to noise, and they do not require specific calibrated cables.

Figure 13: Kistler 8792A50 Tri-axial K-Shear Accelerometer [Billington, 1997]

Figure 14: Wilcoxand 736T High Frequency Accelerometer [Billington, 1997]

A constant current is supplied over a specified to the accelerometers through a Kistler 5134 coupler which, in turn, powers the accelerometers. The signals from a quartz crystal modulating the voltage are sent to the Kistler 5134 coupler. The AC signals which correlate to the measured acceleration flow through a series of filters and buffered circuits.

The high frequency response of an accelerometer is dependent on both the internal components as well as the connection to the mounting surface. The accelerometers were mounted to the bearing test stand at 2.26 N·m (20 in·lbs) torque in order to ensure a dependable stiffness between the coupling and the mounting surface. Another means of ensuring a secure fit between the two, the threaded studs were coated with vacuum grease (Li 1999).

Acoustic Emissions Sensor

Acoustic emission (AE) sensors measure the high frequencies emitted by stress waves. In order for the AE sensor to accurately acquire all pertinent data, it must record at very high frequencies. Frequencies above 100 kHz are very common for most acoustic emission sensors.

The AE sensor used in Li's research is a Physical Acoustic Corporation type R15 sensor. In order to connect the AE sensor to the bearing housing, a cyanoacrylate adhesive couplant was utilized.

There are a few differences between accelerometers and AE sensors that need to be taken into account when determining which sensor is best for the purpose of the research. Stress waves in a material decrease in size when material waves propagate during contact between two surfaces. This is a problem when measuring AE signal outputs. The amplitude response of an AE sensor is also much less uniform than that of an accelerometer. The high data collection rate needed to obtain accurate results with an AE sensor is also difficult to manage. However, this can be somewhat avoided by using low pass filters.

Figure 15 illustrates the frequency response of an Acoustic Emission sensor. Since the modes of the signal and amplitudes might change during a bearing failure, the accelerometer is a more reliable tool than the AE sensor when monitoring bearing defect propagation [Li, 1999].

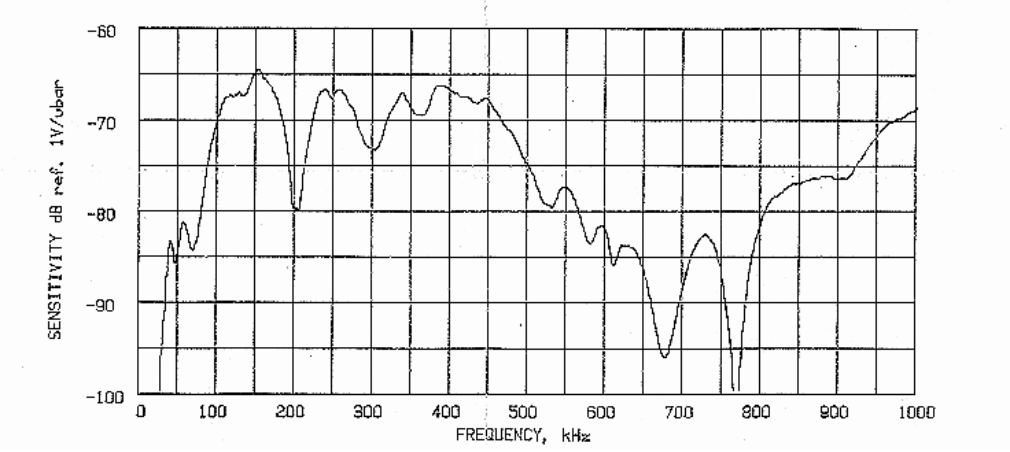

Figure 15: Sensitivity of Acoustic Emission Sensor with Respect to Frequency [Billington, 1997]

For the reasons previously described, only the accelerometer data obtained in the experiments are analyzed in this research. This does not imply that the AE sensors cannot accurately monitor the defect propagation using the modified Paris equation. It simply means that there has been no work done to prove either case.

EDM Groove Initialization

When working with bearings, the time for a crack to initiate is much longer than the crack propagation rate [Paris, 1985]. For this reason, an artificial defect was etched on the inner race of a bearing. Electrical-Discharge Machining, also known as spark erosion, dislodges particles from the work piece through discharging an electrode spark into the surface. In order to break off the particles from the bearing, there must be a strong electrical arc between the bearing and the electrode. The EDM process can be used on any work piece which is electrically conductive [Kalpakjian, 2003]. Figure 16 illustrates the electrode portion of the EDM.

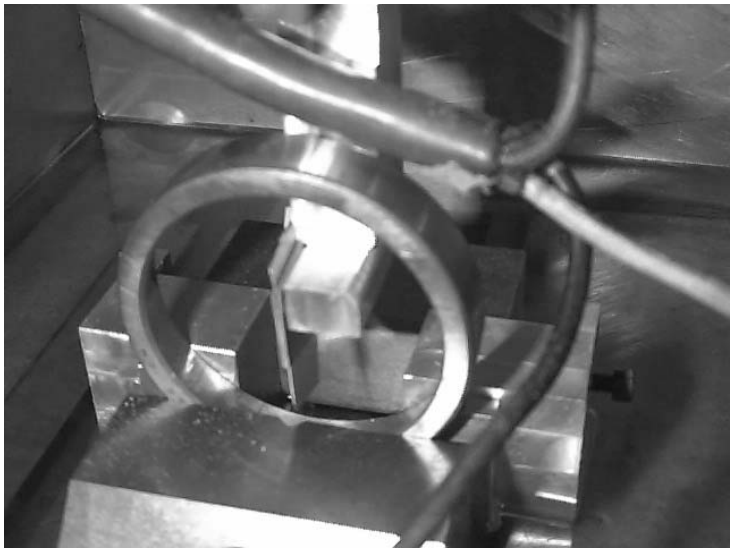

Figure 16: Electrical Discharge Machine [Billington, 1997]

In order to achieve a uniform groove width and depth of cut, the electrode needed to be initially dressed. Dressing the electrode ensures a uniform contact from the electrode to the work piece surface. For this experiment, a second bearing was utilized for the dressing procedure. First the outer race is separated from the internal components. A groove was machined out of the raceway until the entire electrode engaged the metal. Once this is done, the bearing race is rotated slightly until there is a new surface with which the electrode connects. Once the electrode sparks uniformly across the width of the bearing race, the dressing bearing is removed, and the experiment bearing takes its place.

Once the Timken bearing is in place, a groove of desired dimensions is prepared by the EDM. These dimensions are checked through the use of a profilometer. It is the same profilometer used for measuring the defect size for the duration of the experiment whenever the bearing is extracted from the system and checked for crack defect propagation [Billington,1997].

Profilometer

The Hommelwerke Profilometer shown in Figure 17 was the one used for all defect measurements for the experiment pertaining to this research. The diamond stylus of the profilometer moves across the work piece and sends back information electronically to a computer which displays the acquired surface information. The bearing was positioned with the inside of the outer race parallel to the surface plate of the profilometer.

The groove was measured three times. The first pass was across the small diameter of the taper, the second was across the middle of the taper, and the third was over the largest diameter of the cut. The widths and depths were averaged. The measurements of the initial groove were uniform which implies the EDM was an effective method of creating the desired defect [Billington, 1997].

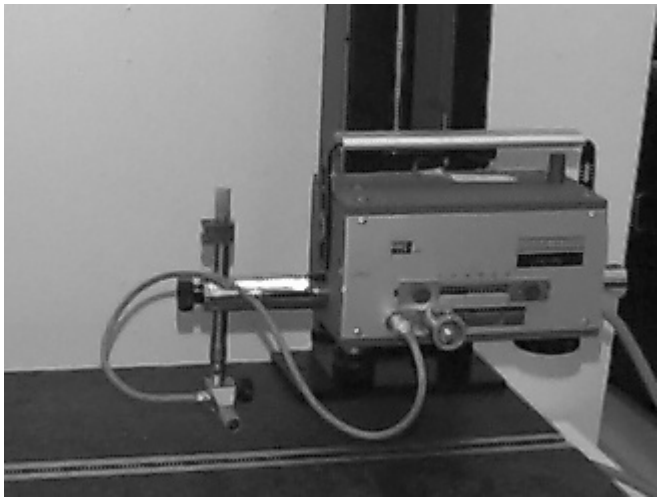

Figure 17: Hommelwerke Profilometer [Billington, 1997]

Experiment Component Descriptions

Resonant Frequency

The resonant frequency of the system needed to be known in order to proceed with this research. The accelerometer signal is often band-passed filtered around the resonant frequency in order to eliminate the high frequencies associated with the accelerometer and the low frequencies associated with the system itself. The resonant frequency was determined by a series of hammer impact tests. These impact tests excited the bearing housing system, and the decaying vibration signal indicates the natural resonant frequency of the system. Several tests were conducted with varied sensor locations, impact points, and loading. From these tests, it was concluded that the resonant frequency of the bearing test system falls between 4000 and 6000 Hz [Billington, 1997].

Determining System Constants

In addition to the resonant frequency, the constants defining the Paris Equation were needed for this research. P_o and m are material constants that are determined experimentally. As previously stated, for the full description of finding P_o and m, one should refer to the ASTM handbook section E647 titled, "Standard Test Method for Measurement of Fatigue Crack Growth Rates." The methods shown in the handbook reflect the methods for determining the variables for the original Paris Model, but the same concepts can be used to find the values in the modified equations.

In order to determine the material constants, a more accurate model is developed which includes the unknown variance probability of the crack growth. After the stochastic nature of the system is taken into account, a recursive least squares algorithm is applied to the system.

Defect propagation is a stochastic process as was shown in Figure 18 by Virkler et al. [1979] in tightly monitored experiments.

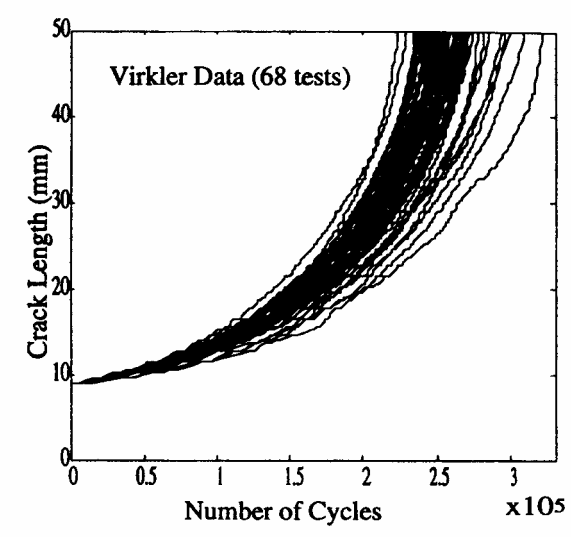

Figure 18: Stochastic Crack Growth Propagation

Since there is a random component involved with the process, a lognormal random variable $e^{Z(t)}$ is multiplied to the right-hand side of the Paris-Erdogan Equation, Equation (2). This results in the model shown as Equation (16).

$$\dot{D} = \frac{dD}{dt} = P_o D^m e^{Z(t)} \tag{16}$$

The natural log of Equation (16) is taken as shown in Equation (17). The defect size, D, can be measured, but the value for $\dot{D}$ must be estimated through a polynomial method.

$$\ln\left(\dot{D}\right) = \ln\left(\frac{dD}{dt}\right) = \ln(P_o) + m\ln(D) + Z(t) \tag{17}$$

A second-order polynomial with an odd number of successive data points are used to fit the defect propagation trend. The rate of growth of the defect is measured by taking the derivative of the center point of the fitted polynomial.

The next item of interest is the stochastic parameter, $Z(t)$. This is done using an on-line recursive least squares (RLS) approximation. The error term of the RLS approximation is estimated to be the stochastic parameter, $Z(t)$. The variances and covariance of $\ln(P_o)$ and m are also obtained through the RLS model parameters.

Further research was done by Li as well as Lin and Yang to indicate that $Z(t)$ is a correlated as a Gaussian-Markov process as shown in Equation (18) where ξ is a colorness parameter, and w_z is Gaussian white noise. When ξ increases, $Z(t)$ becomes less correlated.

$$\dot{Z} = -\zeta(Z) + w_z(t) \tag{18}$$

The stochastic variable needs to be accounted for because it causes much variance in the defect propagation, and it could detract from the true values of P_o and m. The values of P_o and m greatly change the rate of defect propagation as can be seen in Figure 19 and Figure 20, respectively [Li, 1999 and Lin and Yang, 1983].

From previous experiments conducted by Li, the values of P_o and m of the Georgia Institute of Technology's bearing test stand were determined to be 0.13 and 1.1, respectively [Li, 1999].

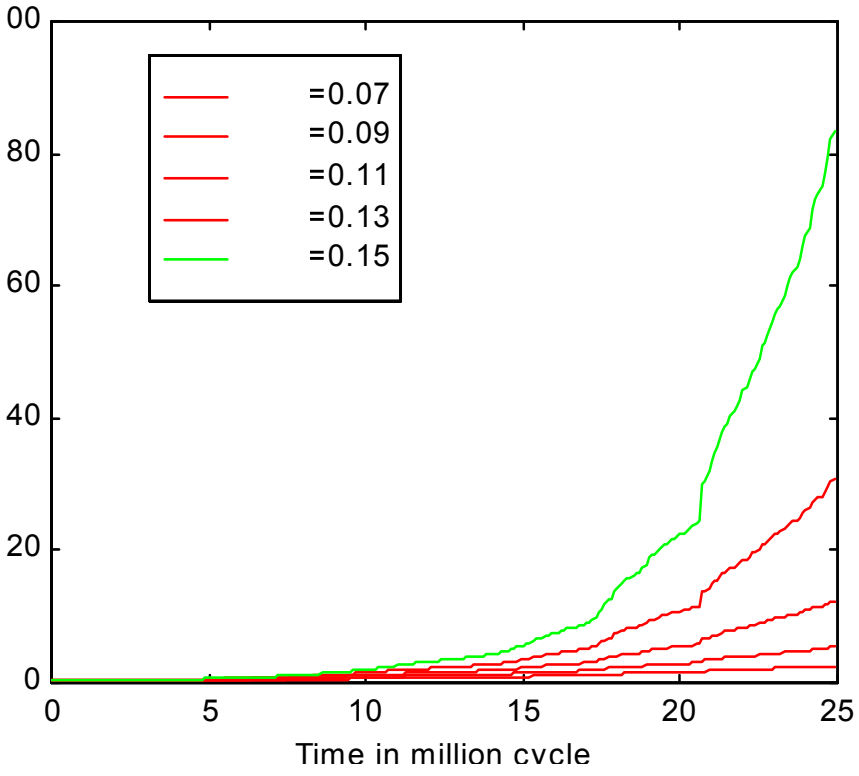

Figure 19: Comparison of Material Constant P_o to defect propagation

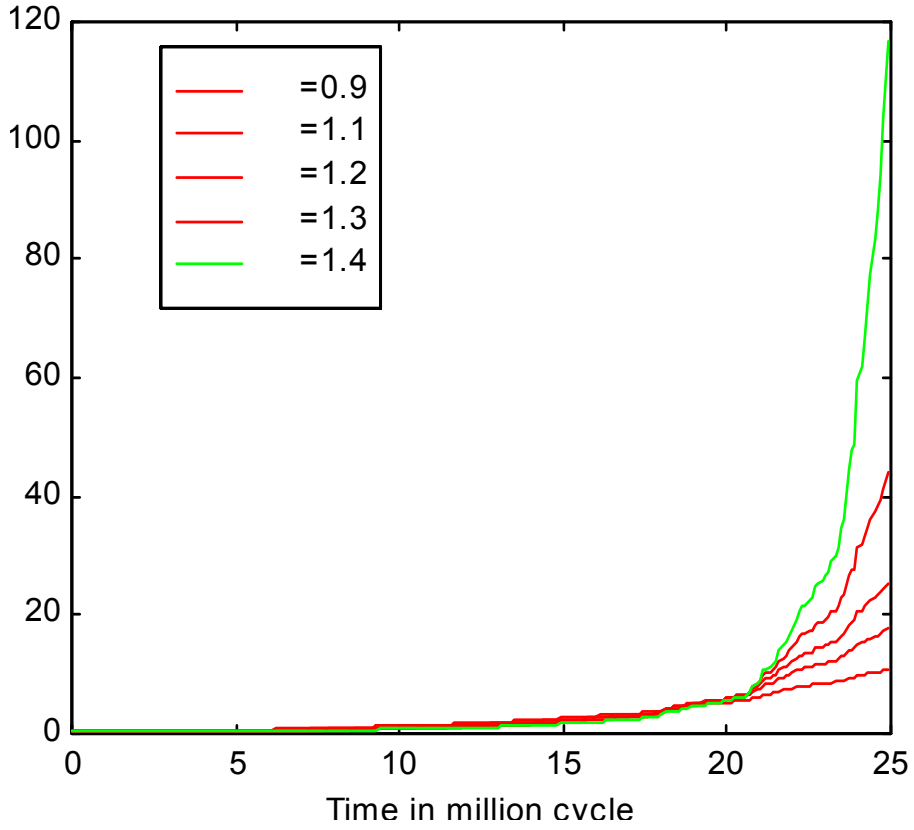

Figure 20: Comparison of Material Constant *m* to defect propagation

Experimental Design and Data Collection

This thesis utilizes the information gathered by the accelerometers when a naturally propagating defect is mounted in the test stand. This data analyzed was acquired by Yawei Li in 1999. A small scratch was placed on the cup of the bearing using an electrode discharge machine. The scratch was aligned in the bearing axial direction in order to simulate a true fatigue defect's orientation. The size of the defect was measured using a profilometer. The bearing was then put in the test stand along with a presumably unscathed bearing. The test stand was run at 1600 rpm with a radial load of 1000 psi. On the first day of testing and every few days thereafter, accelerometers were placed on the housing near the bearings, and the time signals were recorded. Samples

were taken at 30,000 kHz frequency for a one minute duration resulting in 2^{18} samples for every data file. Each time these samples were taken, the bearing crack was measured by the Hommelwerke profilometer, which is described in detail previously in this chapter, and the number of total rotational cycles was recorded [Li et al., 1999].

Since the signals coming from both the accelerometer and the AE sensor are analog, they need to be converted to digital before any work can be done. The signals are also low-pass filtered in order to prevent aliasing of the signal. Aliasing is simply the replication of a signal appearing in an inaccurate location in the frequency spectrum due to low sampling frequencies. Figure 21 illustrates the method used when acquiring the data.

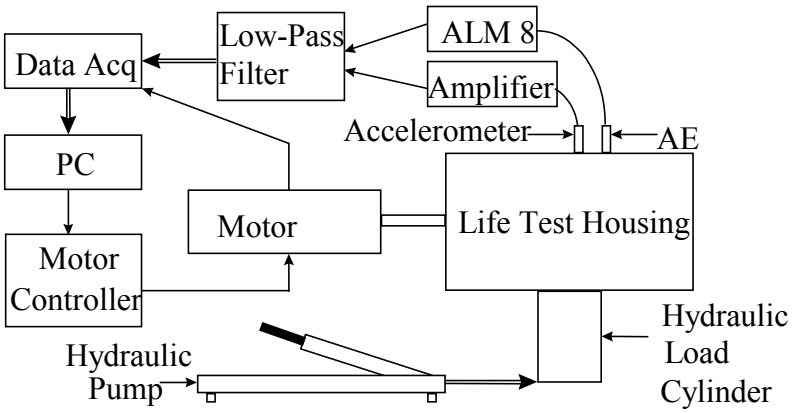

Figure 21: Schematic of Data Acquisition from Propagating Defect

CHAPTER 5

WORK DONE TO PREVIOUSLY ACQUIRED DATA

As mentioned previously, the data for the research presented in this thesis had been acquired by Yawei Li. The information provided was the accelerometer signal, the date which the signal was monitored, the area of the defect, and the number of cycles that had passed since the etched bearing had been placed in the bearing housing system.

Unfortunately, all of the data sets which had been accumulated were not saved. When the original test was run, it was not necessary to keep the instantaneous information because it was used purely for monitoring reasons. There are eight remaining accelerometer signals kept from this particular experiment.

The PSV at the critical defect area is called PSV_{crit}. From these eight data sets, one of the constants for the proposed Modified Paris Equation, PSV_{crit}, needs to be calculated. This is done by the digital signal processing methods of taking the Fast Fourier Transform and then converting to the power spectrum. From the power spectrum, the power spectrum value (PSV) can be determined. This value is then plotted against the defect area to find where the PSV intersects the critical defect area.

Paris Equation Constants

When working with the Paris Equation manipulation, there are three constants which need to be calculated before the bearing's time to failure can be calculated. As previously mentioned, P_o and m were calculated to be 0.13 and 1.1, respectively, for the bearing test stand used to gather the data presented in this thesis. The third, and most

essential constant, for the purposes of this research, is the critical PSV value, PSV_{crit}, above which the bearing is considered to have failed.

The Anti-Friction Bearing Manufacturers Association (AFBMA) standard states that a bearing is considered to have failed at the onset of fatigue failure. However, the useful life of a bearing is considered to be well beyond this point. The Timken Company defines failure criterion to be after the area of the crack surpasses 0.01 in^2 (6.25 mm^2) [Shigley and Mischke, 1989]. Since data are available for a naturally propagating defect, the best means of obtaining the value for the critical PSV was to find the PSV at which the bearing's crack surpassed the failure criterion value. Therefore, the data collected from the bearing test stand were filtered and analyzed in order to obtain the value for PSV_{crit}.

Filtering FFT and PSV description

A Fast Fourier Transform (FFT) was applied to the data in order to convert the information into a more user-friendly format. In vibration analysis, the frequency spectrum is sometimes called the power spectrum [Simmons, 1996]. This is different from the power integration described earlier since the FFT values are not squared. Figure 22 is a plot of one set of the original data output as a function of time, and Figure 23 is the same data in the frequency spectrum.

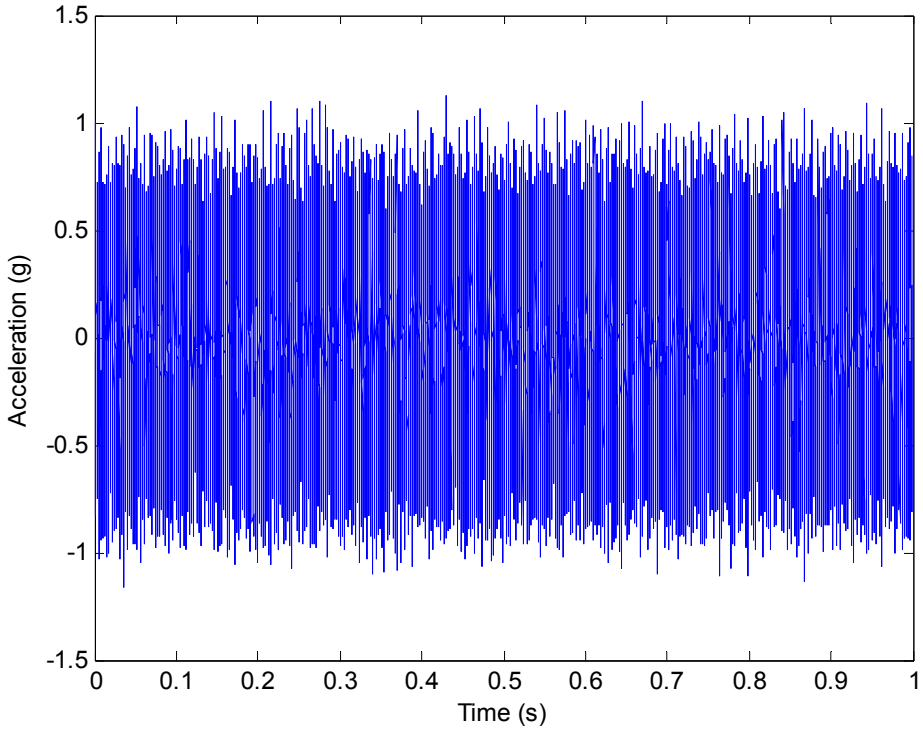

Figure 22: Raw Data

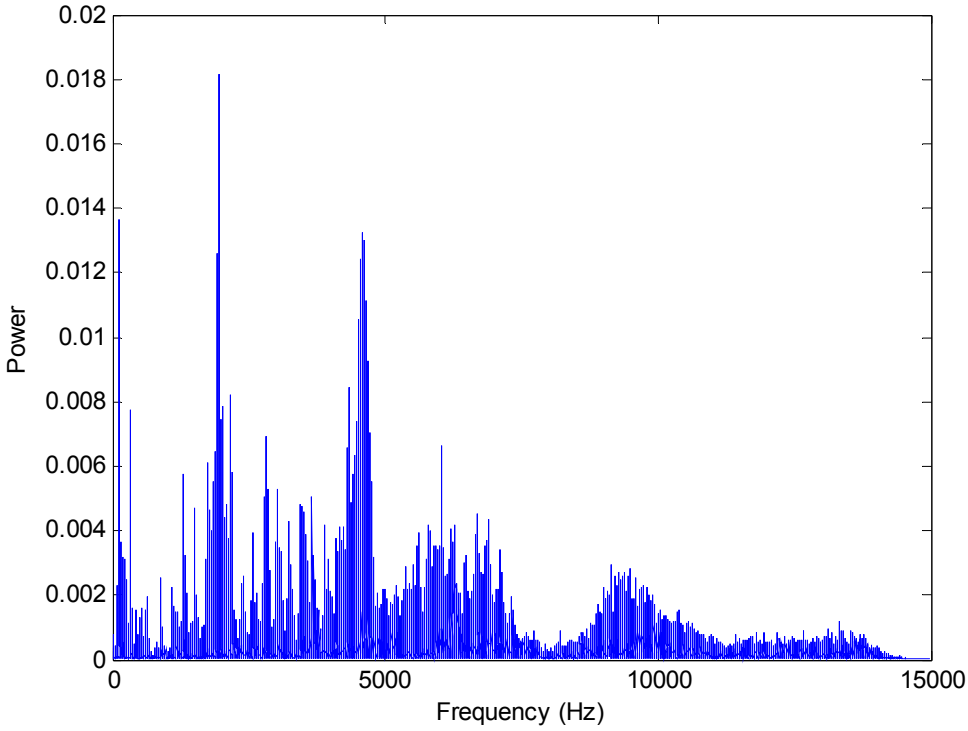

Figure 23: Respective Power Spectrum

Envelope Spectrum Analysis

Diagnostics refers to determining current problems associated with the system. In bearing failures, this often involves both monitoring techniques and digital signal processing. One method of diagnostics utilizes the High Frequency Resonance Technique (HFRT) in conjunction with the Adaptive Line Enhancer (ALE) concept.

In order to determine the bearing defect's location, a high frequency resonance technique was applied to the raw power spectrum data. Figure 24 shows the envelope of the signal after the high frequency resonance technique is applied. Appendix B indicates the procedure for taking the FFT and HFRT of a data set.

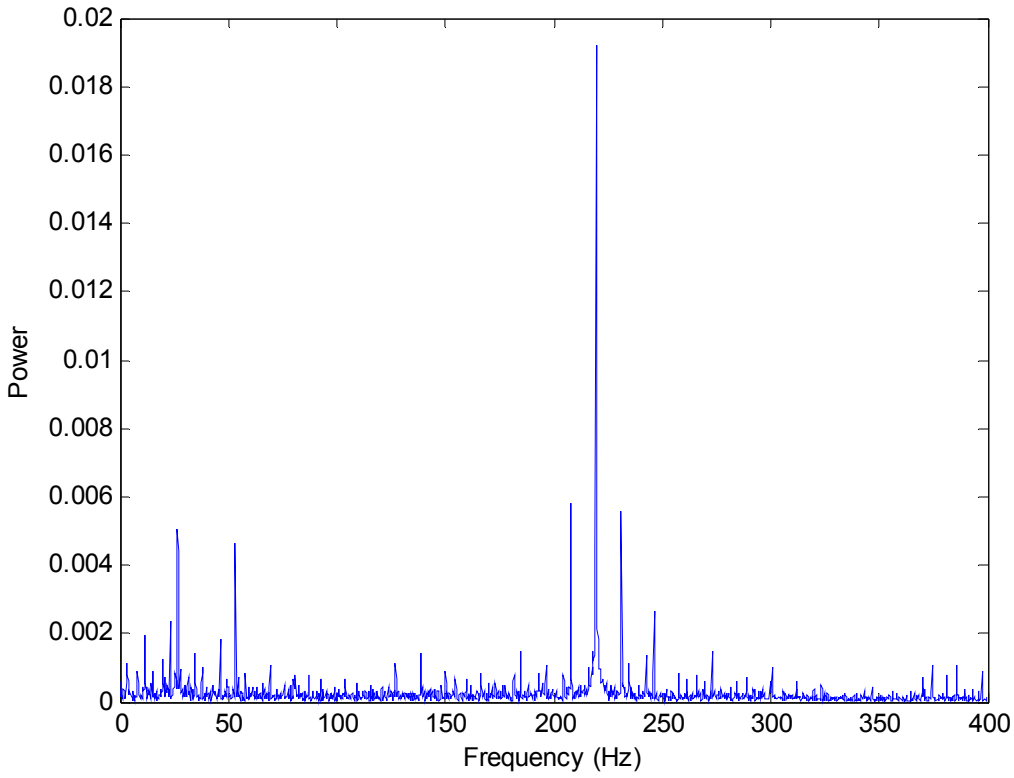

Figure 24: Envelope of Data Indicating Failure is Located Around 220 Hz

From referencing Table 1, one can confirm the failure frequency of the ball pass outer race is equivalent to the frequency having the highest power value in Figure 7.

Frequency Spectrum Analysis

One of the primary purposes of this thesis is to show how the peak amplitude of the raw power spectrum directly indicates the defect severity. The frequency spectrums of all data sets associated with the naturally propagating defect are listed below in Figure 25 thorough Figure 32 . The first set of data comes from just after the initial defect was applied to the bearing, and the final set of data was taken well after the bearing was considered to have failed.

The defect Power Spectrum Value (PSV) is considered to be the highest value in the frequency spectrum obtained from a small region (range is 4000-6000 Hz) around the system's natural frequency of 5000 Hz.

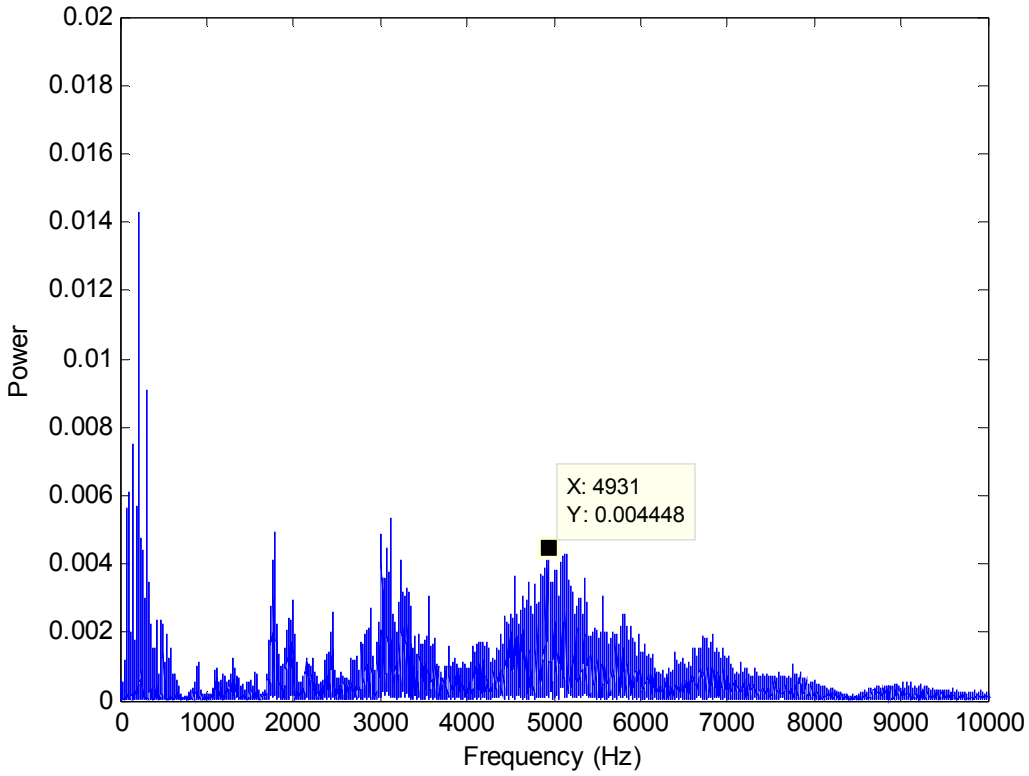

Figure 25: September 24 Frequency Spectrum

This is the first set of filtered data taken on September 24, 1998. The defect has already propagated to 1.78 mm^2 from 1.49 mm^2 after 4.5 million cycles. The value around the resonant frequency is relatively low. This is both desirable and positive because the defect has not yet reached the 6.25 mm^2 fatigue criterion value. Therefore, there is a strong possibility that the power value has room to increase as the defect propagates.

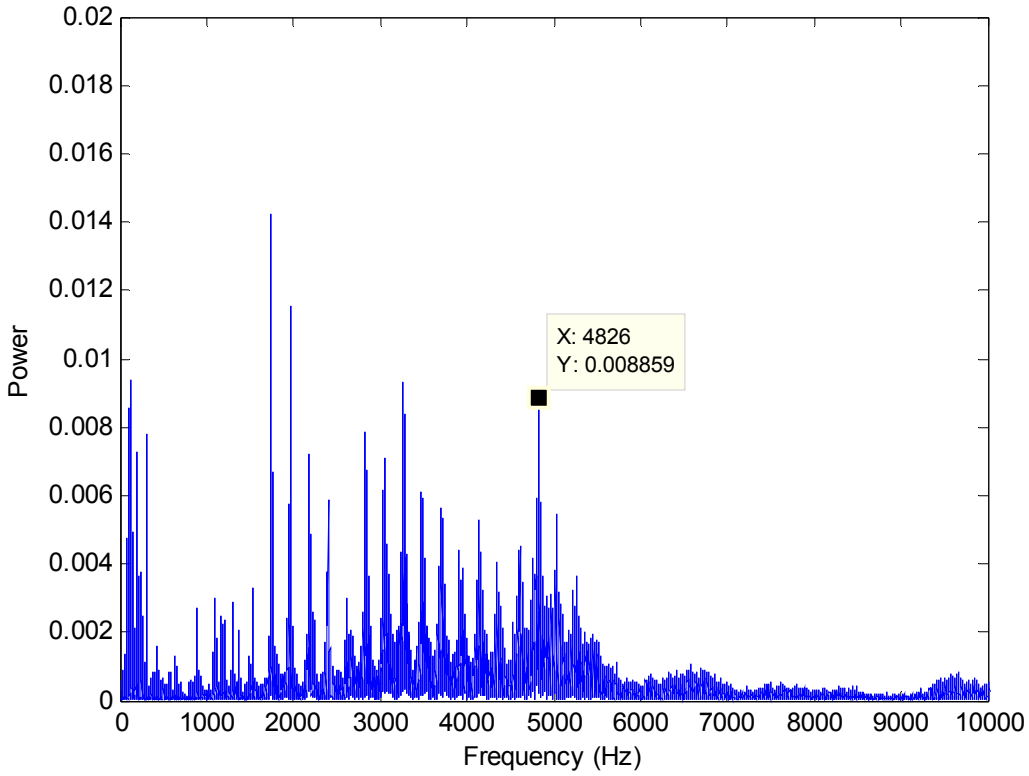

Figure 26: October 21 Frequency Spectrum

This frequency spectrum data was taken 27 days and over 10 million cycles after the first set. The value for the power spectrum doubled when the defect grew from 1.78 mm^2 to 5.56 mm^2. The defect is still less than the 6.25 mm^2 threshold, but it is quickly approaching it. It is noticeable that most values in the frequency spectrum are increasing as the defect increases.

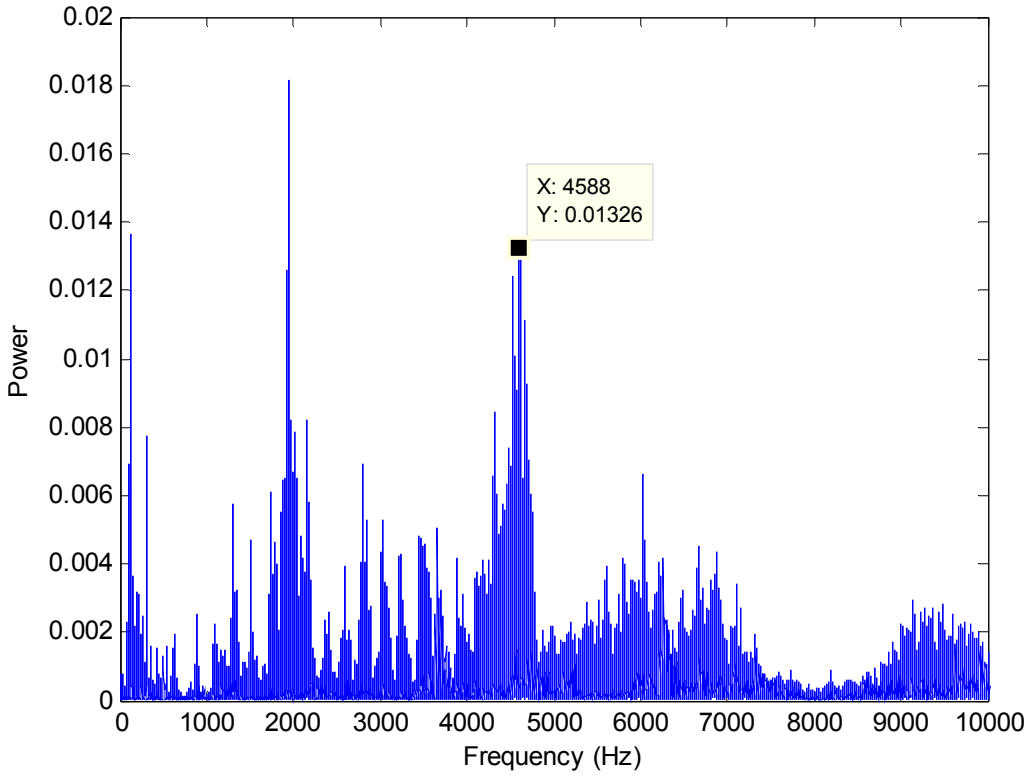

Figure 27: November 14 Frequency Spectrum

The PSV has increased to 0.0134 from 0.00886 after 4.6 million cycles. The higher frequencies are beginning to pick up more energy as the defect approaches the cutoff limit; the defect area is at 5.62 mm^2.

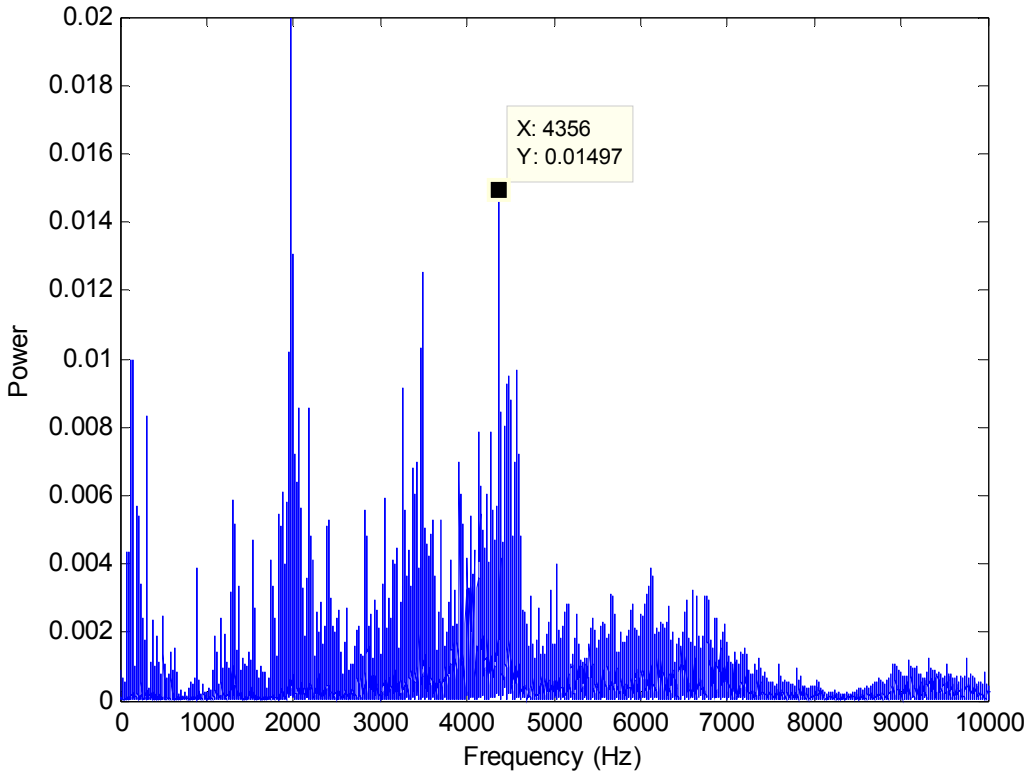

Figure 28: November 16 Frequency Spectrum

November 16 was the last data set collected before the bearing passes the critical defect size. The PSV is at 0.01497 which is considerably larger than that only 1 million cycles before (November 14 data set) which was 0.01326. The defect area at this point is at 5.81 mm^2, a 0.44 mm^2 difference.

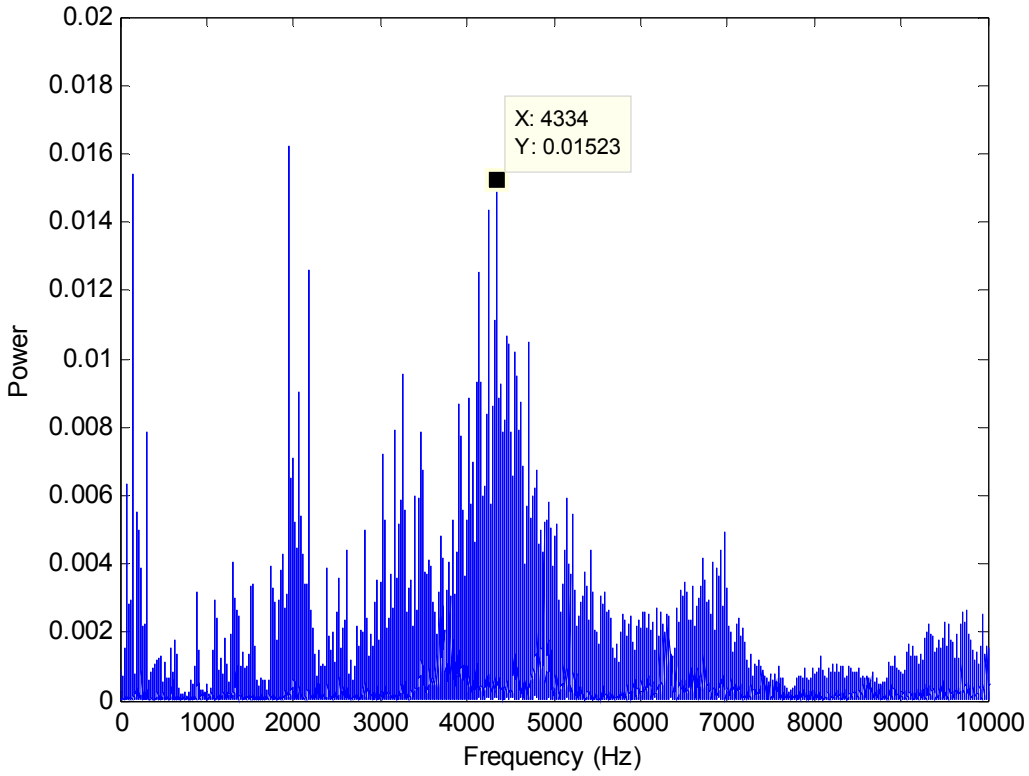

Figure 29: November 20 Frequency Spectrum

The defect size has finally reached the point considered to be beyond bearing failure at 8.09 mm^2. The signal is much busier than what was shown previously. The peak PSV is the highest shown so far at 0.01523. Since the bearing has already reached its failure point, its effects on the other components of the system are going to begin appearing in the system as shown in Figure 30.

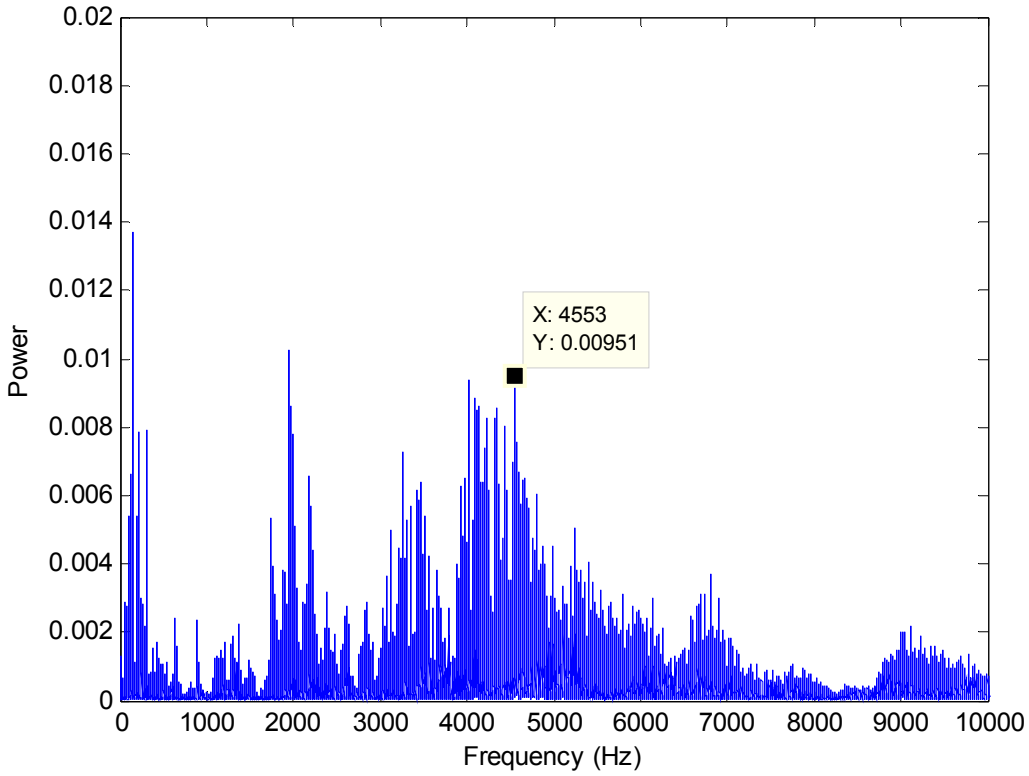

Figure 30: November 22 Frequency Spectrum

The defect is still propagating at this time, but the FFT of the signal is not indicating a strong problem in the system. It is, in actuality, showing a PSV only slightly above that which was determined when the defect size was only 5.57 mm^2. If this signal is compared with the October 21 FFT, there are noticeable changes in the frequencies not associated with the resonant frequency. This is apparent primarily in the higher frequencies.

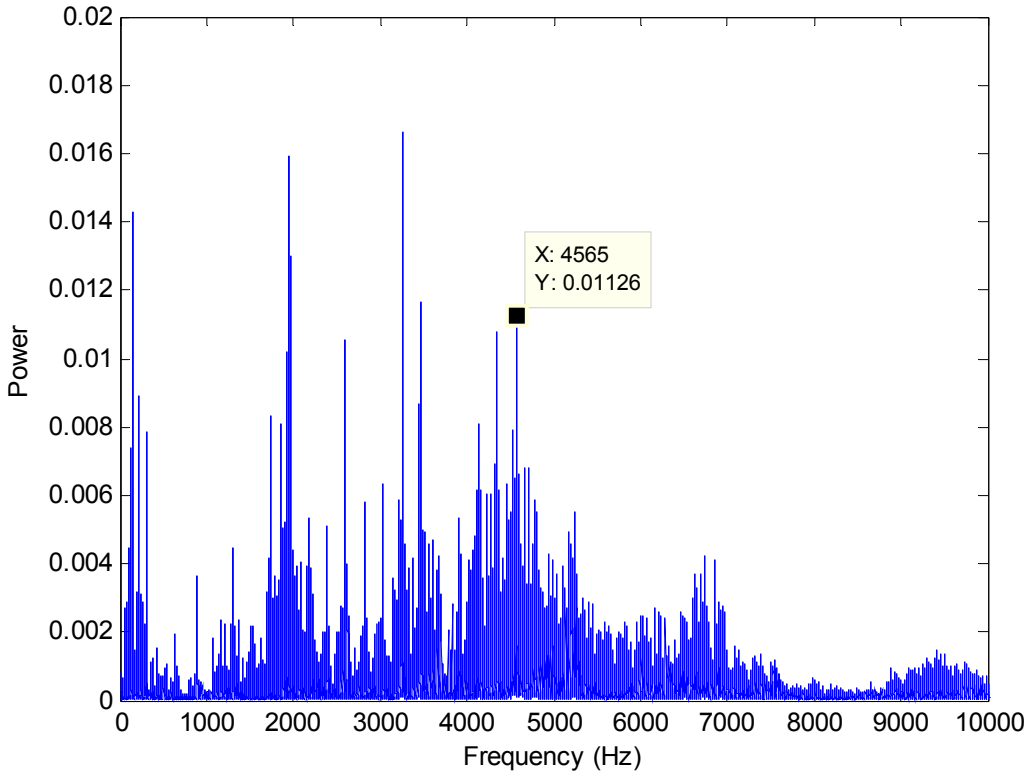

Figure 31: November 25 Frequency Spectrum

The defect size was actually measured to be less than area when the measured PSV had reached its peak. This was probably due to an inaccurate profilometer reading either earlier in the process or, more realistically, for this particular stage in the crack's life. While the peak still has not superceded the value when the defect was at 0.015234, it is still obvious that there is a problem associated with the bearing.

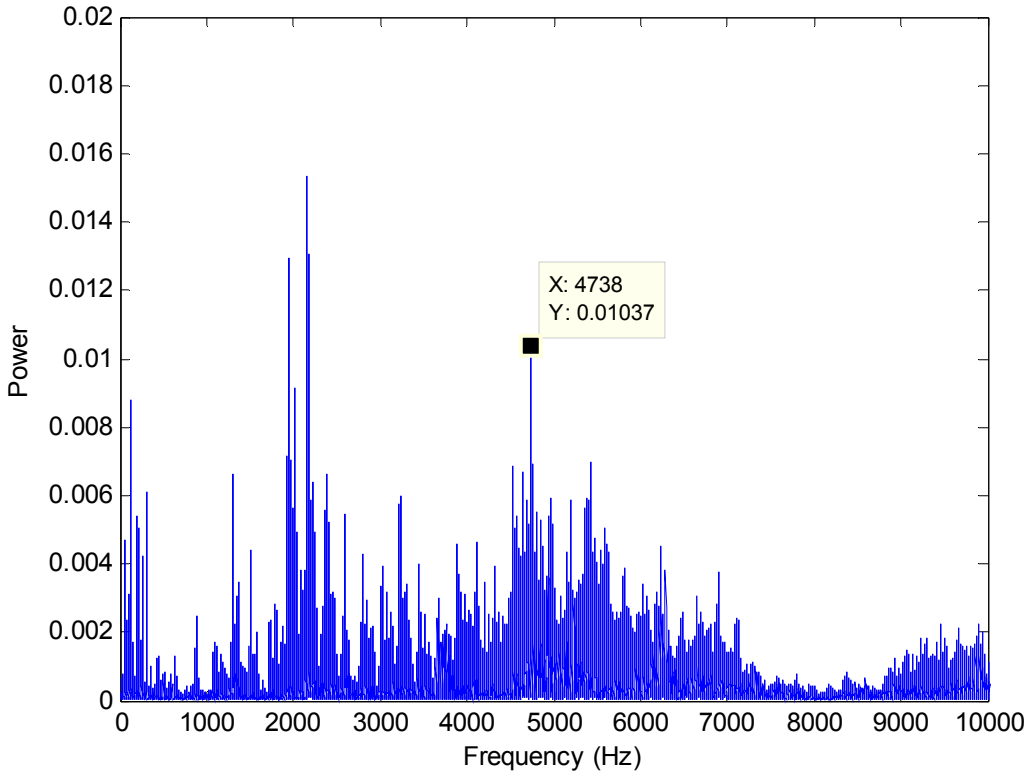

Figure 32: December 17 Frequency Spectrum

December 17 is the last data set available for analysis. Once again, the PSV is lower than when the defect was approaching failure and shortly thereafter. At this point, the defect is measured at 8.432 mm^2, and the number of cycles after the introduced crack was applied to the system is at 33.7 million cycles.

Table 2 shows the bearing defect sizes, the number of cycles associated with the bearing, and the defect PSV associated with the bearing at all stages of the crack propagation process. Appendix C supplies a Matlab code for finding the PSV for an accelerometer signal.

Table 2: Naturally Propagating Defect Pertinent Information

Date	Area (mm^2)	Cycles (millions)	PSV
24-Sep	1.785	4.56	0.004448
21-Oct	5.5683	14.832	0.008859
14-Nov	5.6175	19.408	0.013257
16-Nov	5.8092	20.688	0.01497
20-Nov	8.0904	24.208	0.015234
22-Nov	8.2242	26.016	0.00951
25-Nov	8.0415	27.072	0.011261
17-Dec	8.4329	33.72	0.010365

The values from this chart are useful when determining the critical PSV at which the bearing is considered to have failed. The procedure for estimating the critical PSV is described in the next section.

Calculation of the Critical PSV

The PSV obtained from the raw power spectrum was plotted against defect area as shown in Figure 33. Where the crack area reaches the industrial guideline of failure is the point when the spall reaches $6.25mm^2$, it intersects the plot at PSV_{crit}=0.015. This value is considered to be the critical PSV upon which the following information is analyzed. The PSV_{crit} is system dependent, and should be determined for each individual system in order to apply information provided by this thesis. It is possible that there is a connection between certain system characteristics and PSV_{crit}, but research has yet to be conducted in this area.

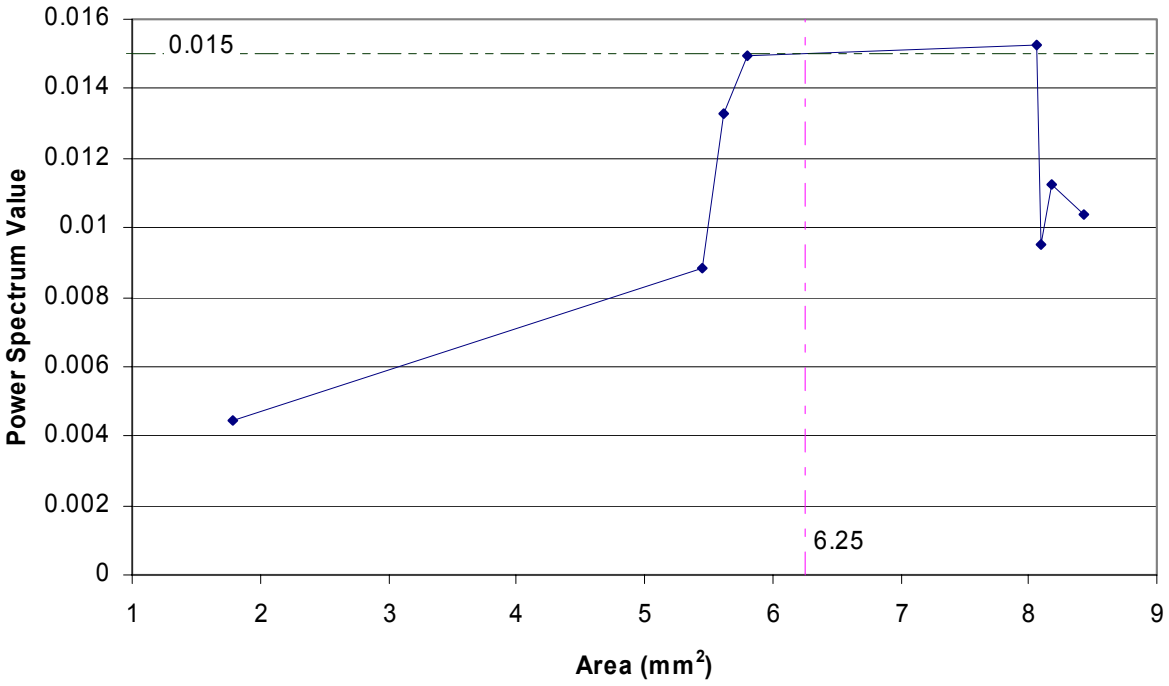

Figure 33: Defect PSV versus Area

In a similar manner, in was concluded from Li's test, the defect for this particular bearing exceeds the 6.25 mm^2 threshold between 20.69 and 24.21 million cycles after the onset of the experiment. From linear interpolation between the points on either side of the failure point, 21.4 million cycles is the point which the bearing failed as shown in Figure 34.

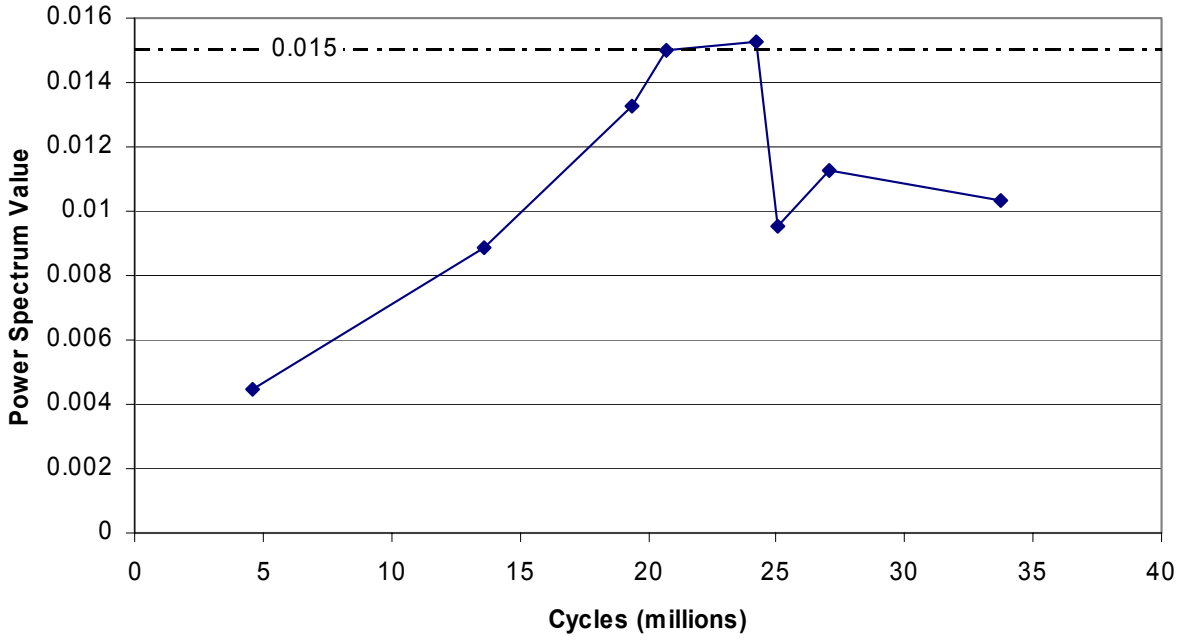

Figure 34: Power Spectrum Value as a Function of Cycles

Now that the value for PSV_{crit} is known, Paris's equation can be rewritten as a more conclusive comparison between remaining cycle time and defect PSV as shown in Equations (19) and (20). Equation (21) indicates the equation specific to Georgia Tech's bearing test stand.

$$\frac{\Delta PSV}{\Delta t} = \frac{PSV_{crit} - PSV_{current}}{\Delta t} = P_0 PSV_{current}^{\ m} \tag{19}$$

$$\Delta t = \frac{PSV_{crit} - PSV_{current}}{P_0 PSV_{current}^{\ m}} \tag{20}$$

$$\Delta t = \frac{0.015 - PSV_{current}}{0.13 PSV_{current}^{\ 1.1}} \tag{21}$$

Equation (21) is the equation which is analyzed for all of the figures in Chapters 6 and 7. The first step towards proving the Modified Paris Model to be true is testing it by simulated data points. It might be possible that the Paris Equation can be modified to analyze other signal characteristics as shown in the next section, but the PSV proved to be the best choice for the given data sets.

Other Signal Characteristics Analyzed

In order to find the best signal characteristic to use in the Modified Paris Equation, several different common properties such as RMS of the band-passed signal, RMS overall, energy in the power spectrum and energy in the envelope spectrum were analyzed to determine which best correlates to the defect propagation. The comparison of this data is shown in Figure 35. In the legend, *E* stands for energy or power spectrum value.

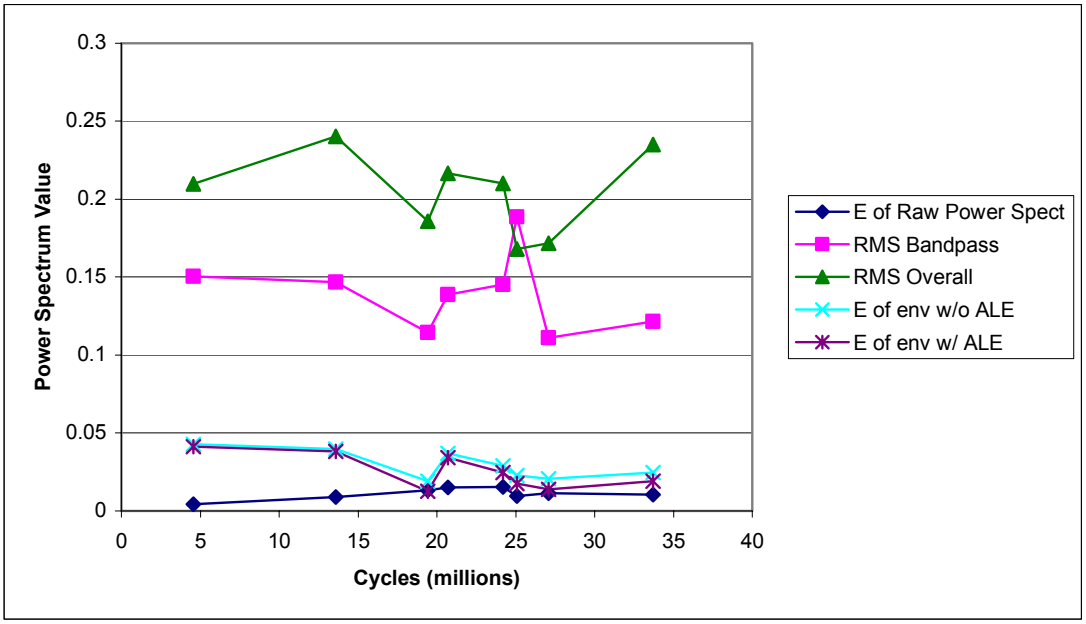

Figure 35: Comparison of Signal Characteristics

From Figure 35, the Power Spectrum Values are the only ones that increase to the point of bearing failure at 21 million cycles. The other monitoring techniques indicate a drop in value on the November 14th data set. This could be caused from a variety of reasons. The data set could simply be a poor one. There might have been a bad connection between the accelerometer and the bearing housing. There is also a possibility that the variance of the system could have caused an inaccurate portrayal of the data.

In any case, the information used for the purpose of this research is the values from the power spectrum. This data characteristic increases while the crack in the cup propagates, and then it tapers down while the movement and disorder from the failed bearing alters the energy in the signal.

CHAPTER 6

SIMULATED DATA POINTS

Now that the constants for the Paris Equation are known, simulated data can be created and analyzed to confirm or reject the validity of the proposed modification to the Paris Equation. As further described within this chapter, simulated data were chosen with equally spaced points with respect to the cycle axis, Gaussian white noise was applied to these points, and then a random selection are chosen for analysis. The reason for applying a Gaussian white noise factor to the data comes from understanding there is some random variance when collecting accelerometer data as well as information acquired from Lin and Yang [1983]. Since data sampling in industry does not occur at regular patterns, the random selection process imitates the non-ideal, real world sampling times.

Development of Simulated Data

Creating simulated data is the first step toward proving the Modified Paris Equation. Since the objective of this research is to see how well the Modified Paris Equation adheres to propagating data, it was important to simulate data that did not fit the same trend as the equation being analyzed. For this reason, the simulated data were constructed to have a linear trend. The primary consideration when determining the slope which the points should follow is to have the initial power spectrum value to be less than the critical spectrum value. Another factor to consider is the slope at which the data

follow. For the purposes of this research, the initial power spectrum value is selected to be $0.002\left(m/s^2\right)$, and the slope of the data is at $8.333x10^{-3}\,\frac{\left(m/s^2\right)}{millioncycles}$.

Figure 36 illustrates the first stage of developing the simulated data for later application in the Modified Paris Equation.

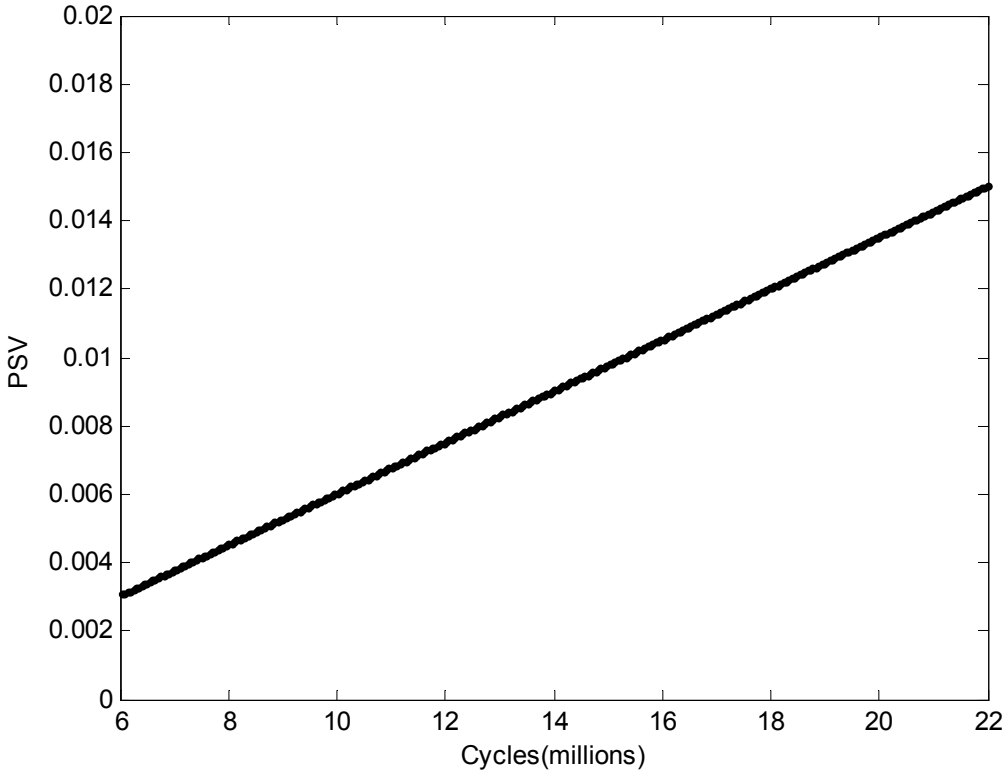

Figure 36: Simulated Data—Linear Equidistant Points

This plot simply shows hundreds of points that are equidistant along the line whose characteristics were described earlier. From this stage, a Gaussian white noise factor was added to the points. This can be shown in Figure 37. The white noise simulates the statistical differences which can be associated with collecting bearing data

with an accelerometer due to system changes and inaccurate mounting methods, for example.

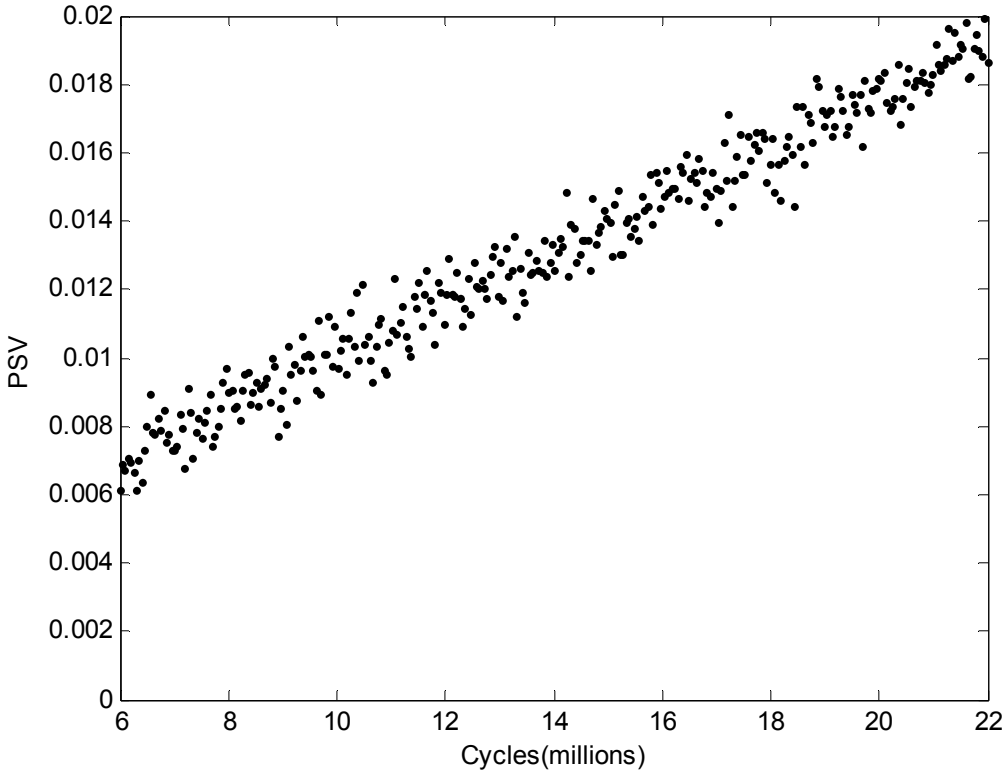

Figure 37: Simulated Data—Gaussian White Noise Applied

Once the Gaussian white noise is in the system, a Matlab code which selects random points from the whole pulls out a few dozen simulated points. Only a few data points are selected in order to simulate the inconsistent defect monitoring that takes place in an industrial environment. The trend is still linear as shown in Figure 38, but the points are no longer equidistant or as predictable as they once were.

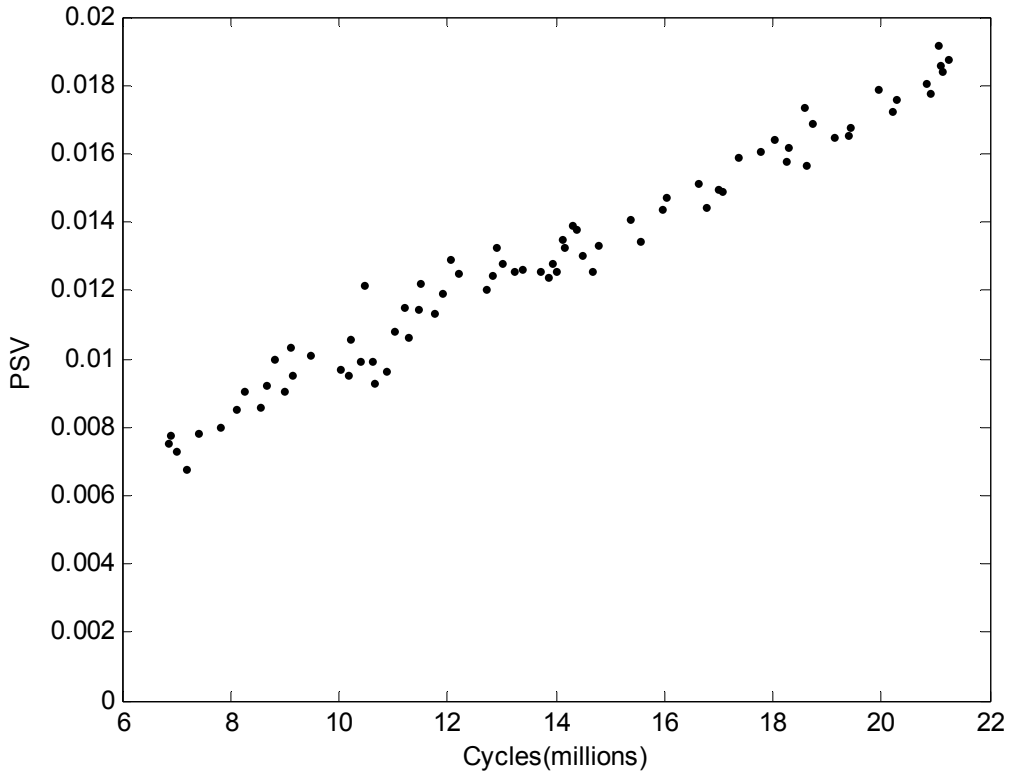

Figure 38: Simulated Data—Random Points Selected from Previous Plot

Appendix D shows the fully annotated Matlab code used when selecting the simulated data points. The the amplitude of the Gaussian white noise is arbitrary. For this research, the value is chosen to be relatively large to emulate the worst possible data collected from a system.

After the simulated points are generated with the desired spacing and amplitude as shown in Figure 38, they are broken up into smaller sets to simulate the defect propagation data collection as would happen in a real-world situation. After the data set is converted into four separate data sets, a least squares algorithm is implemented to estimate the instantaneous PSV.

Least Squares Algorithm

Once the data is arranged and selected so that it is practical and comparable to an actual data set, a Chronologically Weighted Least Squares algorithm exhibits the trend in the data. Figure 39 through Figure 42 shows the adaptation of the algorithm for increased data information as applied to simulated data. These figures illustrate the least squares code output for 20, 50, 70 and 100 percent of the data samples gathered from the simulated points once the extraneous information has been discarded.

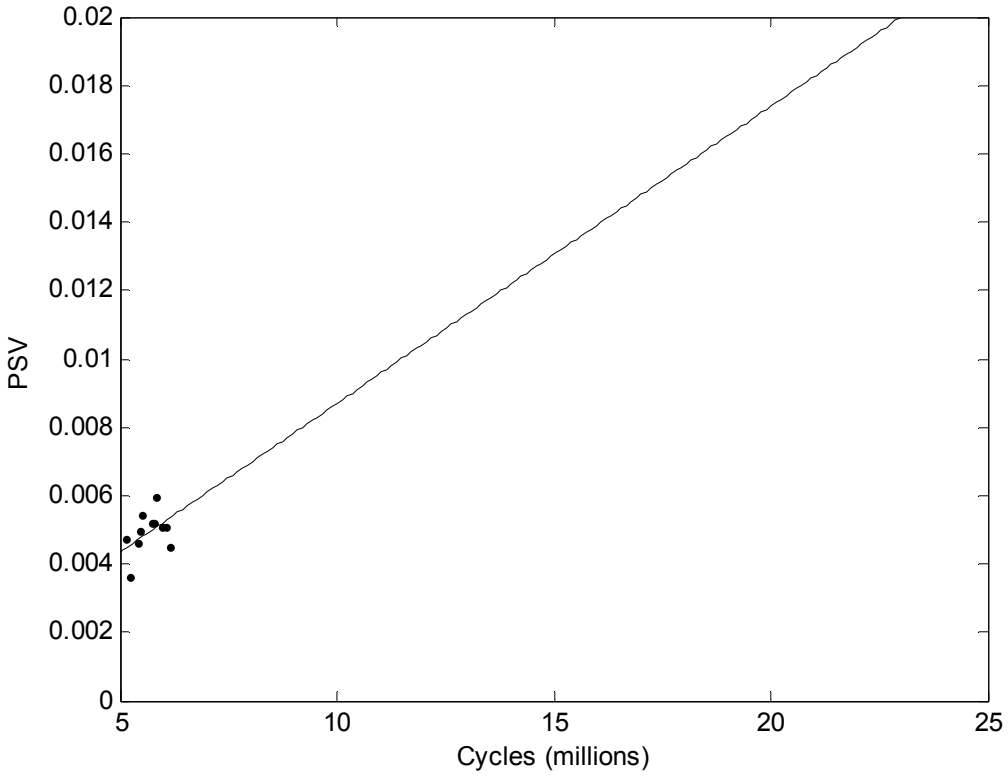

Figure 39: Simulated Data Set 1—Weighted Least Squares Algorithm

After a few cycles have been simulated, the estimated remaining cycles according to the Modified Paris Model is 23.2 million.

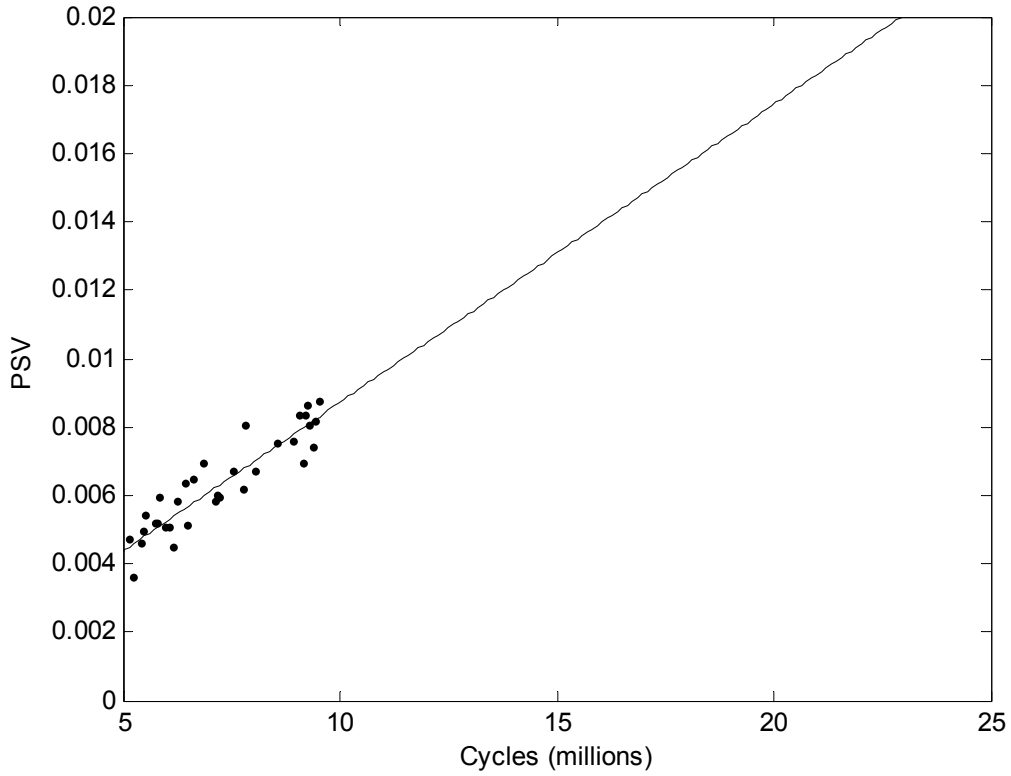

Figure 40: Simulated Data Set 2—Weighted Least Squares Algorithm

Around the 11 million cycle mark, the Modified Paris Model shows the remaining number of cycles to be approximately 10.1 million. This results in a much lower failure time than that which would be estimated from the previous figure. Figure 39 estimates the total time to failure to be 30.2 million while Figure 40 indicates the total time to failure to be 21.1 million cycles. The next data set in Figure 41 illustrates the data points up to 17.5 million cycles.

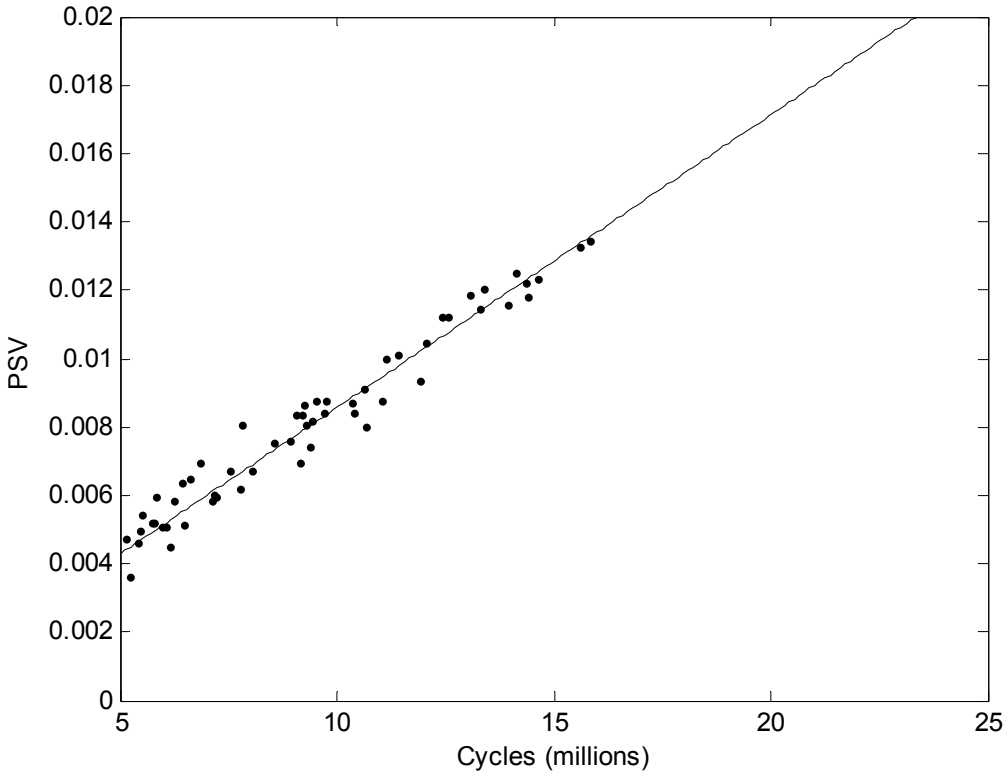

Figure 41: Simulated Data Set 3—Weighted Least Squares Algorithm

At the 17.5 million cycle mark, the Modified Paris Model results in an estimated time to failure of 1.3 million cycles. This shows the time to failure is a total of 18.8 million cycles after the initial analysis point. This value is fairly close to the estimation of 21.1 million cycles calculated from Figure 41.

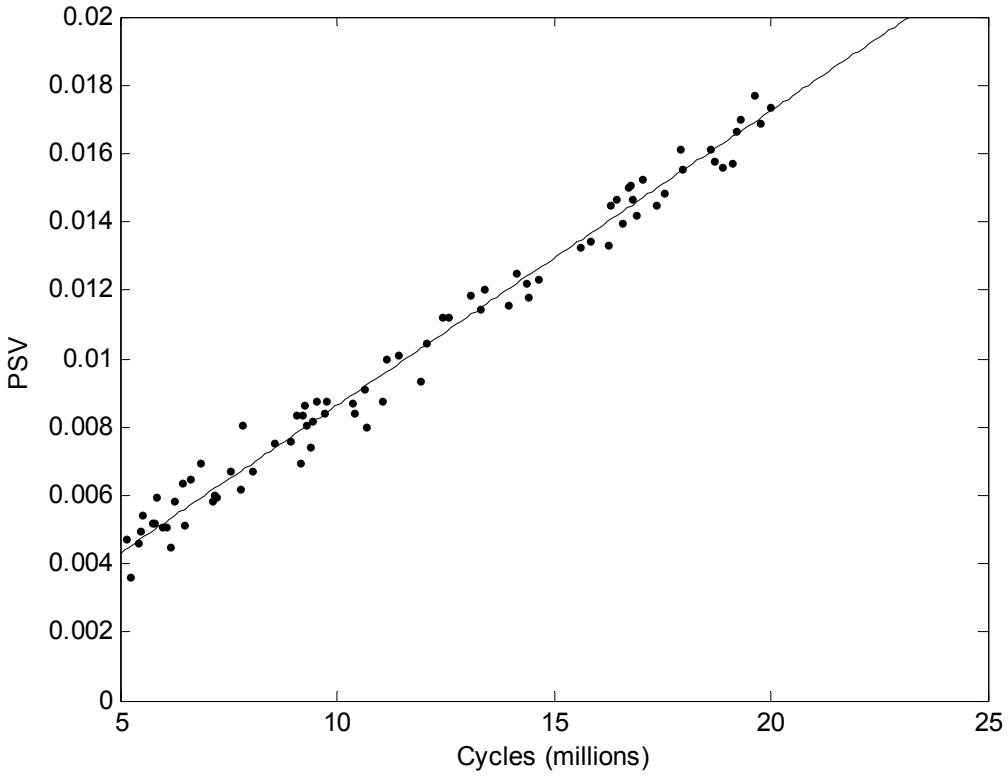

Figure 42: Simulated Data Set 4—Weighted Least Squares Algorithm

In this figure, the number of cycles at the last data point is 20 million. This value is past the 18.8 million cycles estimated failure point found from Figure 41. As expected, the Modified Paris Model indicates that the bearing failed over a million cycles ago.

While this information is a decent indication of how well the theory matches simulated data, the analysis needs to be extended to a larger data set. The modified Paris Equation is applied to thirty sets of data developed in the same manner as the previous sets, and the change in PSV with respect to remaining cycles is plotted against the Modified Paris Equation as shown in Figure 43.

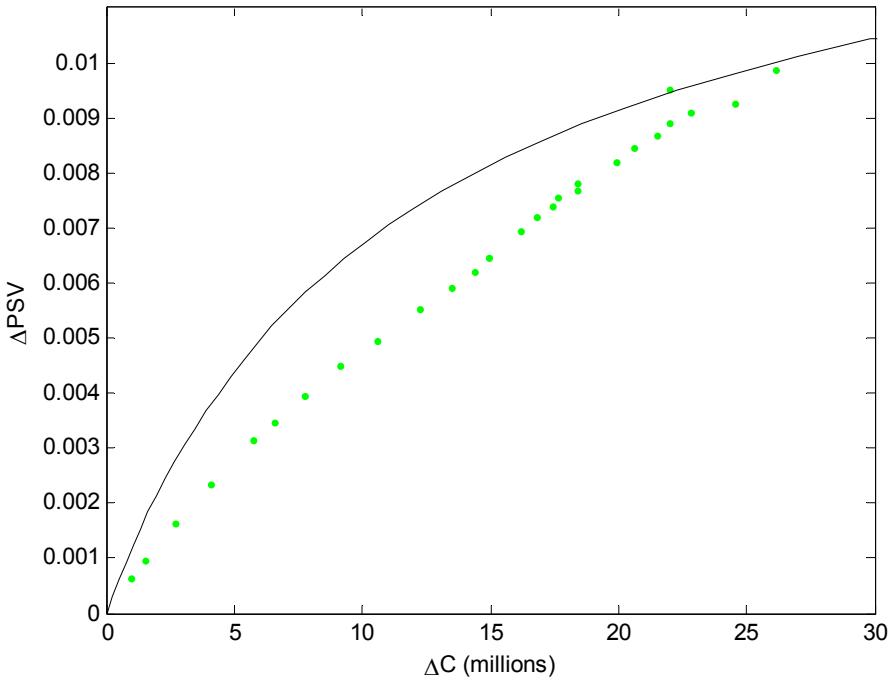

Figure 43: Plot of Simulated Data as Compared to Modified Paris Equation

Validity of the Paris Equation with Respect to the Simulated Data

As understandable, the simulated points follow a linear trend instead of the curved trend indicated by the Modified Paris Equation. However, the important information gathered from this plot is the proximity of the simulated points and the theoretical ones. Figure 44 illustrates the percent difference between the actual remaining cycles and the theoretical remaining cycles.

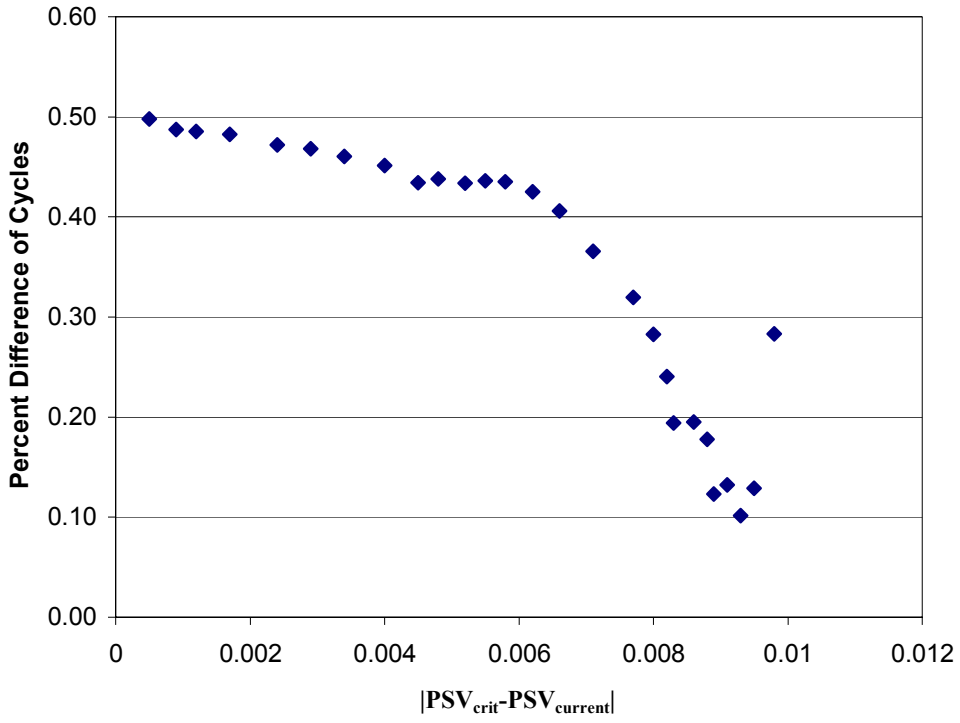

Figure 44: Percent Difference between Estimated Cycles of Simulated and Theoretical Data

This plot indicates that the percent difference between the simulated and theoretical data increases to approximately 50% the closer the bearing is to failure. This is not the most desirable trend, but it is balanced with the information shown in Figure 45. Figure 45 shows the difference between actual and theoretical cycles remaining.

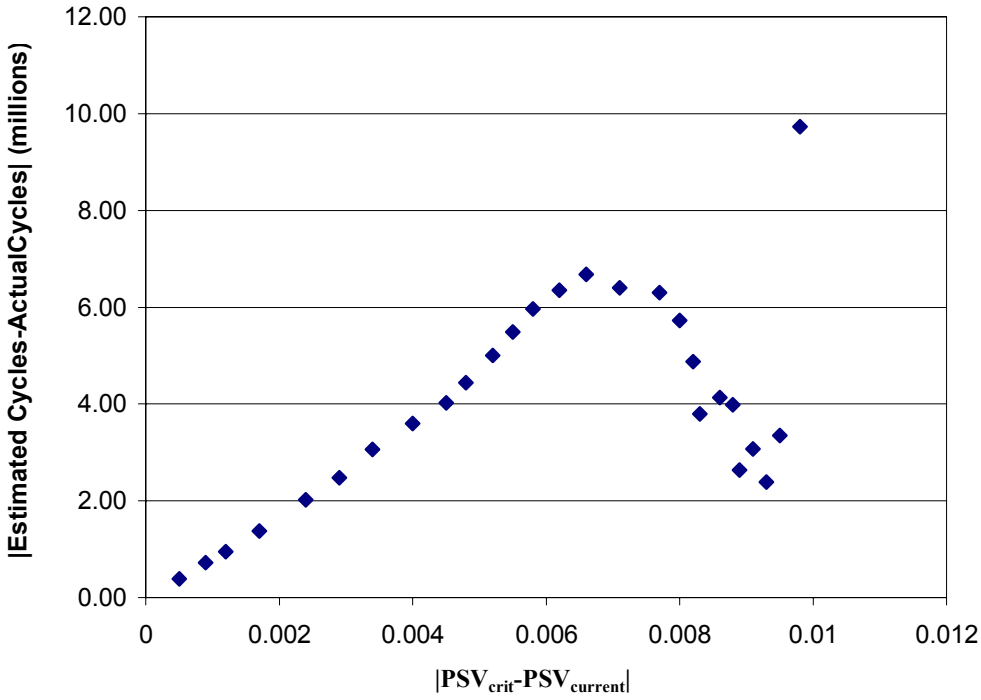

Figure 45: Cycle Difference between Theoretical and Simulated Points

From this plot, the theoretical data tends to approach the simulated data as the PSV reaches PSV_{crit}. This newfound knowledge implies an interesting point. The estimation of failure time is better when the bearing is near failure. In order to find the failure time, more data should be collected closer to the failure point.

The simulated points follow the trend of the Modified Paris equation fairly well, but the true test of the modification comes when it is compared to real data.

CHAPTER 7

EXPERIMENTALLY EXTRACTED DATA

In order to prove the Modified Paris Model is applicable not only in theory, but also in real-world circumstances, the previously acquired data must also relate to the model. The first step towards proving experimental data works with the Modified Paris Model is to work with known data to make it more complete. From there, the points were analyzed in increasingly larger sets to simulate continued accumulation of data from the system. The weighted least squares algorithm was applied to get the instantaneous energy. From there, the most current values were applied to the Modified Paris Equation, and compared to the theoretical values that should be obtained.

Filling Out the Voids in Acquired Data

Since there are few data files remaining in existence from the original experiment, theoretical points needed to be used to ensure the robustness of the model. Figure 46 through Figure 49 describe the procedure implemented for filling out the experimentally extracted data points.

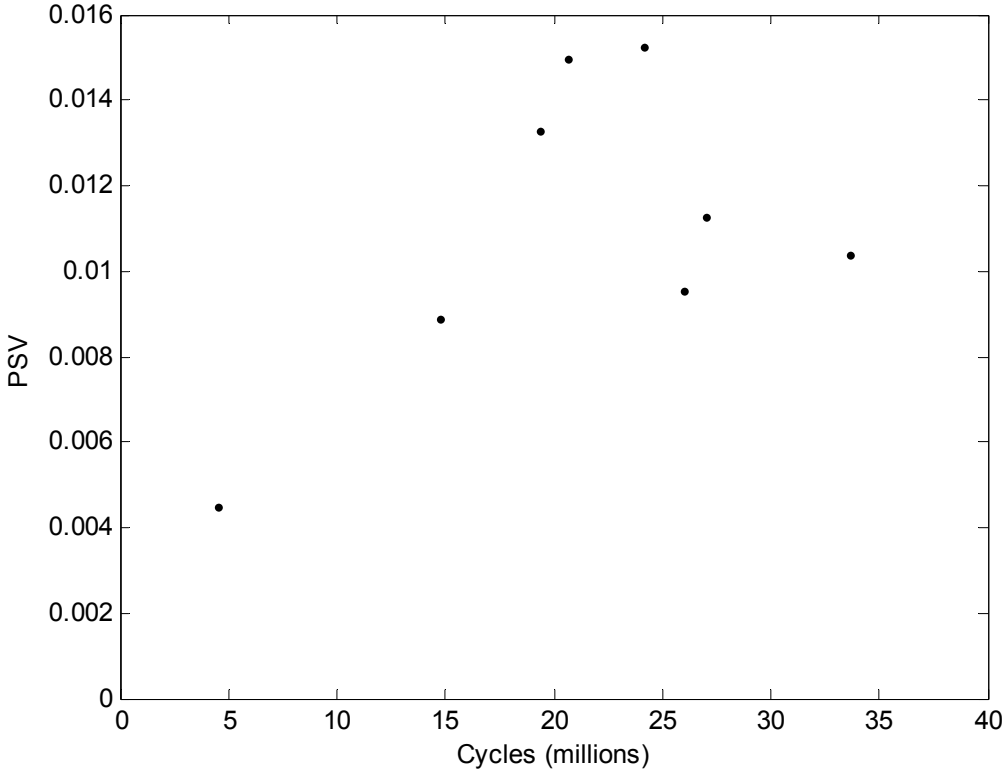

Figure 46: Plot of PSV as a Function of Cycles

This figure shows the known information about the system is not as sufficient as would be expected or preferred. In order to make the model more robust and comparable to the simulated data and Modified Paris Equation, there needs to be more data points.

The points generated to fill in the missing data were selected as linear trend lines between the original data points. Every point is equidistant from the next in the x-direction, and these points are illustrated in Figure 47.

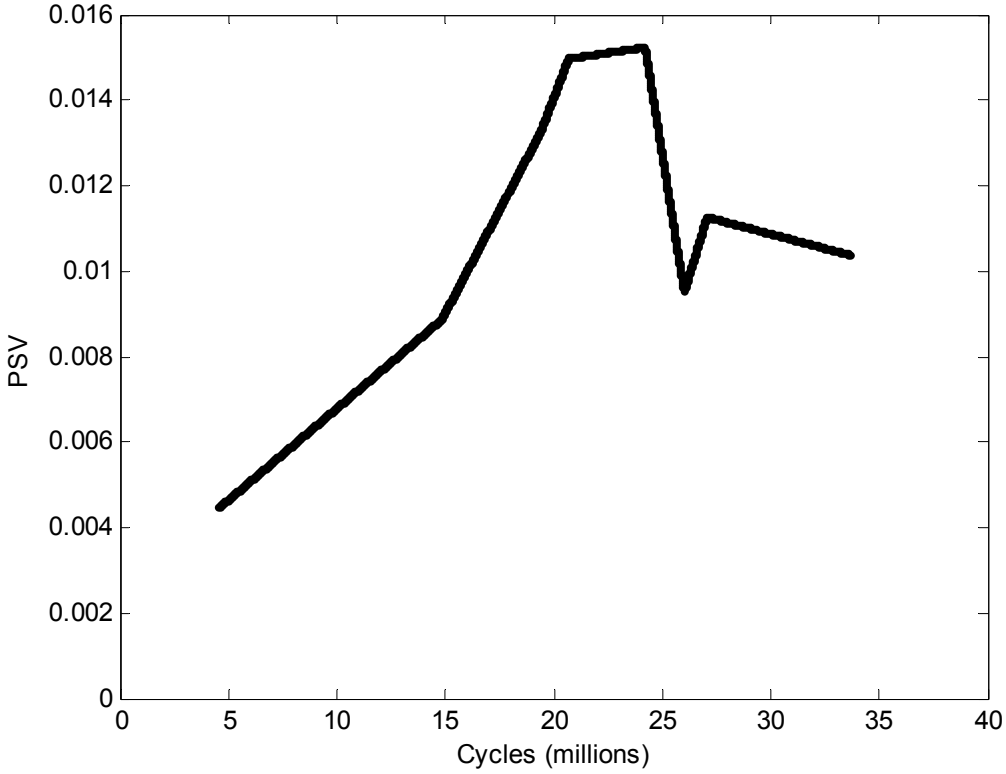

Figure 47: Equidistant Points Filling Out Experimental Data

Figure 47 displays thousands of points; it is not simply lines connecting the points. However, these points are not remotely similar to data that would be collected in industry, so the points have a few more steps of manipulation before they can be applied to the Modified Paris Equation.

Since this is an approximation, and the PSV of the bearing is somewhat in nature, a Gaussian white noise factor is added to the points as shown in Figure 48. This is much like the procedure developed for the simulated data points.

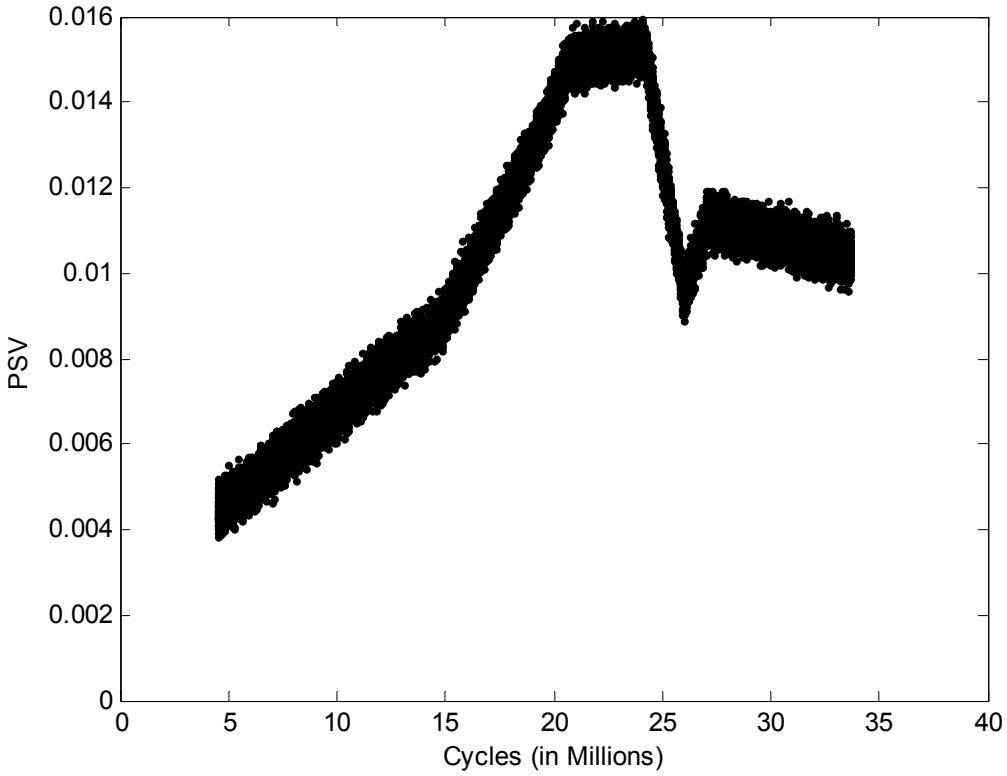

Figure 48: Application of Gaussian White Noise to Equidistant Points

Data is not typically taken periodically and as frequently as these points indicate. In accordance with this rationale, random p1oints from the previous data are selected through implementation of a Matlab code listed in Appendix E. Figure 49 illustrates the same data as Figure 48 but only showing the points extracted by the previously mentioned Matlab code.

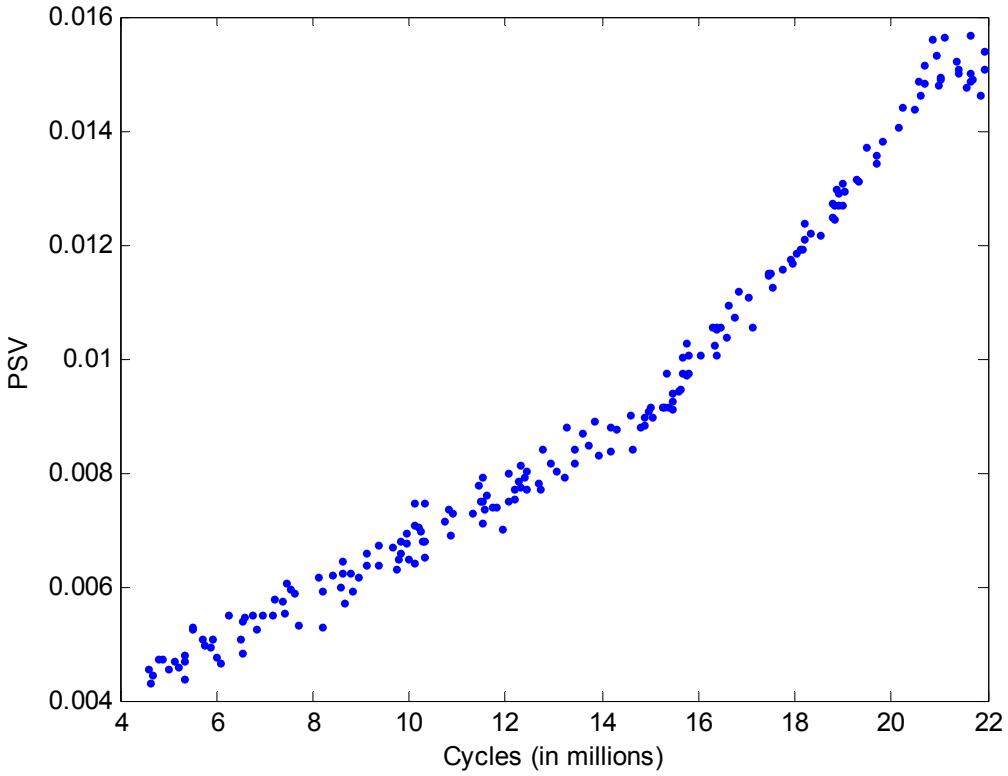

Figure 49: Random Selection of Equidistant PSV Points Obtained from Naturally Propagating Defect

Since it was previously established that the bearing failed around 21.4 million cycles, the data was truncated at the 22 million cycle mark. After the bearing reaches the failure point, the power spectrum value does not follow the same trend it followed while the defect was propagating. For these two reasons, the data after the 22 million cycle mark is no longer regarded as pertinent information.

Applying a Least Squares Algorithm to Increasing Amount of Data

The filled-in, naturally propagating data points selected undergo the same process as the simulated defect data in regards to the simulated data collection procedure and the weighted least squares algorithm that is applied to the system. First, the data are reduced

to a select number of points and gradually increased to the full set in order to simulate data collection in industry. Next, the weighted least squares algorithm is applied to the data sets, as shown in Figure 53. The least squares algorithm is designed to place more emphasis on the most recent data points since those are the ones that best describe the system's current status. For the following figures displaying the weighted least squares algorithm, the weight factor, *c*, is 4.

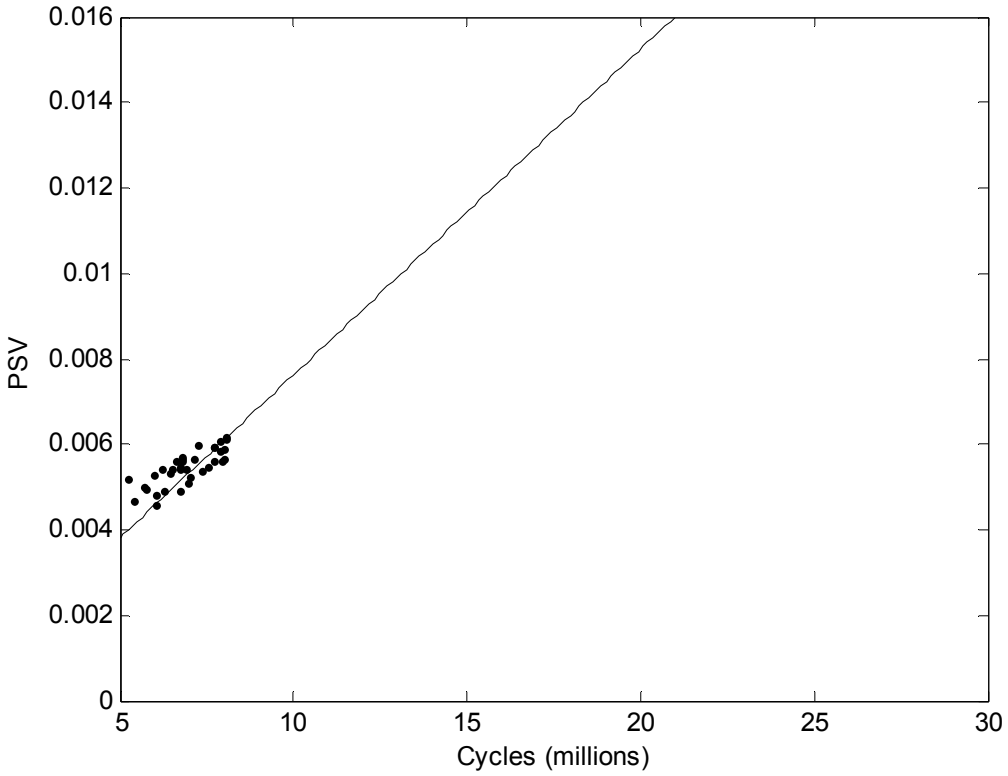

Figure 50: Propagating Experimental Data up to 8.1 Million Cycles and its Respective LS Fit

From just the first few points, it seems that the weighted least squares algorithm takes a larger pull from the latter points. The analysis of this data as well as the proceeding three plots can be found in Table 3.

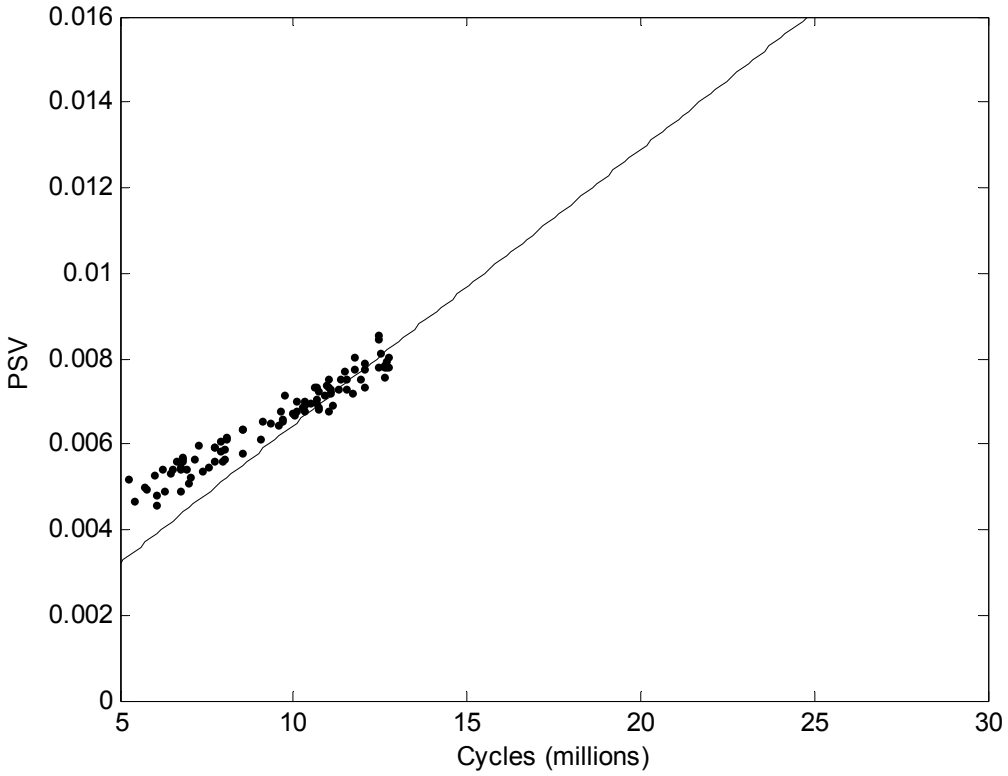

Figure 51: Propagating Experimental Data up to12.8 Million Cycles and its Respective LS Fit

The data shown in Figure 51 is only half the data chosen from the original set. Once the weighted least square algorithm is applied to this data set, the instantaneous approximate PSV for the 12.8 million cycle mark is 0.0082. Once applied to the Modified Paris Equation, the estimated remaining lifetime is 10.2 million cycles. The actual remaining lifetime is 8.6 million cycles; this is a difference of 1.6 million cycles. Even though this cycle difference is not a desirable number, there is still plenty of time to monitor the system before the bearing fails. If this is done, the failure time estimation will probably be more accurate as can be seen in Figure 52.

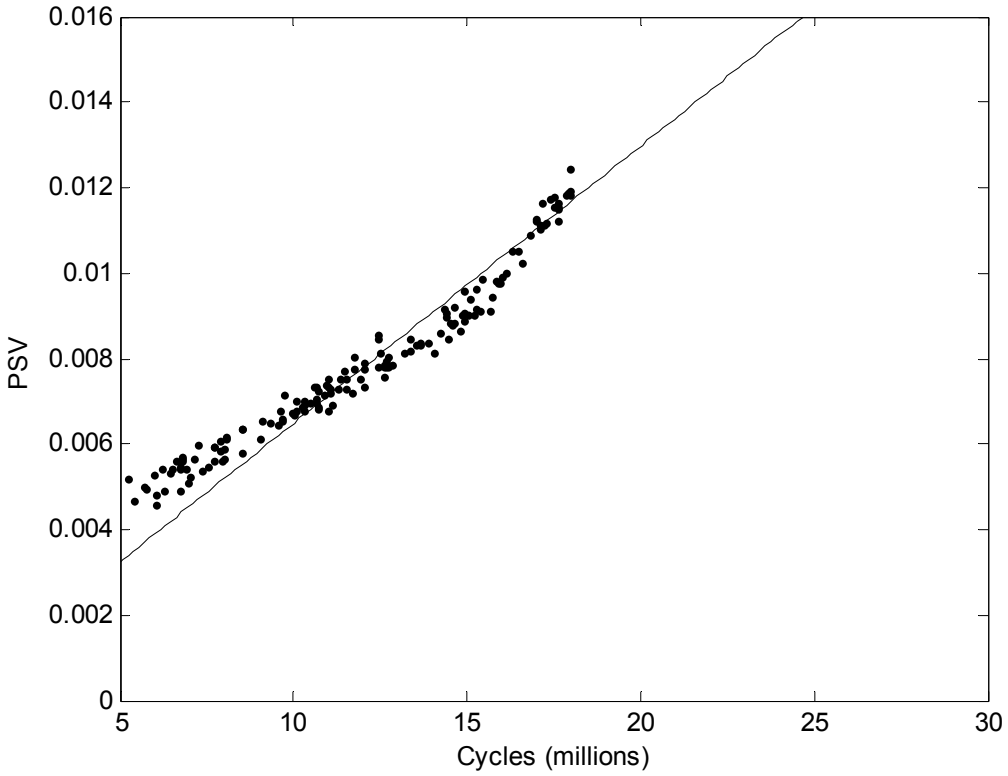

Figure 52: Propagating Experimental Data up to 18 Million Cycles and its Respective LS Fit

The data begins to ascend more rapidly than it had initially in this figure. Since the implemented algorithm places more importance on the most recent points, it is more likely that the estimation will be closer to the actual failure point than the estimation of previous plots. At this point in the data collection, approximately 75 percent of the data points are being analyzed. The estimated time to failure is 3.43 million cycles, and the actual failure point is at 3.40 million cycles. If the stochastic nature of the data points is taken into consideration, the estimation of the failure time is as close as can be expected.

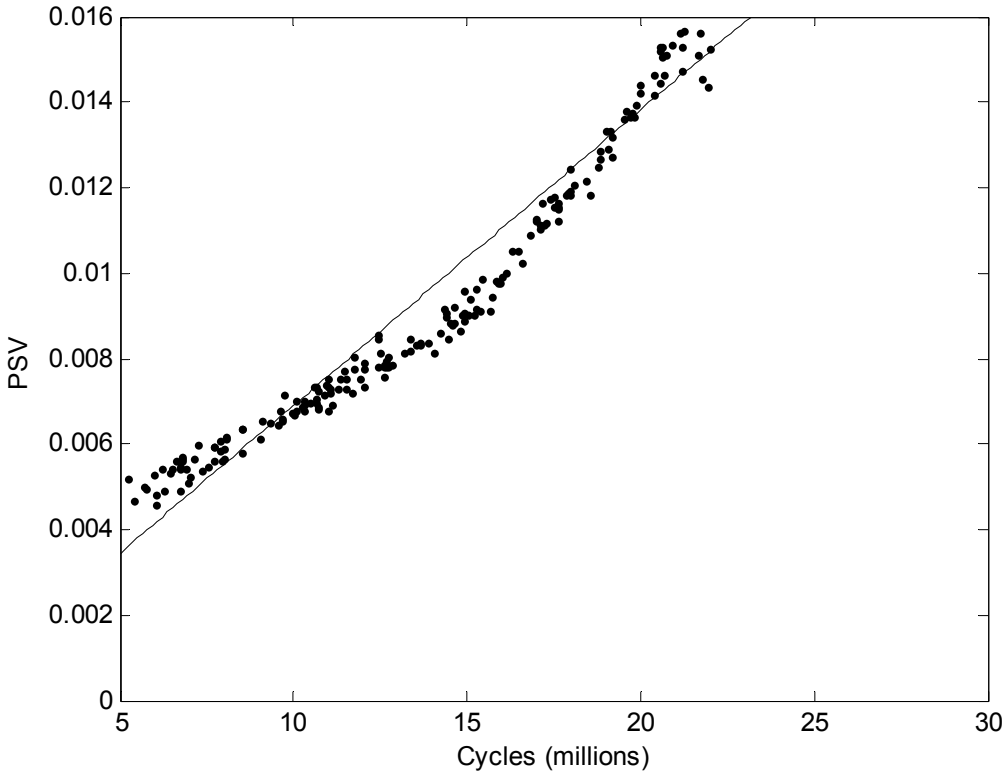

Figure 53: Propagating Experimental Data up to 20.7 Million Cycles and its Respective LS Fit

The data shown above represents 95% of the original data set. According to the weighted least squares fit, the bearing will reach the failure point in 0.57 million cycles. This value is only 100 thousand cycles off from the actual time to failure of 0.67 million cycles. The values from these plots as well as when other least squares algorithms are implemented are located in the next section.

Closeness to Actual Failure Point

From linear previous calculations, it was determined that 21.4 million cycles is the point which the bearing failed. The primary purpose of this research is to be able to determine how closely the data collected in industry relates to the Modified Paris Model.

Another purpose, however, is to show how well the weighted least squares algorithm aids in the estimation of failure times. Table 3 indicates the change between the estimated time to failure and the actual time to failure for the weighted least squares algorithm having a weighting factor of $c = 4$. The data displayed in this table refers to that which was collected for the previous figures showing the propagation of points.

Table 3: Difference Between Paris Estimation and Actual Cycles Remaining Using Weighted Least Squares Approximation with c=4

Defect Stage	Current PSV	Current Cycle	Estimated Time to Failure	Actual Time to Failure	Difference
1	0.0062	8.11	18.3	13.3	5.0
2	0.0082	12.8	10.2	8.6	1.6
3	0.0117	18.0	3.43	3.40	.03
4	0.0143	20.7	0.57	0.67	0.1

It is important to note that the difference between the actual remaining cycles and the estimated remaining cycles reduces as the defect approaches PSV_{crit}. For the most part, Table 3 shows that the estimated remaining cycles is higher than the actual remaining cycles. This is not the ideal trend, but considering how well the estimation correlates with the actual number of remaining cycles as the defect reaches failure, it is tolerable. The next table, Table 4, estimates the same defect propagation data, but the weighted least squares algorithm utilizes a weight of $c = 8$ instead of $c = 4$. The primary purpose of this information is to show that the different weights can give better or worse predictions based upon the collected data.

Table 4: Difference Between Paris Estimation and Actual Cycles Remaining Using Weighted Least Squares Approximation with c=8

Defect Stage	Current PSV	Current Cycle	Estimated Time to Failure	Actual Time to Failure	Difference
1	0.0065	8.35	16.9	13.1	3.9
2	0.0084	13.0	9.87	8.4	1.5
3	0.0117	18.1	3.41	3.3	0.11
4	0.0144	20.8	0.53	0.6	0.07

For the data points used in this research, it seems that $c = 8$ might be a better fit initially, but when $c = 4$, the estimation is closer for the critical time when the bearing is about to fail. Determining which weight value to chose depends upon the collected data. If the data is non-linear, then the recommended approach would be to choose a smaller value for *w* so that there is a greater emphasis on the most recent points. If the data is linear, the emphasis on the most recent points is not as important.

Table 5 shows the estimation of the remaining cycles of the same data when a standard least squares algorithm is implemented.

Table 5: Difference Between Paris Estimation and Actual Cycles Remaining Using Standard Least Squares Approximation

Defect Stage	Current PSV	Current Cycle	Estimated Time to Failure	Actual Time to Failure	Difference
1	0.0059	8.03	19.6	13.4	6.2
2	0.0080	12.8	11.0	8.6	2.4
3	0.0111	18.4	4.3	3.0	1.3
4	0.0139	21.5	0.92	-0.1	1.02

The primary purpose of showing Table 5 is to indicate the importance of using a weighted algorithm when monitoring bearing condtions. For every stage of defect propagation, the column indicating difference between actual and theoretical remaining cycles in the standard least squares algorithm in Table 6 are lower than when the weighted least squares algorithm is implemented—no matter which value of *c* is utilized.

Table 6: Comparison of Differences between Actual and Estimated Remaining Cycles for Three Least Squares Algorithms

% of points	*c*=4	*c*=8	standard
20	5	3.9	6.2
50	1.6	1.5	2.4
80	0.03	0.11	1.3
95	0.1	0.07	0.82

The differences are not very significant for the weighted least squares algorithm since they fall within a few million cycles of each other. The difference between the estimated and actual cycle times decreases the closer it gets to the actual failure point. Therefore, it is recommended to increase data sampling the closer the bearing approaches the failure point.

Since the purpose of this research is to easily predict the remaining number of cycles a bearing has before failure in order to reduce the maintenance costs and maximize the bearing's lifespan, the discrepancy between the estimation and the actual failure time needs to be considered. If a machine is running 24 hours a day at 1800 revolutions per minute, 4 million cycles pass after 1.5 days. The discrepancy between the estimated time to failure and actual time to failure would not really affect the time which the bearing would be extracted from the system.

In order to fully illustrate the comparison between the actual and theoretical data, Figure 54 uses more PSV points than are shown in the analysis of the four propagating figures.

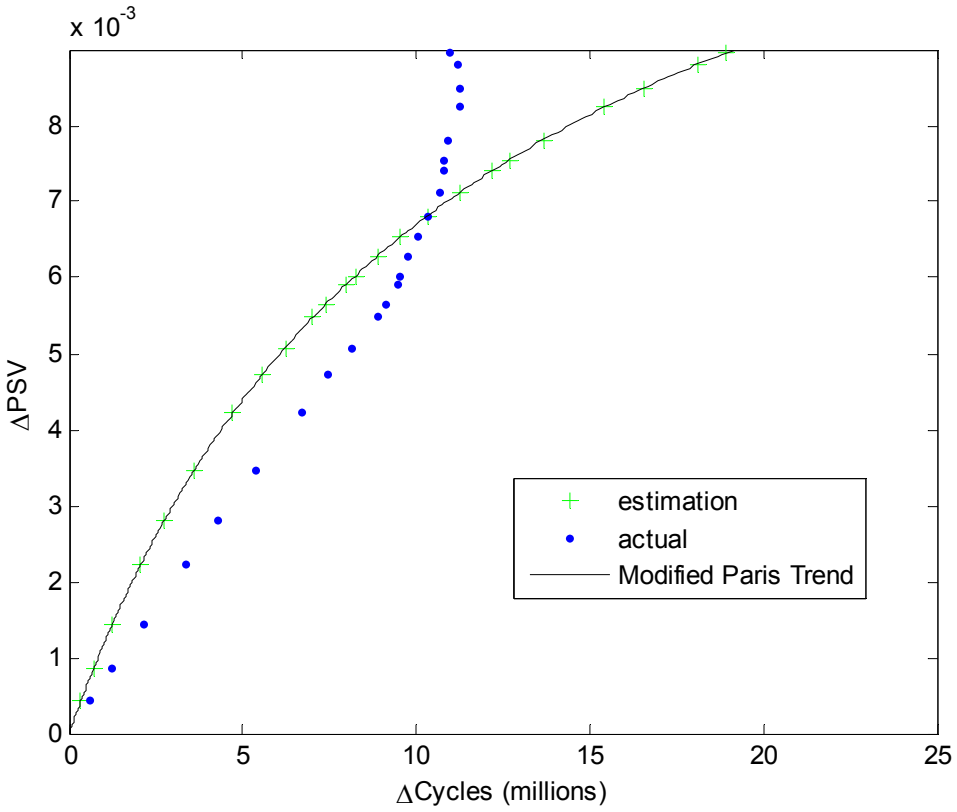

Figure 54: Estimation of Cycles to Failure for Modified Paris Equation

The data closely follow the trend of the modified equation. One positive note concerning the experimentally extracted data points is that the estimation typically errs on the side of caution; one can see that the actual remaining cycles is generally more than that which is estimated. The points for the estimation and the actual data were plotted on the same ΔPSV line so that it is easily visible that the estimation becomes more accurate once the defect has almost reached what is considered the failure point. The code used for plotting Figure 54 is located in Appendix F.

Like the simulated data, it is also important to note the trends in percent difference as well as difference in cycles as the bearing approaches failure.

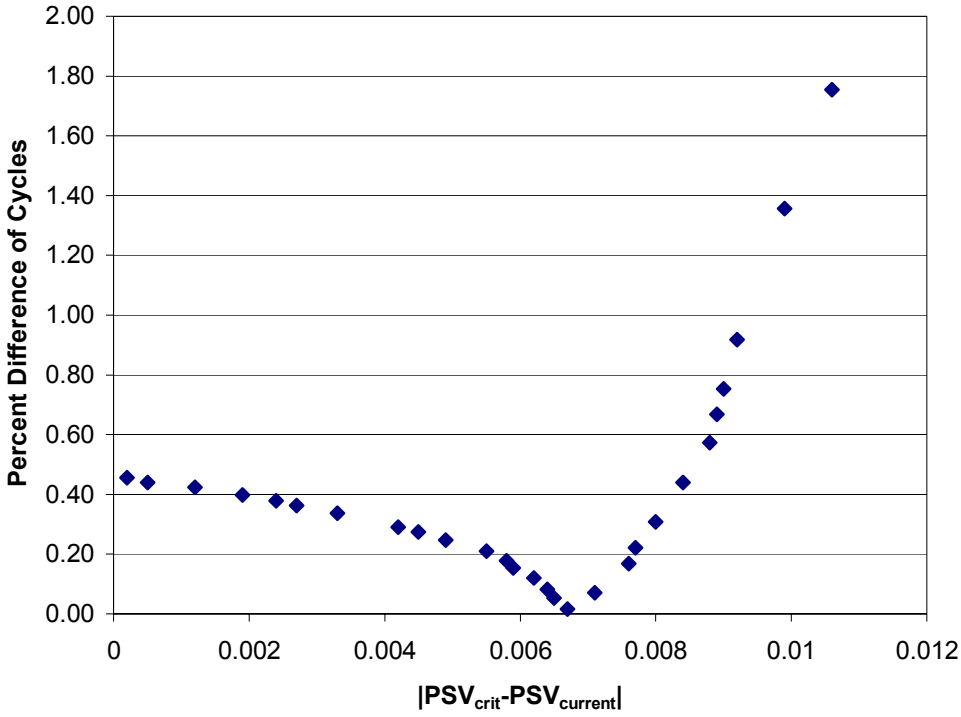

Figure 55: Percent Difference between Estimated Cycles of Experimental and Theoretical Data

Similar to the simulated data points, the experimental data tends to increase in percent difference as the bearing approaches the failure point. Once again, the percent difference approaches approximately 50%. This is an interesting point, but it does not show how closely the data approximates the data in terms of cycles. Figure 56 indicates the cycle difference comparison.

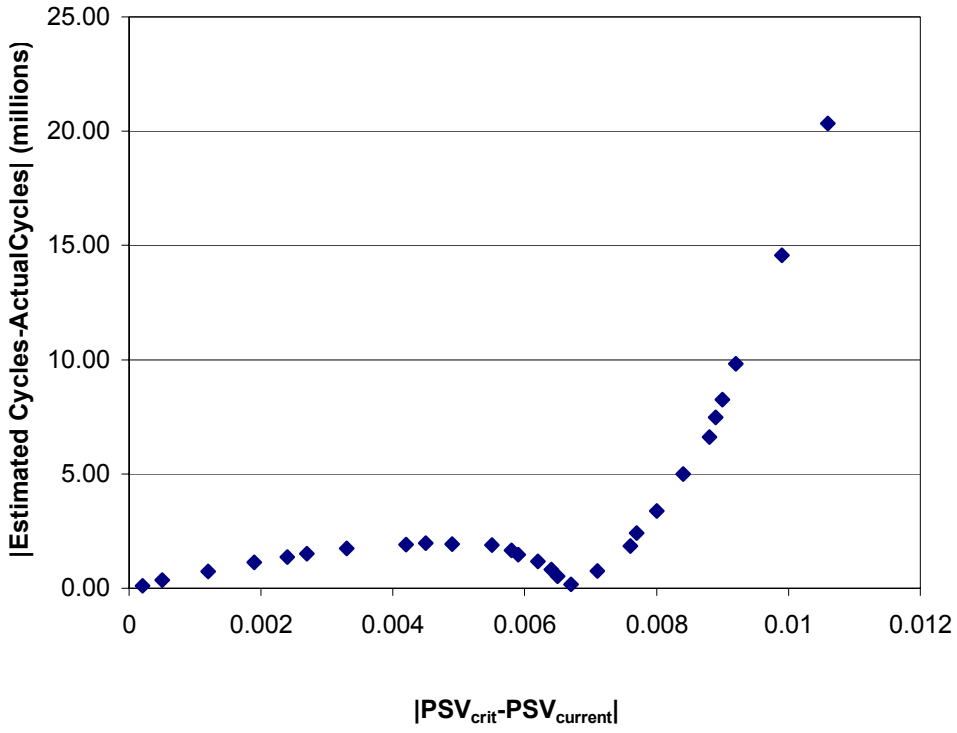

Figure 56: Cycle Difference between Theoretical and Experimentally Extracted Points

Once again, the experimentally extracted points follow the same trend as the simulated points. As the defect approaches failure, the estimation approaches the experimentally extracted time to failure. This also reinforces the belief that the data should be collected more frequently as the bearing reaches the failure criteron.

CHAPTER 8

CONCLUSION

From the information delivered in Chapters 6 and 7, it is shown that the modification to the Paris Equation is a simple, effective means of determining the remaining cycles before a rolling element bearing reaches its failure point. As the defect propagates, the Modified Paris Model becomes more accurate. The estimation is not only close to the true remaining cycles, but it also remains on the conservative side of prediction. It is safer for the sake of the system to remove a bearing prematurely than after it has affected connected components.

In addition to showing that the Modified Paris Model aids to the prediction of failure, this research also shows the importance of using a weighted least squares algorithm as opposed to a standard least squares algorithm. Sometimes the data collection can show power spectrum values which are not truly indicative of the bearing's status. The most recent data points also relay the most accurate current information about the bearing. For these reasons, it is important to put a greater weight on the most recently acquired data. The amount of weight placed on the most recent points is dependent upon the variation of the data, the data's general trend, and the person implementing the code.

Simplicity of the Presented Research

Modification of the Paris equation to utilize a signal's PSV increases bearing efficiency by no longer requiring machine stoppage for inspection or premature replacement; determining the failure time of a defect does not require stopping the system and measuring its size. This research shows that the maximum PSV level around the

resonant frequency of the system implemented in the Modified Paris Equation indicates the remaining lifetime of the bearing.

In order to maximize the lifespan of a bearing, one only needs to collect the time signature of the equipment a few times to obtain the trend line of the defect propagation. As soon as the general trend is known, the data need only be updated a few times to ensure that the PSV is increasing as predicted.

Drawbacks of Presented Research

Some *a priori* information of the system does need to be known. The values for P_o and m are essential to use this prognostic method. This does require on-line monitoring of a bearing when the system is running. If this is impossible to do, then the Modified Paris Equations are probably not useful for application as shown from Figure 20 and Figure 19.

There is a possible means of avoiding determining P_o and m from the on-line monitoring method if the bearings are carefully monitored after a crack is detected. Once the general trends of the defect propagation are known, different values of P_o and m can be iterated to best fit the data. This is not the recommended method for finding these material constants, but there is a possibility that it could be done. After more research is completed on the PSV, this concept could be one to look into for future work in the bearing prognostics area.

Proposed Future Work

Further work can be done to ensure the robustness of this application. In would be beneficial to rerun the experiment with a few new bearings to ensure the critical PSV value at which the bearing fails. It would also be beneficial if the EDM cracks were placed on the cone as well as the cup to see if the deferring components resulted in different PSV_{crit} calculations.

Another important aspect which needs to be confirmed is the critical PSV for all rotational systems. The modified equation should also be tested and confirmed on rotating equipment other than bearings. If all pieces of rotating machinery follow the same trend of the Modified Paris Equation, it would take little effort and equipment to monitor all of the components in a system.

More future work can be done if RMS or envelope spectrum values work in Paris Equation. It is simple to only take the Fast Fourier Transform of the data. If it can be proven that the RMS or envelope spectrum gives a better failure estimate, then the extra steps needed to calculate these values could be worth the effort and time. Unless the equipment is not costly or important, it should always be monitored to ensure the productivity of the system and the plant as a whole.

Contributions

There are several contributions included in this thesis. The primary contributions of this research are as follows:

1. The modification of the Paris-Erdogan Equation from monitoring the defect size to instead determining the energy of the system is a conservative estimate for remaining life for rolling element bearings having a defect on the outer race.

2. This thesis shows how to determine the three constants needed to implement the Modified Paris Equation (C_o, n, and PSV_{crit}).
3. Focusing on the most recent points to estimate the current PSV proves to be the most beneficial when using the Modified Paris Equation.
4. As the defect reaches the critical energy value, the Modified Paris Equation becomes more accurate.

These points are useful for both future research on bearing test stands as well as application in industry. One goal of this research was to determining a means of monitoring a rolling element bearing without interrupting the system, and the contributions described in this thesis prove that it can be done.

APPENDIX A

CHRONOLOGICALLY WEIGHTED LEAST SQUARES MATLAB CODE

```
%Tara R. Lindsay
%Least Squares Linear Fit
%Added weights so that the latter points have more
%impornance than previous points

%%%%%%%%%%%%%%%%%%%%%%%%%%%%%%%%%%%%%%%%%%%%%%%%%%%%%%%%
function [c d]=chronweightlsquares(x_vect,y_vect,weight)
%y=cx+d

n=length(x_vect);
x2=0;    %x^2
y1=0;    %y
xy=0;    %x*y
x1=0;    %x

for ii=1:1:n
   w=1/(n-ii+weight);
   x2=x2+w*x_vect(ii)^2;
   y1=y1+w*y_vect(ii);
   xy=xy+w*x_vect(ii)*y_vect(ii);
   x1=x1+w*x_vect(ii);
end
d=(x2*y1-xy*x1)/(n*x2-x1^2);
c=(n*xy-x1*y1)/(n*x2-x1^2);
```

APPENDIX B
FFT AND HFRT CODE

```
%Tara Lindsay
%This code takes data received from a bearing and converts it from the time
%domain to the frequency domain in order to determine bearing defect size.
%This code also includes the HFRT to determine where the bearing fails.

%  Figures generated
%  Figure 1 = Raw Data
%  Figure 2 = Raw data spectrum (fft)
%  Figure 3 = Envelope spectrum

clear;
close all;
%constants for the system for paris's equation
Co=0.13;
n=1.1;

%The following variables dimention the bearing used in research at Tech
rpm=1600;           %[rev/minute] bearing rotation speed
f=rpm/60;           %[rev/minute] bearing rotation speed
ID=1.625;           %[inches] inside diameter
OD=2.891;           %[inches]  outside diameter
no_balls=19;        %[balls]  number of balls in the bearing
ball_d=0.309;       %[inches]  ball diameter
alphadeg=13.13;     %[degrees]
alpha=alphadeg*(pi/180);%[radians]  taper angle
dm=2.25;            %[inches] pitch diameter
%determine frequencies of ball pass inner race, ball pass outer race,
%and rollers. Defect is on outer race for this research.
f_bpir = no_balls*f/2*(1+(ball_d/dm)*cos(alpha))
f_bpor = no_balls*f/2*(1-(ball_d/dm)*cos(alpha))
f_r = no_balls*(f*dm)/2*(1-((ball_d/dm)*cos(alpha))^2)
f_c =f/2*(1-(ball_d/dm)*cos(alpha))

%Load data and find pertinent parameters
load 'C:\Documents and Settings\Tara\My
Documents\GaTech\Research\Data4Research\nov14.txt';
vib_datapoints=length(nov14);    %number of vibration data points
vib=nov14(1:vib_datapoints,1);  %pulls out the correct column of data
vib_time=1.0;                %[seconds] length of time data was sampled
vib_fs=30000;                %[samples/second]sampling frequency

% This is a plot of the raw data
```

```
figure(1);
plot(0:1/vib_datapoints:(1-1/vib_datapoints),vib);
title(['raw data'])
xlabel('Time (s)');
ylabel('Acceleration (g)');

% Next step is to find fft/power spectrum
X=fft(vib)/vib_datapoints;
df=vib_fs/vib_datapoints;

%This is a plot of the Power Spectrum (fft(rawdata))
figure(2)
plot(df:df:vib_fs/2-df,abs(X(2:vib_datapoints/2)));
title(['Power Spectrum'])
xlabel('Frequency (Hz)');

%Third step of program is to find the envelope spectrum of the data
%This shows the defect location.

%Resonant frequency of the system is around 5500 Hz
Wn_vib=[4000 6000]*2/vib_fs;
cutoff=400;
cutoff_vib=cutoff*2/vib_fs;     %cutoff frequency for bandpassed filtration of data

[top,bottom]=butter(5,Wn_vib); %use a butterworth filter for bandpassing
[t,b]=butter(5,cutoff_vib);
xx=filter(top,bottom,vib);
X=fft(vib)/vib_datapoints;
xxx = abs(xx);
xxx=filter(t,b,xxx);
XXX=fft(xxx)/vib_datapoints;          %envelope spectrum output

figure(3)
plot(df:df:cutoff-df,abs(XXX(2:floor(cutoff/df))));
title('Envelope Spectrum w/o ALE');
xlabel('Frequency (Hz)');
```

APPENDIX C
POWER SPECTRUM VALUE EXTRACTION CODE

```
%Tara Lindsay
%This code finds the maximum energy surrounding the resonant frequency of
%the data

function [energy_nov20]=energy_nov20(low_lim, up_lim)

%Vibration sensor data information
%Loaded file is measured in volts
load 'C:\Documents and Settings\tlindsay.PMRC_DOMAIN\My
Documents\Research\Research\My
Thesis\April24\DataAndDescriptions\nov20_08p30_0.txt';
vib_datapoints=length(nov20_08p30_0);      %number of vibration data points

vib=nov20_08p30_0(1:vib_datapoints,1);
vib_time=1.0;              %[seconds] length of time data was sampled
vib_fs=30000;              %[samples/second]sampling frequency

% %begin filtering process
fast_data=fft(vib)/vib_datapoints;
df=vib_fs/vib_datapoints;

x_vect=df:df:vib_fs/2-df;
y_vect=abs(fast_data (2:vib_datapoints/2));
lxv=length(x_vect);

% Cutting down Power Spectrum plot to encompass only the energy
%around the resonant frequency of the system.
index_low=round(low_lim/df);
index_high=round(up_lim/df);
diff=index_high-index_low;
for ii=1:1:diff;
   x_res(ii)=x_vect(index_low+ii-1);
   y_res(ii)=y_vect(index_low+ii-1);
end

format long g;
energy_nov20=max(y_res);
```

APPENDIX D
SIMULATED DATA POINTS PLOTS

```
%Tara Lindsay
%Strictly Simulated Data
%This code forms the plot showing the selection of random points, and the
%comparison plot of the theoretical Paris Equation with the sim points.
%(This is known as deltaCdeltaPSV plot)
%FakeGenSignal
%Used for checking algorithm for simulated points
pts=400;
int=0.002;
FakeCycles=linspace(2,20,pts);
Base=linspace(0,0.015,pts);
figure(1)
plot(FakeCycles,abs(Base),'k.')
ylabel('PSV')
axis([6 20 0 .02])
xlabel('Cycles(millions)')
axis([6 20 0 .02])

%Same as above plot, but each point has a gaussian white noise factor
%associated with it.
gaussian_noise=0.0005*wgn(1,400,2);
Base_Gauss=gaussian_noise+Base+int;
figure(2)
plot(FakeCycles,abs(Base_Gauss),'k.')
ylabel('PSV')
axis([6 20 0 .02])
xlabel('Cycles(millions)')

%Take random points from plot #2
rndpts=pts/4;
random_pts_vector=sort(round(rand(rndpts,1)*pts));
%**********need to determine how to pull out indicies*********
inew=1;
jnew=1;
for jj=1:1:rndpts;
   for ii=inew:1:pts;
      if random_pts_vector(jj)==ii;
         rndpts_eng(jj)=Base_Gauss(ii);
         rndpts_cyc(jj)=FakeCycles(ii);
         inew=ii;
      end
   end
end
```

```
figure(3)
plot(rndpts_cyc,rndpts_eng,'k.')
axis([6 20 0 .02])
xlabel('Cycles(millions)')
ylabel('PSV')
%~~~~~~~~~~~~~~~~~~~~~~~~~~~~~~~~~~~~~~~~~~~~~~~~~~~~~~~~~~~~~~~~~~~~~~~~

E_final=0.015022;
Co=.13;
n=1.1;
lnevm=length(rndpts_cyc);
goodenoughpoints=4;
new_eng_val=zeros(lnevm,goodenoughpoints);
new_cyc_val=zeros(lnevm,goodenoughpoints);

for kk=1:goodenoughpoints
   percent=kk/goodenoughpoints;
   vector(kk)=round(lnevm*percent);
   for ii=1:1:vector(kk);
      new_eng_val(ii,kk)=rndpts_eng(ii);
      new_cyc_val(ii,kk)=rndpts_cyc(ii);
   end
end

Y_lin=0.001:.0001:.02;
for jj=1:goodenoughpoints
   [c(jj)
d(jj)]=chronweightlsquares(new_cyc_val(1:vector(jj),jj),new_eng_val(1:vector(jj),jj));
   CurrentC(jj)=max(new_cyc_val(:,jj));
   CurrentE(jj)=c(jj)*CurrentC(jj)+d(jj);
   deltaE(jj)=E_final-CurrentE(jj);
   deltaC(jj)=(deltaE(jj))/(Co*CurrentE(jj)^n);
   for zz=1:1:length(Y_lin)
      X_lin(jj,zz)=(Y_lin(zz)-d(jj))/c(jj);
   end
   figure(jj+3)
   plot(X_lin(jj,:), Y_lin(1,:),'k-', new_cyc_val(1:vector(jj),jj),
new_eng_val(1:vector(jj),jj),'k.')
   axis([5 25 0 .02])
   ylabel('PSV')
   xlabel('Cycles (millions)');
end
deltaC

figure(8)
```

```
plot(CurrentC(1:jj),CurrentE(1:jj),'k.')
xlabel('Delta Cycles(millions)');
ylabel('Delta Power Spectrum Value ((m/s^2)^2)');
axis([0 20 0 .016]);
```

APPENDIX E
NATURALLY PROPAGATING FIGURES

```
% This code shows how the propagating points were chosen and the implementation
% of the chronologically weighted least squares algorithm

clear all;
close all;
E_final=0.015022;
weight=4;
Co=.13;
n=1.1;

%Days corresponding to Energy and Cycles
D= [924   1021   1114   1116   1120   1122   1125   1217]';

% # of cycles the bearing has undergone on given day
C=  [4.560    14.832    19.408   20.688   24.208    26.016    27.072    33.720]';

%Area associated with number of cycles and day
Area=[1.785    5.5683    5.6175    5.8092    8.0904    8.2242    8.0415    8.4329]';

%Maximum Energy near resonant freq. after signal has been filtered
E=[0.00444783222028835
  0.0088591945233774
  0.0132573959978724
  0.0149704390918183
  0.0152343720991011
  0.00951013385028358
  0.0112612969517493
  0.0103651024541256];

% Equidistant x-points
deltaC=(C(8)-C(1));
no_pts=1000*deltaC;
delta=1/1000;
delta_c(1)=C(1);

for ii=2:1:no_pts
   delta_c(ii)=delta_c(ii-1)+1/1000;
end

for ii=1:1:7;
   m(ii)=(E(ii+1)-E(ii))/(C(ii+1)-C(ii));
   b(ii)=E(ii)-m(ii)*C(ii);
end
```

```
ii=1;
val=1;
for jj=val:1:no_pts
   energy(jj)=m(ii)*(delta_c(jj))+b(ii);
   if delta_c(jj)>=C(ii+1);
      ii=ii+1;
   end
   val=jj;
end

%Plot of energy versus bearing cycles
fig=1
figure(fig);
fig=fig+1;
plot(C, E,'k.')
axis([0 40 0 .016])
ylabel('PSV')
xlabel('Cycles (millions)')

%Plot of energy versus bearing cycles 29260 points
figure(fig);
fig=fig+1;

plot(delta_c, energy,'k.')
axis([0 40 0 .016])
ylabel('PSV')
xlabel('Cycles (millions)')

figure(fig);
fig=fig+1;
y=wgn(1,no_pts,2);
scale=0.0002;
new_energy=y*scale+energy;

plot(delta_c, new_energy,'k.')
axis([0 40 0 .016])
xlabel('Cycles (in Millions)')
ylabel('PSV')

%~~~~~~~~~~~~~~~~~~~~~~~~~~~~~~~~~~~~~~~~~~~~~~~~~~~~~~~~~~~~
cutoff_cyc_val=22;
delt_cutoff=cutoff_cyc_val-delta_c(1);
nopts=delt_cutoff*1000;
number_of_desired_samples=200
random_points=rand(number_of_desired_samples,1);
sort_rand_pts=sort(random_points)*nopts;
```

```
new_cyc_index=round(sort_rand_pts);
new_cyc_val=C(1)+delta*new_cyc_index;

%Find the energy values corresponding to this cycle vector
delta_c=round(delta_c*1000)/1000;
val=1;
for jj=1:1:number_of_desired_samples;
   for ii=val:1:nopts;
      if new_cyc_index(jj)==ii;
         new_eng_val_max(jj)=new_energy(ii);
      end
   end
end

Y_lin_4=0.001:.0001:.016;
for jj=1:1:length(Y_lin_4)
   X_lin_4(jj)=(Y_lin_4(jj)-d_4)/c_4;
end

%~~~~first set of data points~~~~~~~~~~~~
for ii=1:1:round(length(new_eng_val_max)*.2)
   new_eng_val_first(ii)=new_eng_val_max(ii);
   new_cyc_val_first(ii)=new_cyc_val(ii);
end

[c_1 d_1]=chronweightlsquares(new_cyc_val_first, new_eng_val_first, weight);
% C_final_1=(E_final-d_1)/c_1
% deltaT_lin_1=C_final_1-new_cyc_val_first(ii)
CurrentCycle_1=new_cyc_val_first(ii)
CurrentEnergy_1=c_1*CurrentCycle_1+d_1
deltaT_lin_1=(E_final-CurrentEnergy_1)/(Co*CurrentEnergy_1^n)

Y_lin_1=0.001:.0001:.016;
for jj=1:1:length(Y_lin_1)
   X_lin_1(jj)=(Y_lin_1(jj)-d_1)/c_1;
end
%~~~~~~~~~~~~~~~~~~~~~~~~~~~~~~~~~~~~~~~~~~~~~~~~~~~~~~~~~~~~~~~~~~~~~~~~~~~~~~~~
%~~~~~~~~~~second set of data points~~~~~~~~~~
for ii=1:1:round(length(new_eng_val_max)*.5)
   new_eng_val_second(ii)=new_eng_val_max(ii);
   new_cyc_val_second(ii)=new_cyc_val(ii);
end

[c_2 d_2]=chronweightlsquares(new_cyc_val_second, new_eng_val_second, weight);
% C_final_2=(E_final-d_2)/c_2
% deltaT_lin_2=C_final_2-new_cyc_val_second(ii)
```

```
CurrentCycle_2=new_cyc_val_second(ii)
CurrentEnergy_2=c_2*CurrentCycle_2+d_2
deltaT_lin_2=(E_final-CurrentEnergy_2)/(Co*CurrentEnergy_2^n)

Y_lin_2=0.001:.0001:.016;
for jj=1:1:length(Y_lin_2)
   X_lin_2(jj)=(Y_lin_2(jj)-d_2)/c_2;
end

%~~~~~~~~~~~~~~~~~~~~~~~~~~~~~~~~~~~~~~~~~~~~~~~~~~~~~~~~~~~~~~~~~~~~~~~~~~~~~~~~
%~~~~~~~~~~third set of data points~~~~~~~~~~
for ii=1:1:round(length(new_eng_val_max)*.80)
   new_eng_val_third(ii)=new_eng_val_max(ii);
   new_cyc_val_third(ii)=new_cyc_val(ii);
end

[c_3 d_3]=chronweightlsquares(new_cyc_val_third, new_eng_val_third, weight);
% C_final_3=(E_final-d_3)/c_3
% deltaT_lin_3=C_final_3-new_cyc_val_third(ii)
CurrentCycle_3=new_cyc_val_third(ii)
CurrentEnergy_3=c_3*CurrentCycle_3+d_3
deltaT_lin_3=(E_final-CurrentEnergy_3)/(Co*CurrentEnergy_3^n)

Y_lin_3=0.001:.0001:.016;
for jj=1:1:length(Y_lin_3)
   X_lin_3(jj)=(Y_lin_3(jj)-d_3)/c_3;
end

%~~~~~~~~~~~~~~~~~~~~~~~~~~~~~~~~~~~~~~~~~~~~~~~~~~~~~~~~~~~~~~~~~~~~~~~~~~~~~~~~
%~~~~~~~~~~fourth set of data points~~~~~~~~~~
for ii=1:1:round(length(new_eng_val_max)*.95)
   new_eng_val_fourth(ii)=new_eng_val_max(ii);
   new_cyc_val_fourth(ii)=new_cyc_val(ii);
end

[c_4 d_4]=chronweightlsquares(new_cyc_val_fourth, new_eng_val_fourth,weight);
% C_final_4=(E_final-d_4)/c_4
% deltaT_lin_4=C_final_4-new_cyc_val_fourth(ii)
CurrentCycle_43=new_cyc_val_fourth(ii)
CurrentEnergy_43=c_4*CurrentCycle_43+d_4
deltaT_lin_43=(E_final-CurrentEnergy_43)/(Co*CurrentEnergy_43^n)

Y_lin_4=0.001:.0001:.016;
for jj=1:1:length(Y_lin_4)
   X_lin_4(jj)=(Y_lin_4(jj)-d_4)/c_4;
end
```

APPENDIX F
NATURALLY PROPAGATING DATA ΔC AND ΔPSV

```
%This code plots the theoretical versus actual points for delta C and delta PSV
clear all;
close all;
fig=1
E_final=0.015022;
weight=4;
Co=.13;
n=1.1;

%Days corresponding to Energy and Cycles
D= [924   1021   1114   1116   1120   1122   1125   1217]';

% # of cycles the bearing has undergone on given day
C=  [4.560    14.832    19.408   20.688   24.208    26.016    27.072    33.720]';

%Area associated with number of cycles and day
Area=[1.785    5.5683    5.6175    5.8092    8.0904    8.2242    8.0415    8.4329]';

%Maximum Energy near resonant freq. after signal has been filtered
E=[0.00444783222028835
  0.0088591945233774
  0.0132573959978724
  0.0149704390918183
  0.0152343720991011
  0.00951013385028358
  0.0112612969517493
  0.0103651024541256];

% Equidistant x-points (cycles)
deltaC=(C(8)-C(1));
no_pts=1000*deltaC;
delta=1/1000;
delta_c(1)=C(1);

for ii=2:1:no_pts
   delta_c(ii)=delta_c(ii-1)+1/1000;
end

% energy(1)=E(1);

%slope is constant between points y=mx+b
for ii=1:1:7;
   m(ii)=(E(ii+1)-E(ii))/(C(ii+1)-C(ii));
```

```
   b(ii)=E(ii)-m(ii)*C(ii);
end

ii=1;
val=1;
for jj=val:1:no_pts
   energy(jj)=m(ii)*(delta_c(jj))+b(ii);
   if delta_c(jj)>=C(ii+1);
      ii=ii+1;
   end
   val=jj;
end

%implementing Gaussian white noise
y=wgn(1,no_pts,2);
scale=0.0002;
new_energy=y*scale+energy;

cutoff_cyc_val=22;
delt_cutoff=cutoff_cyc_val-delta_c(1);
nopts=delt_cutoff*1000;
number_of_desired_samples=200;
random_points=rand(number_of_desired_samples,1);
sort_rand_pts=sort(random_points)*nopts;
new_cyc_index=round(sort_rand_pts);
new_cyc_val_max=C(1)+delta*new_cyc_index;

%Find the energy values corresponding to this cycle vector
delta_c=round(delta_c*1000)/1000;
val=1;
for jj=1:1:number_of_desired_samples;
   for ii=val:1:nopts;
      if new_cyc_index(jj)==ii;
         new_eng_val_max(jj)=new_energy(ii);
      end
   end
end

lnevm=length(new_eng_val_max);
goodenoughpoints=30;
new_eng_val=zeros(lnevm,goodenoughpoints);
new_cyc_val=zeros(lnevm,goodenoughpoints);

for kk=1:goodenoughpoints
   percent=kk/goodenoughpoints;
   vector(kk)=round(lnevm*percent);
```

```
   for ii=1:1:vector(kk);
      new_eng_val(ii,kk)=new_eng_val_max(ii);
      new_cyc_val(ii,kk)=new_cyc_val_max(ii);
   end
end
Co=.13;
n=1.1;

for jj=1:goodenoughpoints
   [c(jj)
d(jj)]=chronweightlsquares(new_cyc_val(1:vector(jj),jj),new_eng_val(1:vector(jj),jj),
weight);
   C_final(jj)=(E_final-d(jj))/c(jj);
   CurrentC(jj)=max(new_cyc_val(:,jj));
   CurrentE(jj)=c(jj)*CurrentC(jj)+d(jj);
   deltaCact(jj)=C_final(jj)-CurrentC(jj);
   deltaE(jj)=E_final-CurrentE(jj);
   deltaC(jj)=deltaE(jj)/(Co*CurrentE(jj)^n);
end

%Plotting theoretical points to actual time to failure.
ParisDeltaE=linspace(E_final-.000001,0,500);

for pp=1:1:length(ParisDeltaE)
   ParisDeltaC(pp)=ParisDeltaE(pp)/(Co*(E_final-ParisDeltaE(pp))^n);
end

figure(fig)
fig=fig+1
plot(deltaC,deltaE,'g.', deltaCact, deltaE, 'b.',ParisDeltaC,ParisDeltaE,'k-')
% plot(ParisDeltaC,ParisDeltaE,'k-')
xlabel('DeltaC (millions)');
ylabel('DeltaPSV');
axis([-100 400 0 .016]);
legend('estimation', 'actual','Modified Paris Trend');

figure(fig)
fig=fig+1
plot(deltaC,deltaE,'g.', deltaCact, deltaE, 'b.',ParisDeltaC,ParisDeltaE,'k-')
xlabel('DeltaC (millions)');
ylabel('DeltaPSV');
legend('estimation', 'actual','Modified Paris Trend')
axis([0 25 0 .009]);
```

REFERENCES

Al-Balush, K. R., and Samanta, B. "Gear Fault Diagnosis Using Energy-Based Features of Acoustic Emission Signals." Journal of Systems and Control Engineering 216.1 (2002): 249-263.

ASTM E647, "Standard Test Method for Measurement of Fatigue Crack Growth Rates," ASTM International.

Billington, Scott A. Sensor and Machine Condition Effects in Roller Bearing Diagnostics. Diss. Georgia Institute of Technology, 1997.

C. Cempbel "A New Method of Symptom Based Processing for Machinery Condition Recognition and Forecasting." Mechanical System and Signal Processing (1995): 129-137.

Davis, M. H. A. Markov Models and Optimization. 1st ed. New York: Chapman & Hall, 1993.

Goldman, Steve. Vibration Spectrum Analysis: A Practical Approach. 2nd ed. New York: Industrial Press, Inc, 1999.

Harris, Tedric. Rolling Bearing Analysis. 3rd ed. New York: John Wiley & Sons, Inc., 1991.

Hoeprich, M.R. "Rolling Element Bearing Fatigue Damage Propagation." Transactions of the ASME Journal of Tribology 114 (1992): 328-333.

Hoffman, Joe D. Numerical Methods for Engineers and Scientists. 2nd ed. New York: Marcel Dekker, Inc., 2001.

Kalpakjian, Serope and Schmid, Steven R. Manufacturing Processes form Engineering Materials. 4th ed. Upper Saddle River, NJ: Prentice Hall, 2003.

Kay, S. M. and Marple, S. L. "Spectrum Analysis—A Modern Perspective." Modern Spectrum Analysis, II. New York: IEEE Press, 1986: pp. 1-41.

Key to Metals Task Force. "Fatigue Crack Growth." INI International. 31 October, 2005. < http://www.key-to-steel.com/ViewArticle.asp?ID=49>

Li, Yawei. Dynamic Prognostics of Rolling Element Bearing Condition. Diss. Georgia Institute of Technology, 1999.

Lin Y. K., and J. N. Yang. "On Statistical Moments of Fatigue Crack Propagation." Engineering Fracture Mechanics 18.2 (1983): 243-256.

NIST/SEMATECH. e-Handbook of Statistical Methods. 31 October, 2005. <http://www.itl.nist.gov/div898/handbook.>

P. C. Paris and F. Erdogan. "A Critical Analysis of Crack Propagation Laws." ASME Transactions, Journal of Basic Engineering (1985). 528-534.

Qiu, Jing, Cheng Zhang, Brij Seth, Steven Liang. "Damage Mechanics Approach for Bearing Lifetime Prognostics." Mechanical Systems and Signal Processing (2002): 817-829.

Roberts, Richard A., and Clifford T. Mullis. Digital Signal Processing. 1st ed. Reading, MS: Addison-Wesley Company, 1987.

Sensorland. "The Piezoelectric Accelerometer." 31 October, 2005. <http://www.sensorland.com/HowPage003.html>

Shigley, Joseph and Mischke, Charles. Mechanical Engineering Design. 5th ed. New York: McGraw-Hill, Inc, 1989.

Shiroishi, J., Y. Li, S. Liang, T. Kurfess, and S. Danyluk. "Bearing Condition Diagnostics Via Vibration and Acoustic Emission Measurements." Mechanical Systems and Signal Processing (1997): 693-705.

Simmons, Ryan. "MOLA: Random Vibration Analysis." Mechanical Systems Analysis and Simulation Branch. NASA's Goddard Space Flight Center. 22 January, 1996. 31 October, 2005. <http://analyst.gsfc.nasa.gov/ryan/MOLA/random.html>.

Virkler, D. A., Hillberry, B. M., and Goel, P. K. "the Statistical Nature of Fatigue Crack Propagation." *ASME Journal of Engineering Materials and Technology*, Vol. 101, No. 2: 1979, pp.148-153.

Williams, J. A. Engineering Tribology. New York: Oxford University Press, 2000.

Wikipedia. "Spectral Density." 3 September, 2005. 31 October, 2005. <http://en.wikipedia.org/wiki/Spectral_density>

Zhang, C. et al. "Impact Dynamics Modeling of Bearing Vibration fro Defect Size Estimation." International Journal of COMADEM: 2000, pp.37-42.